



**INSROP WORKING PAPER**

**NO. 66 - 1996, I.1.10**

**Ice Environment and Ship Hull Loading along  
the NSR**

**Mikko Lensu, Stephanie Heale, Kaj Riska  
and Pentti Kujala**

**INSROP International Northern Sea Route Programme**



Central Marine  
Research & Design  
Institute, Russia



The Fridtjof  
Nansen Institute,  
Norway



Ship and Ocean  
Foundation,  
Japan



# International Northern Sea Route Programme (INSROP)

Central Marine  
Research & Design  
Institute, Russia



The Fridtjof  
Nansen Institute,  
Norway



Ship & Ocean  
Foundation,  
Japan



## INSROP WORKING PAPER NO. 66-1996

Sub-programme I: Natural Conditions and Ice Navigation

Project I.1.10: Ice Environment and Ship Hull Loading along the NSR

Supervisor: Kaj Riska

**Title:** Ice Environment and Ship Hull Loading along the NSR

Authors: Mikko Lensu, Stephanie Heale, Kaj Riska and Pentti Kujala

Adresse: Helsinki University of Technology,  
Ship Laboratory,  
Tietotie 1,  
02150 Espoo,  
FINLAND

Date: 18 October 1996

Reviewed by: Professor Claude Daley, Memorial University of  
Newfoundland, Canada

### *What is an INSROP Working Paper and how to handle it:*

This publication forms part of a Working Paper series from the **International Northern Sea Route Programme - INSROP**. This Working Paper has been evaluated by a reviewer and can be circulated for comments both within and outside the INSROP team, as well as be published in parallel by the researching institution. A Working Paper will in some cases be the final documentation of a technical part of a project, and it can also sometimes be published as part of a more comprehensive INSROP Report. For any comments, please contact the authors of this Working Paper.



## FOREWORD - INSROP WORKING PAPER

INSROP is a five-year multidisciplinary and multilateral research programme, the main phase of which commenced in June 1993. The three principal cooperating partners are **Central Marine Research & Design Institute (CNIIMF)**, St. Petersburg, Russia; **Ship and Ocean Foundation (SOF)**, Tokyo, Japan; and **Fridtjof Nansen Institute (FNI)**, Lysaker, Norway. The INSROP Secretariat is shared between CNIIMF and FNI and is located at FNI.

INSROP is split into four main projects: 1) Natural Conditions and Ice Navigation; 2) Environmental Factors; 3) Trade and Commercial Shipping Aspects of the NSR; and 4) Political, Legal and Strategic Factors. The aim of INSROP is to build up a knowledge base adequate to provide a foundation for long-term planning and decision-making by state agencies as well as private companies etc., for purposes of promoting rational decisionmaking concerning the use of the Northern Sea Route for transit and regional development.

INSROP is a direct result of the normalization of the international situation and the Murmansk initiatives of the former Soviet Union in 1987, when the readiness of the USSR to open the NSR for international shipping was officially declared. The Murmansk Initiatives enabled the continuation, expansion and intensification of traditional collaboration between the states in the Arctic, including safety and efficiency of shipping. Russia, being the successor state to the USSR, supports the Murmansk Initiatives. The initiatives stimulated contact and cooperation between CNIIMF and FNI in 1988 and resulted in a pilot study of the NSR in 1991. In 1992 SOF entered INSROP as a third partner on an equal basis with CNIIMF and FNI.

The complete series of publications may be obtained from the Fridtjof Nansen Institute.

## SPONSORS FOR INSROP

- Nippon Foundation/Ship & Ocean Foundation, Japan
- The government of the Russian Federation
- The Norwegian Research Council
- The Norwegian Ministry of Foreign Affairs
- The Norwegian Ministry of Industry and Energy
- The Norwegian Ministry of the Environment
- State Industry and Regional Development Fund, Norway
- Norsk Hydro
- Norwegian Federation of Shipowners
- Fridtjof Nansen Institute
- Kværner a.s.

## PROFESSIONAL ORGANISATIONS PERMANENTLY ATTACHED TO INSROP

- Ship & Ocean Foundation, Japan
- Central Marine Research & Design Institute, Russia
- Fridtjof Nansen Institute, Norway
- National Institute of Polar Research, Japan
- Ship Research Institute, Japan
- Murmansk Shipping Company, Russia
- Northern Sea Route Administration, Russia
- Arctic & Antarctic Research Institute, Russia
- ARTEC, Norway
- Norwegian Polar Research Institute
- Norwegian School of Economics and Business Administration
- SINTEF (Foundation for Scientific and Industrial Research - Civil and Environmental Engineering), Norway.

## PROGRAMME COORDINATORS

- **Yury Ivanov, CNIIMF**  
Kavalergardskaya Str.6  
St. Petersburg 193015, Russia  
Tel: 7 812 271 5633  
Fax: 7 812 274 3864  
Telex: 12 14 58 CNIMF SU
- **Willy Østreng, FNI**  
P.O. Box 326  
N-1324 Lysaker, Norway  
Tel: 47 67 11 19 00  
Fax: 47 67 11 19 10  
E-mail: sentralbord@fni.no
- **Ken-ichi Maruyama, SOF**  
Senpaku Shinko Building  
15-16 Toranomom 1-chome  
Minato-ku, Tokyo 105, Japan  
Tel: 81 3 3502 2371  
Fax: 81 3 3502 2033  
Telex: J 23704



# CONTENTS

## 1. INTRODUCTION 1

## 2. PARAMETERISATION OF THE ICE COVER 3

- 2.1. Existing ice codes 3
  - 2.1.1. WMO Ice Code 3
  - 2.1.2. Russian codes 6
  - 2.1.3. Ice characterisation in the INSROP information system 7
  - 2.1.4. Navigability oriented descriptions 9
    - 2.1.4.1. Canadian Ice Regime 10
    - 2.1.4.2. Russian approach 11
  - 2.1.5. Shortcomings of the conventional ice codes 12
- 2.2. Parameterisation in terms of distributions 13
- 2.3. Level ice; Ice thickness distribution 17
  - 2.3.1. Maximum level ice thickness 17
  - 2.3.2. Level ice strength 17
  - 2.3.3. The statistics of level ice thickness 18
- 2.4. Ice floes 19
- 2.5. Ice ridges 20
  - 2.5.1. Ridging model 20
  - 2.5.2. Sail and keel geometry 20
  - 2.5.3. Sail and keel structure 23
  - 2.5.4. Distribution of cross-sectional sail heights 24
  - 2.5.5. Distribution of ridge link sizes 25
  - 2.5.6. Distribution of ridge spacings 27
  - 2.5.7. Extrapolation of ridge density 28
  - 2.5.8. Extremal statistics 30
- 2.6. Leads 33
- 2.7. Dynamics 33

## 3. ICE CONDITIONS ALONG THE NORTHERN SEA ROUTE 34

- 3.1. Geography of the area 34
- 3.2. Hydrographic conditions 36
- 3.3. The selected parameterisation 38
- 3.4. The ice data matrices 40
  - 3.4.1. Area I, Pechora Sea 40
  - 3.4.2. Area II, Western Kara Sea 41
  - 3.4.3. Area III, Eastern Kara Sea 42
  - 3.4.4. Area IV, Laptev Sea 42
  - 3.4.5. Area V, Western East Siberian Sea 43
  - 3.4.6. Area VI, Eastern East Siberian Sea 44
  - 3.4.7. Area VII, Chukchi Sea 45
- 3.5. Data summaries 45



## **4. SHIP TRANSIT ALONG THE NSR 52**

- 4.1. Transit modelling 52**
- 4.2. Ship's speed in the NSR sea areas 54**
- 4.3. The transit results 55**

## **5. SHIP SAFETY ALONG THE NSR 61**

- 5.1. Description of the approach applied 61**
  - 5.1.1. General description 61**
  - 5.1.2. Formulations for the long term loads 61**
  - 5.1.3. Effect of the maximum ice breaking capability 65**
  - 5.1.4. Effect of ship hull shape 66**
  - 5.1.5. Evaluation of failure probability for the frames 68**
- 5.2. Application to the NSR 69**
- 5.3. Results of the damage probability calculations 70**

## **6. CONCLUSION 77**

## **ACKNOWLEDGMENTS 78**

## **REFERENCES 79**

- APPENDIX 1. Monthly mean temperatures on five weather stations 84**
- APPENDIX 2. Sectionwise monthly concentrations along NSR 87**
- APPENDIX 3. Damage probability tables 97**
- APPENDIX 4. Graphs of damage probability vs month 110**
- APPENDIX 5. Project review 114**



# 1. INTRODUCTION

The projects on the navigation along the Northern Sea Route (NSR) were initiated in the Ship Laboratory at the Helsinki University of Technology for several purposes. One initiative came from the research programme 'Shipyards 2000' run by Finnish shipyards. The project for this programme collected sea ice data along the NSR. Another initiative came from the Regional Fund of Lapland of the Finnish Cultural Foundation which granted to Dr. Pentti Kujala a scholarship to study the risk of hull damage of ships navigating along the NSR. Thus it was very welcome initiative when Dr. H. Kitagawa contacted us with an invitation to participate the INSROP programme. The present project is the result of this invitation. The INSROP funding made it possible to collect our somewhat scattered results together.

The Project I.1.10 belongs to the INSROP sub-programme I, Natural Conditions and Ice Navigation, and its objective is to combine existing knowledge on ice conditions with methods of calculating transit parameters and damage probabilities of ice going ships along the NSR. Thus the project has three rather independent parts. The first includes the development of appropriate methods of ice cover parameterisation and the characterisation of ice conditions along NSR with it. The second part describes the transit of ships in these ice conditions. Here a simplified simulation approach, based on physical description of ice-ship interaction processes and able to use detailed ice cover statistics as an input, is applied. The third part calculates ice load distributions and damage probabilities. It is directly connected with the long term statistics of ice cover.

Ice conditions and ship transit in ice-infested waters is addressed in nearly all projects of the sub-programme I, Natural Conditions and Ice Navigation. Numerous INSROP Working Reports contain data or methods that are closely related to those of this report. For these an acronym IWP has been used when referring to them in appropriate sections of this report. The work on the description of the ice conditions is also closely related to the MAST III 'Ice State' project coordinated by Helsinki University of Technology.

Chapter 2 discusses the current ice codes and their shortcomings. The codes originate from the era before ice forecast models and real time high resolution satellite imagery and they are not optimal if a high level integration of all possible components relevant to ice navigation is a focus. As a first step towards more geophysical ice cover Parameterisation the use of statistical distribution models for floe size, thickness, ridges etc. is suggested. A detailed model for ridging statistics is presented. This is the most important input data about ice cover for transit simulations. The development of new methods of ice cover description will be continued in the 'Ice State' project.

Chapter 3 contains a description of ice conditions along the NSR using a subdivision to seven sea areas. These data are then used for transit simulations and damage probability calculations. The data is from publicly available sources; the inclusion of much more extensive Russian databases would greatly increase the detail and reliability of the description. However, the major problem of relating the values used



in large scale ice cover characterisation to certain statistical models required by the transit and damage modelling will probably remain.

The transit speed calculations are described and applied to NSR in Chapter 4. These are obtained as the average transit speed of a vessel with specified parameters through a certain mixture of ice conditions which are: channel ice, level ice and ridged ice. An SA-15 type vessel is used as an example of a typical merchant vessel navigating on the NSR. The transit speeds are calculated for the seven sea areas and for different ice conditions described in Chapter 3.

The approach to ship safety and damage probability is described in Chapter 5. It is based on the extrapolation of observed long term statistics of ice loads from the Baltic. The Baltic conditions have thus been scaled up to correspond to the ice conditions on different NSR seas. The ice conditions from Chapter 3 are used as an input.

The results of transit simulations and damage probability calculations should be regarded as tentative. The main reason is that the description of ice conditions is quite rough. For example, the overall ice concentration values do not take into account such features as areas with lower concentration occur by the fast ice edge. In addition much relevant data, especially on ice thickness distribution, is lacking and much of other data, especially on ice ridges, is merely descriptive. For reliable calculations the existence probability of certain ice conditions for each route point would be needed and as result distributions pertaining to ship transit and damage would be obtained. Therefore the main content of this report is on the methodological side. However, as the Russian data becomes available in the INSROP data base the developed tools will increase in operative value. Further development of the approach is suggested in Chapter 6, Conclusions.

Further, the transit calculations use only the average ice conditions along a route segment. Once more thorough transit information is needed, a full transit simulation should be done. Then the ice data distributions are used to create by a Monte Carlo method an example of ice conditions along the route. Ship progress through these conditions is simulated on time step basis. The repetition of this calculation creates transit statistics and the relationship of these to the statistics of ice conditions. This task is a large one and thus the simpler approach was used here.

The hull damage risk calculations is based on Baltic ice conditions. These do not include multi-year ice. This load component should be added to the present calculations. Also the consolidation of ridges should be taken into account more directly in load calculations. Even with these shortcomings the present report contains a presentation of the elements to be studied in assessing the navigability of the NSR.

## 2. PARAMETERISATION OF THE ICE COVER

### 2.1. EXISTING ICE CODES

An ice code is a predefined set of ice parameters and their ranges that are used to characterise the ice cover. To these codes are associated special nomenclatures and symbols. Two main uses of ice codes are ice charts and characterisation of ice observations. The following desiderata can be imposed on an ice code:

- It should describe relevant ice conditions without being too detailed
- It should be presentable in a synoptic visual form
- The relation with ice navigability should be straightforward
- It should be determinable by remote sensing methods
- It should be determinable by shipboard observations
- The parameters should be related to those used in geophysical ice models

What comes to navigation in ice, two choices are available. An ice code may seek to describe in an optimal way the ice conditions relevant for ship transit. The other possibility is to use the navigational ability of ships, categorised according to a certain system, as a descriptor of the ice cover.

#### 2.1.1 WMO Ice Code

A special nomenclature and symbol system have been developed by the World Meteorological Organisation (WMO) to describe sea ice fields. Sea ice is like a thin film between the atmosphere and the ocean with highly complicated morphology, thermodynamics and dynamics. Its state is mainly determined by the following parameters:

- 1) Ice concentration
- 2) Age or stage of development
- 3) Thickness
- 4) Form (e.g. floe size)
- 5) Surface features (e.g. ridges)
- 6) Motion.

Coordination of the work of the Ice Services in the whole world has been made through the Sea Ice Working Group of the WMO. An internationally agreed illustrated nomenclature was published in 1970 (WMO, 1970). This book attempted to standardise the sea ice terminology and give definitions to the various terms. Updates of the nomenclature have been made since 1970.

For the preparation of an ice chart, symbol systems have been introduced to describe, mainly based on visual observations, the type and the concentration of ice. This has been a very useful way of illustrating the structure and development of an ice cover.



The application for navigation has, however, been rather complicated as in different regions different systems of symbols are used. In 1981 WMO introduced "The International System of Sea-Ice Symbols", a unique set of symbols to be used in all sea areas (WMO 1985). Figure 1.1 shows as an extract the symbols for the ice concentration and some additional symbols used on Baltic ice charts



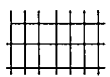

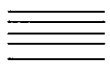







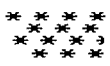

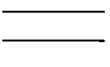
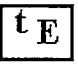

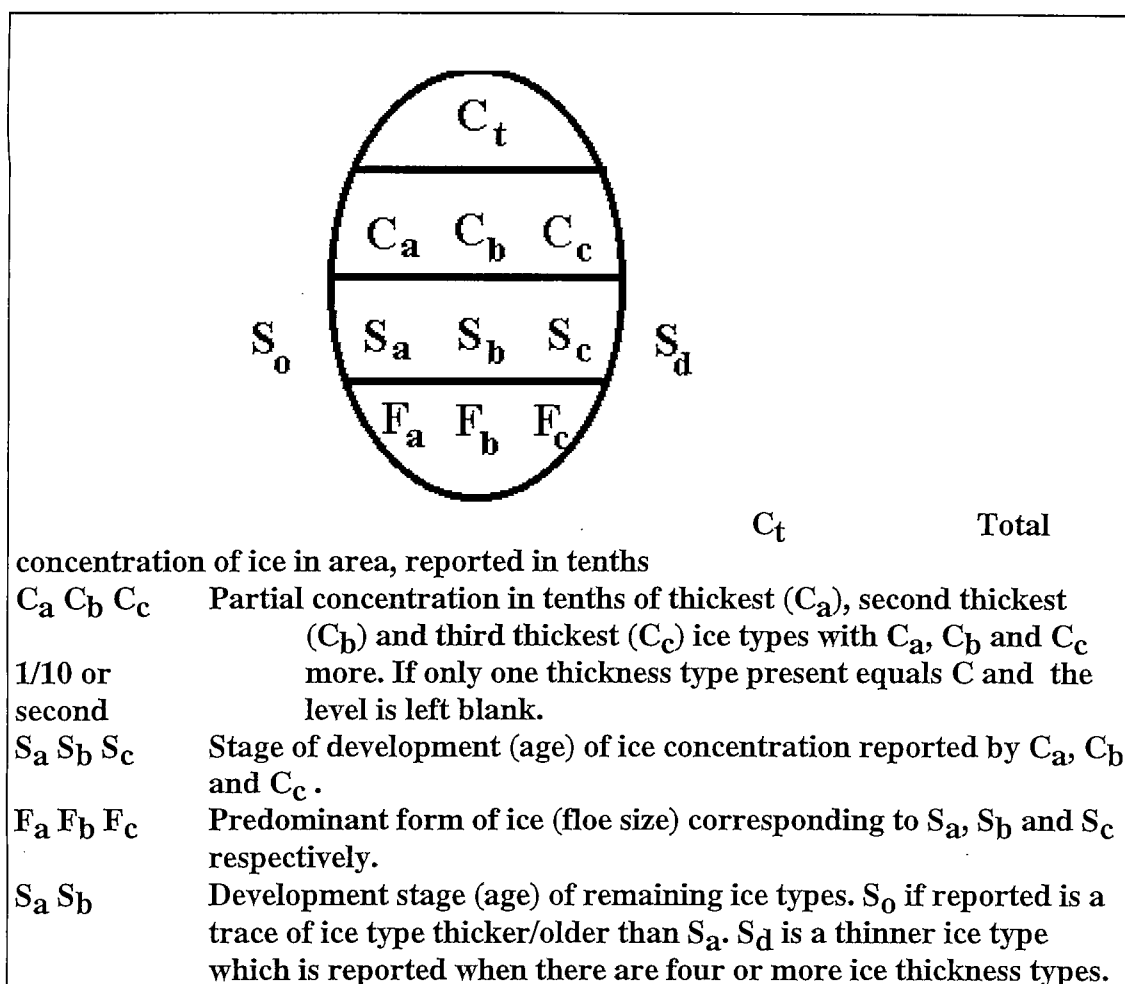
	Fast Ice		Ridged or hummocked ice C=concentration
	Consolidated, compact or very close ice (9-10/10)		Rafted ice C=concentration
	Close ice (7-8/10)		Windrow, Jammed brash barrier
	Open ice (4-6/10)		Ice edge or ice boundary
	Very open ice (1-3/10)		Estimated ice edge or ice boundary
	Open water (<1/10)		Lead
	New ice		Crack
	Level ice		Thickness measured in cm
			Floebergs/Floe bits

Figure 2.1. WMO ice symbols adopted for use in the Baltic

As step towards a digital form of ice charts, the WMO Sea Ice Working Group created as main symbol the "egg". This egg code provides numerical values of ice concentration, the stage of development (thickness) and the form of the ice (floe size) for a more or less homogeneous sea ice cover within given ice boundaries. The scheme is presented in Figure 2.2. How the ice symbols and egg codes are used in ice charts is highly variable.



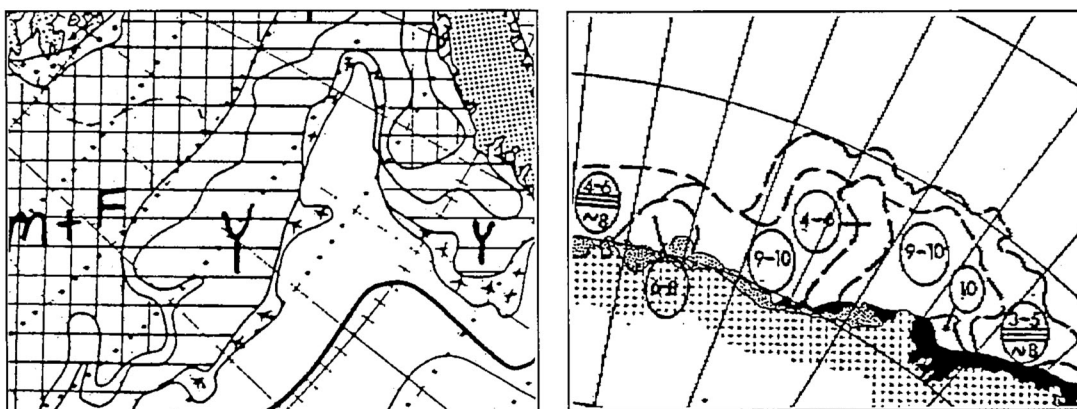
$F_a F_b F_c$ Form of ice (width)			$S_a S_b S_c$ Stage of Development (thickness cm)		
0	Pancake		1	New	<10cm
1	Brash		2	Nilas	<10cm
2	Ice Cakes	<20m	3	Young	10-30 cm
3	Small floe	20-100 m	4	Grey	10-15 cm
4	Medium floe	100-500 m	5	Grey-white	15-30 cm
5	Big floe	500-2000 m	6	First Year	> 30 cm
6	Vast floe	2-10 km	7	Thin First Year /White	30-70 cm
7	Giant floe	>10 km	1.	Medium First Year	70-120 cm
8	Fast ice		4.	Thick First Year	> 120 cm
9	Icebergs		7.	Old	
X	No Form		8.	Second Year	no
C	Ice is in strips in which concentration is C		9.	Multi-year	defined ranges
			$\Delta$	Icebergs	

Figure 2.2 . Scheme of the WMO Egg code

Ice charts for the NSR are delivered by various institutions. The Norwegian Meteorological Institute supplies ice charts covering Barents and Kara Seas. These apply the graphical presentation of compactness classes (Figure 2.3) with the additional indicators of the relative abundance of first year and multi-year ice:

- M(+)
  - M
  - M+F
  - F+M
  - F
- very thick multi-year ice  
dominance of multi-year ice  
multi-year and first year ice  
first year and multi-year ice  
dominance of first year ice

These charts are based on NOAA/AVHRR 1.5 km resolution data and on DMSP/SSM/I 25 km resolution data. National Ice Center in USA uses the same data but applies the Egg Code instead. In addition the theoretical thickness of the season's growth based on freezing degree days is given. These charts cover the whole NSR.



**Figure 2.3.** Ice map styles of NSR and National Ice Center.

### 2.1.2 Russian codes

NSR ice surveillance is based on analyses made in the meteorological centers of Dikson and Pevek. The analysis is based on information gathered from satellites, aeroplanes, ships and scientific stations. The center works out a simplified ice map and transmits it on facsimile. The details can be found in several INSROP Working Papers, for example Makarov et al. (1995, IWP 24) and Grishchenko et al. (1995, IWP 25).

Russian ice charts are typically much more detailed than other ice charts. They use an extensive set of symbols that differs in several respects from the WMO symbols (Figure 2.4). It allows more detailed graphical description of local characteristics, for example the floe sizes and ice compression. In addition features typical to the Russian Arctic like stamukhas and characterisation of fast ice is included. How the ice symbols are used in individual charts depends on the available data and the ability of

the chartist, but increasing the details easily makes the chart to lose its synoptic character.

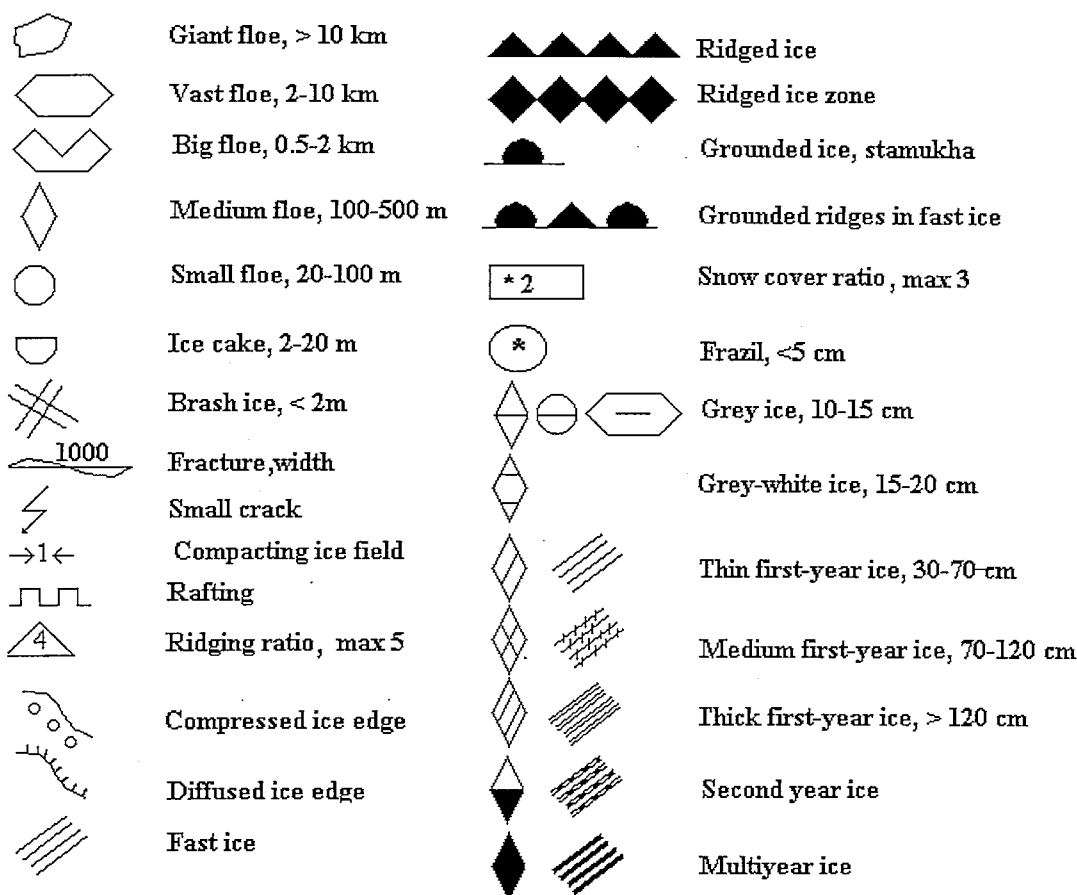


Figure 2.4. A selection of Russian ice symbols.

### 2.1.3. Ice characterisation in the INSROP information system

The INSROP information system (Løvås et al. 1994, IWP 4) has database entities for ice and snow characterisation and, on the other hand, for ice observations. The database uses the formats and concepts of a GIS (geographical information system) which can be based on a PC terminal with ArcView software.

In the system are defined three basic kinds of objects: entities, attributes and relations. Entities are database objects to be characterised. Geographic entities may be features, profiles, layers or composites, corresponding roughly to 0, 1, 2, and 3-dimensional entities respectively. The dimensions can refer to horizontal position (x,y), vertical position or height (z), time (t), and to themes or topics (c, for example: classification of ice types). Attributes are database objects characterising the entities; they are more commonly called characteristics. Relations are links between database objects. Thus in a GIS it is (however, not in the present version of INSROP information system) possible, for example, to characterise different types of thickness measurements and link them with ice maps, satellite images, ice cover time series or ship navigability.



With the system various queries can then be made, like: what is the probability of meeting ice more than 1.5 m thick in a certain area at a certain time.

In the present version of the INSROP information system the entities and attributes relating to ice are arranged under two entity themes: ice and snow, and NSR navigability. The first is related to geophysical ice characterisation and ice mapping. It uses to some extent the same terminology as the WMO ice code although the sets of numbers or letters used as attribute domains are different. The attributes and their domains are given in Table 2.1.

**Table 2.1.** Ice and snow attributes in INSROP information system.

Ice origin	S,I R	S Sea ice I Ice of land origin	R River ice
Stage of development	N,P,Y F,S,M	N New ice P Pancake ice Y Young ice	F First-year ice S Second-year ice M Multi-year ice
Forms of fast ice	1-4	1 Young coastal ice 2 Icefoot	3 Anchor ice 4 Grounded ice
Forms of pack ice	0-9	0 Consolidated pack ice 1 Compact pack ice 2 Very close pack ice 3 Close pack ice	4 Open ice 5 Very open ice 8 Open water 9 Ice-free
Forms of floating ice	1-9	1 Pancake ice 2 Vast floes 3 Big floes 4 Medium floes 5 Small floes	6 Floeberg 7 Ice breccia 8 Brash ice 9 Iceberg
Ice arrangement	1-9	1 Ice field 2 Ice massif 3 Ice belt 4 Ice tongue	6 Ice strip 7 Ice bight 8 Ice jam 9 Ice edge
Pack-ice motion processes	D,C,S	D Diverging C Compacting	S Shearing
Ice deformation processes	1-5	1 Fracturing 2 Hummocking 3 Ridging	4 Rafting 5 Weathering process
Openings in the ice	1-4	1 Crack 2 Fracture zone	3 Lead 4 Polynya
Ice-surface features	1-9	1 Level ice 2 Rafted ice 3 New Ridges 4 Weathered ridges 5 Consolidated ridges	6 Hummocked ice 7 Bare-ice 8 Snow-covered ice 9 Sastrugi
Ice drift	cm/s degree	Speed Direction	

Stage of melting	1-5	1 Puddles 2 Thaw holes 3 Dried ice	4 Rotten ice 5 Flooded ice
Snow cover	cm 1-5	Snow thickness 1 New snow 2 Dry snow	3 Wet snow 4 Snowdrift 5 Sastrugi

The second set of ice attributes is under the entity theme NSR Navigability. These attributes are intended to be used for ship based ice observations only. In addition to ice information the theme contains information on vessels, ship routes, voyages and ship accidents. The ice information is coded according to the shipboard ice code as described in the Canadian Ice Manual. (AES 1994). It consists a WMO ice code (Figure 2.2) with some additional attributes, which are:

- Partial concentration of rafted ice
- Partial concentration of ridges and hummocks
- Snow coverage
- Snow depth
- Mean ridge height
- Extreme ridge height
- Direction of ice drift
- Speed of ice drift
- Trend in behaviour of ice
- Number of growlers and/or bergy bits
- Number of icebergs
- Polynya characterisation

The attribute domains are equal to those of WMO and Canadian ice codes. The classifications of the information system may change in the future. For example, Løset and Vefsnmo (1994, IWP 5) include floe size and ridge distributions into their list of requirements for INSROP data base.

#### 2.1.4 Navigability oriented descriptions

One problem of WMO related ice codes is that not all variation of ice cover that they describe is relevant for navigation. On the other hand it is difficult to define a single parameter or a small set of parameters that would describe the navigability of the ice cover by starting from the morphological description. One possibility is to use the ability of certain ships to navigate in the ice. The parameters related to this, speed, energy consumption and damage probability, are then in a way integrals of the variable ice conditions. Thus very different compositions of the ice cover can be considered as equivalent from a navigational point of view if the chosen trafficability descriptors are identical for them.

### 2.1.4.1 Canadian Ice Regime

The Ice Regime Shipping Control System (IRS) is an aspect of the Arctic Shipping Pollution Prevention Regulations (ASPPR) for Canadian Arctic sea areas. It extends and will eventually replace the former system, known as Zone/Date system, where the Canadian Arctic was divided into 16 control zones with earliest/latest entry days for certain ship categories. The Zone/Date system has also been recommended for NSR by Torrens (1994, IWP 1) to be used as a basis of insurance policy. With the IRS is associated a new Arctic vessel classification system and a new directive of navigation safety (Subcommittee, 1989).

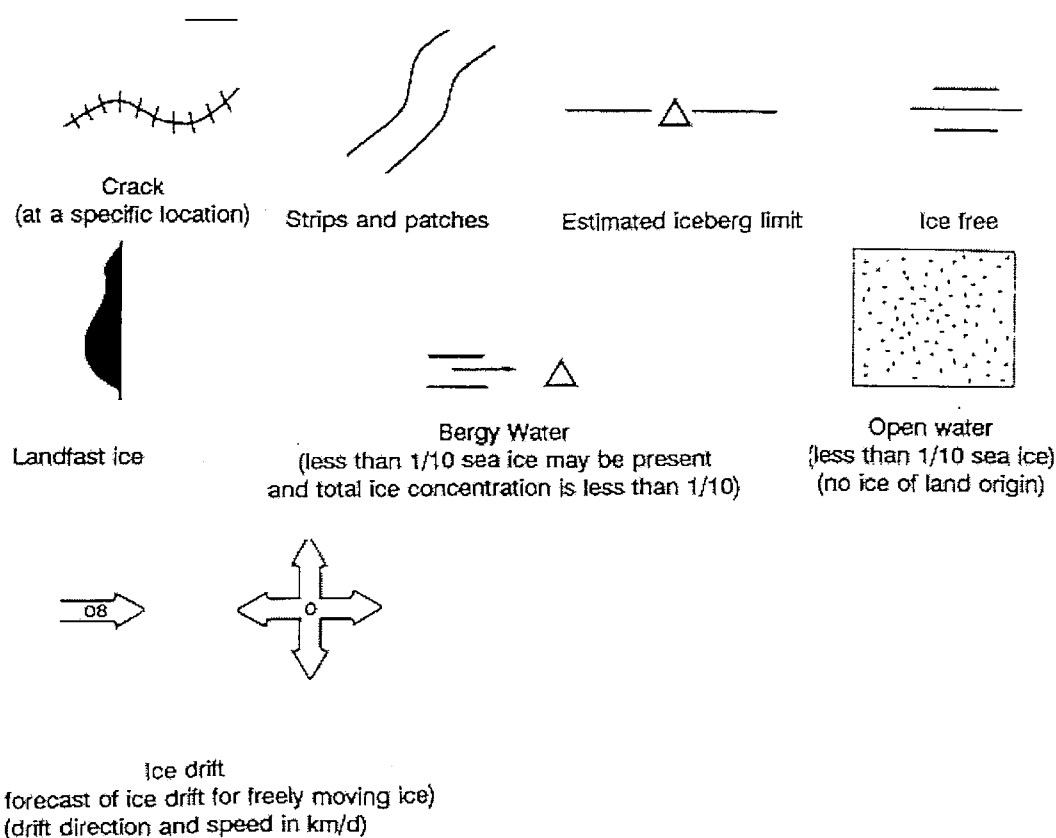
The concept of ice regime is an attempt to characterise ice conditions in a way that would have a connection to navigation from the outset and would be more flexible than the Zone/Date system. The ice cover is a complex mixture of different ice types and a detailed description of it is often not the best possible one for navigational purposes. An ice regime is defined as an area of relatively homogeneous ice conditions but without no predefined size or location. The ice cover within an ice regime may consists of several ice types but their properties and relative coverages should not vary much.

The IRS stresses damage probability rather than speed or other measures of navigational effectivity. The basic idea is to calculate an 'ice numeral' (IN), or an index of hazardousness, for each ship type as a sum of relative coverages of ice types weighted by their hazardousness to the ship. The weights are called 'ice multipliers' and are tabulated. Thus the ice numeral is

$$IN = (C_1 \cdot IM_1) + (C_2 \cdot IM_2) + \dots$$

where  $C_i$  is concentration for ice type  $i$  and  $IM_i$  the corresponding ice multiplier. The ice numeral must be nonnegative for a ship to be allowed to enter the ice regime. The ice multipliers may be increased if the ice is decaying (has thaw holes) or contains brash (floes < 2 m in diameter), or they may decreased if the ice is ridged; these parameters are known as 'modifiers' in the system. Available icebreaker escort modifies also the multipliers. However, the IRS has not yet fully been incorporated with the Canadian ice charting. These rely on the ice codes with some additional symbols, Figure 2.5.

The IRS has been applied to the NSR in Hagen and Jones (1996, IWP 32). The ice data was mainly from Russian ice charts completed with ridging, decaying and brash ice content data from various sources. The calculations were made for four years (1987-1990) and for four phases of the ice season (late January, mid May, mid July and early September). The ice numerals were calculated and the minimum ice class allowed to navigate in a certain ice regime at certain time was determined.



**Figure 2.5.** Additional Canadian ice symbols.

#### 2.1.4.2 Russian approach

The concept of ice regime is related to the Russian approach of 'specialised ice information'. This is considered to be a set of ice, operating and ice-navigation characteristics. They are intended to indicate ice conditions directly on the route of ships and present a quantitative estimate of their effect to navigability (Bovin et al. 1995, IWP 23).

The basic concept is QAD or quantitative assessment of the difficulty of ice navigation. It has been developed in Russia mainly by Buzuyev and his collaborators (see Bovin et al. 1995, IWP 23, and references therein). Its objectives are

- To identify various ice cover characteristics affecting the ship motion
- To describe the effect of ice conditions to ship motion
- To classify ice cover in terms of ship motion
- To obtain en route ice information from more regional ice information
- To collect relevant data

The main division of ice types are given in Table 2.2. An unique feature in QAD is a method of deriving along the route ice conditions from regional ice conditions given, for example, by ice charts. This is necessary because ice navigation does not proceed along linear tracks but continuously seeks optimal routes, that is, areas of lower concentration, smaller floes and less ridging. Therefore the ice conditions experienced



by a ship are moderated versions of those prevailing regionally; certain rules for estimating these are given. The effect of the ice cover to ship motion is calculated on the basis of empirical formulas. The speeds obtained thereby are 'theoretical speeds' from which the 'operating speed' is obtained according certain rules that take into account the speed decrease due to safety requirements and other factors. The operating speed is then used for route planning.

**Table 2.2.** Ice condition classes in QAD.

Ice conditions	Main ice-ship interaction	Parameters relevant for ice resistance
Fast ice, large floes	Breaking of continuous cover	Thickness, ridging, snow cover, degree of destruction
Medium size floes	Breaking, pushing aside of the floes	Concentration, ridging, degree of destruction, pressure
Small floes, channel ice	Pushing ice aside	Concentration, friction coefficient, pressure, channel width

A related approach is that of Makarov et al. (1995, IWP 24). It describes a complex system of data flow for navigational purposes which includes also forecasts. The ice conditions and forecasts are allowed to contain uncertainties and the decisions of entering a certain region are assisted by theoretical decision formulas. The idea is that the ice regimes along the NSR are so large that the decisions must not be made on the basis of real time ice information but on short and long term forecasts for the date of transit through a certain region.

### 2.1.5. Shortcomings of the conventional ice codes

The main shortcomings of the conventional ice codes from the point of view of NSR trafficability are:

- 1) The classification of ice types is unnecessarily detailed for younger and thinner ice types that are found during a short period after the freeze-up and are transitory later during the ice season. On the other hand, thicker, deformed and multi-year ice types are insufficiently characterised. The gradations in various characterisations should be in proportion to decrease of ship speed or increase of damage probability.
- 2) There is no quantitative reference to deformed ice types like rafted ice although these can be predominant and several times thicker than level ice.
- 3) There is no quantitative reference to ice ridges, to their size and frequency of occurrence.
- 4) There is no reference to lead sizes, frequencies and orientations.

- 5) The relation of regional ice characteristics to what is experienced by an ice going ship is uncertain.
- 6) The codes cannot optimally use the information that is available from SAR images.
- 7) The terminology has no clear connection to geophysical ice models used for forecasting.

The main reason for these shortcomings is that when the WMO ice code was coined in 1970,

- no operative ice models existed,
- no high resolution satellite data was available, and
- very little data on the thickness, floe size and ridge distributions existed.

The code is clearly aimed at the codification of visual and mainly qualitative observations, for example those made on board. However, it is not feasible that one ice code would satisfy all possible requirements. Therefore a possible scenario for the future development of the ice codes could contain

- a geophysical ice code with theoretically sound concepts which can be related to satellite imagery and ice modelling,
- a navigational ice code which can be related to ship speed and damage probability, and
- an observational ice code as a further development of the WMO code.

This threefold description is truly applicable only if the connecting relations between these parts are simultaneously developed.

## **2.2. PARAMETERISATION IN TERMS OF DISTRIBUTIONS**

The parameters appearing in ice charts and ice codes are regional values pertaining to ice concentration, ice thickness, ice floe size, and possibly ridging, that is, to morphological characteristics. These values are usually derived from visual observations, reconnaissance flights, occasional in situ sampling, and various satellite images. The most difficult parameter to quantify is ice thickness as no basinwide scale remote sensing method exists. If, for example, the ice is rafted to multiple thickness only the thickness of component ice pieces is given since no easy means to determine the average thickness exists. Therefore the thickness values in ice charts are expected to be less than what actually exists.

The variation in ice morphology is typically very large even in a local scale. It is seldom possible to derive unambiguously from a set of singular regional values of morphological properties a description on how difficult the ice conditions are for shipping. A complete map of the ice cover, for example a high resolution satellite image, is on the other hand often too specific. If the regional values of relevant parameters, appearing in ice charts and longer term statistics, are equal to the true

regional average values of ice properties it is possible to obtain a more detailed description of ice conditions by statistical distribution models. These in a way mediate between the regional values and complete mapping. Thus, for example, if the ridge density and mean sail height are known, it is possible with the assumed ridge spacing and sail height distribution models to calculate various probabilities and make transit simulations. However, for most parameters the relation between given regional values and true averages is unclear as no precise methodology for determining these values is prescribed in the ice codes. The given values of ice floe size and ice thickness are rather 'typical' values that are often dependent on subjective choice.

The use of morphological distributions would be a step towards more geophysical ice codes. As a result the characterisation of ice conditions would become less ambivalent and less dependent on subjective interpretation. It would also be possible to estimate the relative coverage of 'easy' and 'difficult' ice conditions without increasing the detailedness. Many distributions, like that for floe size, are semiautomatically derivable from imagery. What is most important, however, is that for the morphological distributions  $f$  it is possible to write evolution equations

$$\frac{\partial f}{\partial t} = \Phi + \Theta + \Psi$$

where  $\Phi$ ,  $\Theta$  and  $\Psi$  describe the change due to ice motion, thermodynamics and mechanics (deformation) respectively. These equations may then be connected to the dynamic-thermodynamic ice models.

As the first step the parameters in ice codes should be defined in such a way that they are connectable with certain distribution parameters, for example with mean values and variances. The basic distributions are as follows:

*Ice thickness distribution.* Various versions of this distribution are defined and applied, but there is no general agreement. The thickest ice is due to ice ridges which are described in much more detail by ridge distributions. Therefore the practical use of the thickness distribution can be restricted to the level and rafted ice types.

*Floe size distribution.* The small floes are most numerous but cover only an insignificant part of the total ice area. Therefore the floe size distribution is most conveniently defined in terms of relative coverage of floes instead of relative frequency of floe sizes.

*Ridge distributions.* Two basic ridge distributions are size and spacing distributions. It is possible to define also a distribution of ridge directions.

*Lead distributions.* The leads are described by distributions for lead width, length and direction. Usually only lead widths are considered. In the winter pack the lead system geometry can be related to the atmospheric forcing. For the summer pack lead distributions are difficult to define since the ice consists of rounded randomly arranged floes. Lead distributions and floe distribution together define the ice concentration.

*Dynamical distributions.* Only large scale ice drift patterns are usually available. From SAR images it is possible to determine local drift speeds and areas of ice convergence and divergence. Areas of compact divergent ice are characterised by lead formation and areas of compact convergent ice by ice pressure and ridge formation; both are typically elongated directed objects. Thus the areas with ice pressure can, similarly to leads, be described by distributions of their width, length and direction. However, these matters have been thus far little studied.

For certain distribution models one parameter, the mean value, is enough. These models can then be readily applied if the average value of the respective quantity is known. For other distributions, however, two or more parameters are needed. If the second parameter is not available (from standard deviation, for example) it must be assumed. The generally accepted basic distribution hypotheses are given in Table 2.3 (see sections 2.3-2.7 for references). The overall coverage of distribution data is yet rather small and the models are to be regarded as tentative; it is possible that the competing hypotheses lead eventually to the same, more general distribution family.

**Table 2.3.** Basic distributions to describe sea ice cover.

Distribution	Suggested models	Parameters	Comments
Thickness distribution	Unsettled	Three or more parameters?	Exponential tail
Floe size distribution	Lognormal	Mean floe size Floe size median or standard deviation	Mean value not defined
	Power law	Power law exponent	
Ridge spacing distribution	Exponential	Ridge density	
	Lognormal	Ridge density Spacing median or standard deviation	
Ridge sail height distribution	$\propto \exp(-h^2)$	Mean sail height	
	Exponential	Mean sail height	
Lead width distribution	Power law	Power law exponent	Mean value not defined
Dynamical distributions	Unsettled		

The use of distributions for the real time operative description of ice conditions has become feasible due to the development of remote sensing methods. This applies especially to the use SAR imagery that provides high resolution highly structured images with good spatial and reasonable temporal coverage. Conditions important for



favourable navigation are open water leads, first year ice and polynyas in areas of old ice, avoiding ridges and ice pressure. These require ideally a resolution comparable to ship dimensions, that is, 15-35 m which is currently provided only by SAR with 10-100 m resolution. The relation between imagery and morphological distributions goes in both directions. The various distributions should be derivable from the images. On the other hand, the interpretation of the images depends on the distribution models. For example, for the estimation of backscattering intensity due to ice ridges and for the construction of interpretation algorithms one should know the distribution of number of ridges per pixel.

The most common remote sensing methods of different morphological parameters are listed in Table 2.4. See Sandven and Kloster (1994, IWP 3) for various satellites available for NSR and the descriptions of different sensors.

**Table 2.4.** Remote sensing methods and their accuracy

Parameter	Method	Accuracy	Comments
Thickness	Airborne electromagnetic	Good	Presently not applicable over shallow or fresh water Cold conditions needed, problems with snow cover Indirect; requires highly developed interpretation algorithms
	Thermal infrared	Fair	
	SAR	Nominal	
Floe size	Visual satellite imagery	Good	Difficulties with closed winter pack ice
	SAR	Excellent	It is possible to discern multi-year floes
Ridges	Laser profilometer	Excellent	Measures sails only, keel properties obtained from a model
	Upward looking sonar	Good	Non-realtime, limited in space
	Submarine borne sonar	Good	Bad accessibility
	SAR	Fair	Spacings and directions; requires interpretation algorithms
Leads	AVHRR, microwave	Good	Coarse resolution
	SAR	Good	Difficulties in discerning smooth new ice from open water
Dynamics	Visual imagery	Fair	
	SAR	Good	

## 2.3. LEVEL ICE; ICE THICKNESS DISTRIBUTION

### 2.3.1. Maximum level ice thickness

The growth of undeformed ice is controlled by the air temperature  $T_a$  and the thickness of the snow cover  $h_s$ . If the thickness of the snow cover is assumed to be constant throughout the ice growth, then the ice thickness may be determined from the so called Zubov's equation (Nakawo and Sinha 1981),

$$L\rho_i \left( \frac{h_i^2}{2k_i} + \frac{h_s h_i}{k_s} \right) = \int_0^t (T_m - T_a) dt = DDF \quad (2.1)$$

where  $k_s$  and  $k_i$  are the thermal conductivities of snow and ice,  $\rho_i$  ice density,  $L$  the latent heat of infusion of ice and  $T_m$  the freezing temperature of sea water. Zubov (1945) derived an empirical version of equation (1) which is

$$h_i^2 + 50h_i - 8DDF = 0. \quad (2.2)$$

where  $h$  is in cm and  $DDF$  in °Cdays. Once the average temperature is known and  $DDF$  can be calculated, equation (2) can be used to obtain ice thicknesses if these are not measured directly. The other application of thermal growth equations is to the thickness of consolidated layer of ice ridges.

The ice which does not melt during the summer season becomes multi-year ice. There exists an equilibrium thickness for multi-year ice attained in the end of melting season. The equilibrium is reached when the growth during the winter season equals the melt during summer. It is dependent on the solar radiation, albedo of the snow surface, temperature, oceanic heat flux and snow thickness. For average values in the Polar Basin the equilibrium thickness is about 3 m (Maykut and Untersteiner 1971). The default value of level multi-year ice thickness may be taken to be this equilibrium thickness. This is also in a good agreement with the maximal ice thicknesses encountered along the NSR.

### 2.3.2. Level ice strength

The strength of level ice is mainly dependent on the temperature and salinity of ice, and of the strain rate. Other parameters like the crystal structure influence in practice the strength very little and moreover this influence disappears under the natural scatter (Cox et al. 1985, Timco and Frederking 1990). For practical purposes multi-year ice may be considered salt free and the salinity of first-year ice to be  $S_i=0.4\%$ . The strength parameters for level ice for practical applications are given in Table 2.5. These are needed later in the hull ice load formulations.

**Table 2.5.** Standard ice strength values.

Quantity	First-year ice, $S_i=0.4\%$		Multi-year ice	
	$T=-2^{\circ}\text{C}$	$T=-10^{\circ}\text{C}$	$T=-0^{\circ}\text{C}$	$T=-10^{\circ}\text{C}$
Compressive strength kPa	3000	6000	4000	9000
Bending strength kPa	300	600	800	1600

### 2.3.3. The statistics of level ice thickness

The variation of ice thickness is typically large. This variation derives from two sources. The ice cover is a mixture of ice types having different typical thicknesses: level ice, deformed ice and multiyear ice. In addition the thickness variation within each type can be large, especially for deformed ice. The thickness variation depends also on what is the reference of ice thickness. If the thickness is understood refer to a single point the variation is much larger than if thickness averages for, say, 1 sq. km. are considered, as the latter smooth out individual peaked formations.

The variation in ice thickness can be given in terms of an ice thickness distribution. Assume a region with total ice area  $A$  within the ice cover and with minimum, maximum and mean ice thicknesses  $h_{min}$ ,  $h_{max}$  and  $\bar{h}$  respectively. Let  $A(h,t)$  be the area of ice thicker than  $h$ . Then  $A(h,t)/A$  can be understood as decreasing cumulative distribution that decreases from unity at  $h=h_{min}$  to zero at  $h=h_{max}$ . The thickness distribution is defined as

$$f(h,t) = -\frac{d}{dh} \frac{A(h,t)}{A} \quad (2.3)$$

or 'relative area of ice with thickness  $h$ '. It can also be interpreted as the probability to find thickness  $h$  in a random measurement. The expectation of  $f(h,t)$  is  $\bar{h}$ . The thickness distribution can also be defined for each ice type separately.

It is possible to define an equation governing the time evolution of the thickness distribution (Thorndike et al. 1975) and connect it with ice dynamics. However, the status of thickness distribution theory is unsettled and the mean ice thicknesses reported in ice charts and ice codes cannot be usually taken to be mean values of a certain ice thickness distribution. This is mainly due to the difficulty of measuring ice thickness over large areas and in real time. No generally accepted statistical models have been found. What is known is that the tail of the distribution mirrors the exponentiality of ridge size distributions. Bovin et al. (1995, IWP 23) reports on Russian research on thickness distribution. Empirical fits, mainly due to Buzyev, have

been defined. Although difficult to justify physically these can be used to quantify the variance of ice thickness along NSR.

## 2.4 ICE FLOES

Consider a region with total ice area  $A$  within the ice cover and let  $a$  be ice floe area. Let  $A(a, t)$  be the area covered by floes with area larger or equal to  $a$ . Analogically to ice thickness the floe size distribution is defined as

$$f(a, t) = -\frac{d}{da} \frac{A(a, t)}{A} \quad (2.4)$$

or 'relative area covered by floes with size  $a$ '. There are two hypothesis on the possible form of the floe size distribution. The first is lognormal (Lensch 1989)

$$f(a, t) = \frac{1}{\ln \sigma \sqrt{2\pi}} \frac{1}{a} \exp \left\{ -\frac{1}{2} \left( \frac{\ln(a / \mu)}{\ln \sigma} \right)^2 \right\} \quad (2.5)$$

where  $\mu(t)$  is the geometric mean which is equal to areal median. This means that 50 % of the ice area consists of floes with area larger than  $\mu$  and another 50 % of floes smaller than  $\mu$ . The parameter  $\mu$  can thus be determined by finding a floe area  $\mu$  such that larger floes cover half of the total ice area, without bothering of the smaller floes that are often below resolution.  $\sigma(t)$  is the geometric standard deviation. The area weighted mean, as defined for a set of floe areas  $a_i$ , is

$$\bar{a} = \frac{\sum_i a_i^2}{\sum_i a_i} = \mu \exp \left\{ \frac{1}{2} \ln^2 \sigma \right\} \quad (2.6)$$

This is also the expectation of  $f(a, t)$ . From this equation (knowing  $\mu$ ) the parameter  $\sigma$  can be obtained. The area weighted mean is larger than the areal median and corresponds roughly to what is visually estimated to be a dominant floe size. Thus an ex tempore parameterisation of the model can be made by dividing the ice area into two halves, small and large floes, by a median value  $\mu$  and estimating typical large floe  $\bar{a}$ . The effect of subjective bias in this procedure should be studied in order to minimise the errors.

Another model for the floe size distribution is the power law (Matsushita 1985). Then the relative area of ice covered by floes larger than  $a$  obeys the dependence

$$A(a) \propto a^{-\rho} \quad (2.7)$$

The power law has a merit of simplicity and it is based on the observation of visual scale-similarity of floe sizes: images with different scales from the ice pack 'look the

same'. The area weighted mean, however, depends on the maximum allowed floe size. The parameter  $p$  is a measure of increase in detail with decreasing  $\alpha$ . There are indications that the applicability of power law is limited to smaller floe sizes (Lensu 1990).

A thumb rule for selecting the floe size distribution can thus be to apply the power law when the ice cover has clear self-similar appearance and lognormal when a dominant floe size can be discerned. If the ice cover has clear thickness categories (first-year and multi-year ice) the corresponding floe distributions can be treated independently.

## 2.5. ICE RIDGES

### 2.5.1 Ridging model

Ridging is quantified in terms of linear transects across the ridge field as no generally accepted two-dimensional description of ridged ice fields exists. This is satisfactory when modelling ice loads on ships traversing along straight track through an ice field. The basic quantification of ridging includes four components

- Ridge spacing distribution or ridge density
- Distribution of ridge size
- Model of sail and keel geometry
- Model of ridge sail and keel structure

The geometric model describes the profiles of the sail and keel (height and width and their variation along the ridge). The structural model describes the piece size and porosity of the block rubble in the ridge and the thickness of the consolidated layer which can then be related to the strength properties of the ridge. The structural and geometric models thus enable the calculation of ice loads pertaining to an encounter of a ridge of certain size. From the ridge size distribution the corresponding distribution of ice loads is obtained while the ridge density gives the frequency of their occurrence.

The following approach refers more to the statistical properties of ridge sails since most measurements or estimates on ridge size are based on surface observations only. As the majority of data on ridge sail distributions is obtained by laser profilometers that give the ice surface profile along linear track the approach is intended for the estimation of ridge sizes from such data.

### 2.5.2 Sail and keel geometry

The basic unit of a ridge field is called a ridge link (following Hibler et al 1972). Ridge links are defined as ridge segments of certain constant length  $L$  which are of the same order magnitude as typical ship breadth (Figure 2.6). They are convenient units of decomposing the ridge field; the total length of ridge sail per unit area is  $NL$  where  $N$  is the number of links per unit area.



The ridge model is shown in Figure 2.7. Considering sail only, the crest of the ridge link defines a longitudinal profile and the crest height is denoted by  $h$ . The average crest height of a single link is defined to be ridge link size  $s$ . The crest height has typically large variation with peaks and troughs: links can contain gaps where  $h=0$  and values of  $h>2s$  are often found (Figure 2.8). This variation is described by a crest height distribution  $k(h,s)$ . This can be interpreted to be the probability that a randomly chosen crest point has height  $h$  in a ridge link with size  $s$ . Such a random choice occurs, for example, when a profiling device measures a cross-sectional profile from which the highest point is determined. Thus  $s$  is the expectation of  $k(h,s)$

$$s = \int h k(h,s) dh$$

In addition the average thickness of the consolidated layer  $h_c$  and the cutoff value related to the measurement method  $h_0$  are defined.

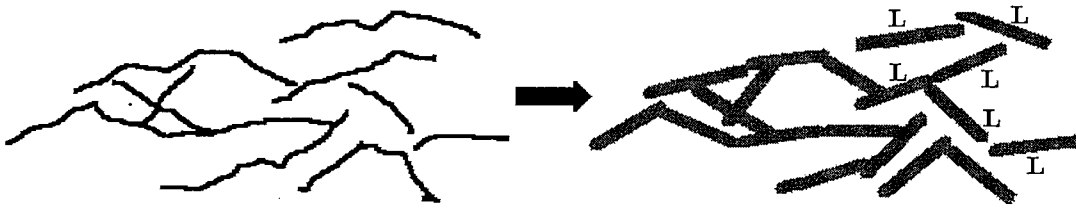


Figure 2.6. Decomposition of a ridge field into links.

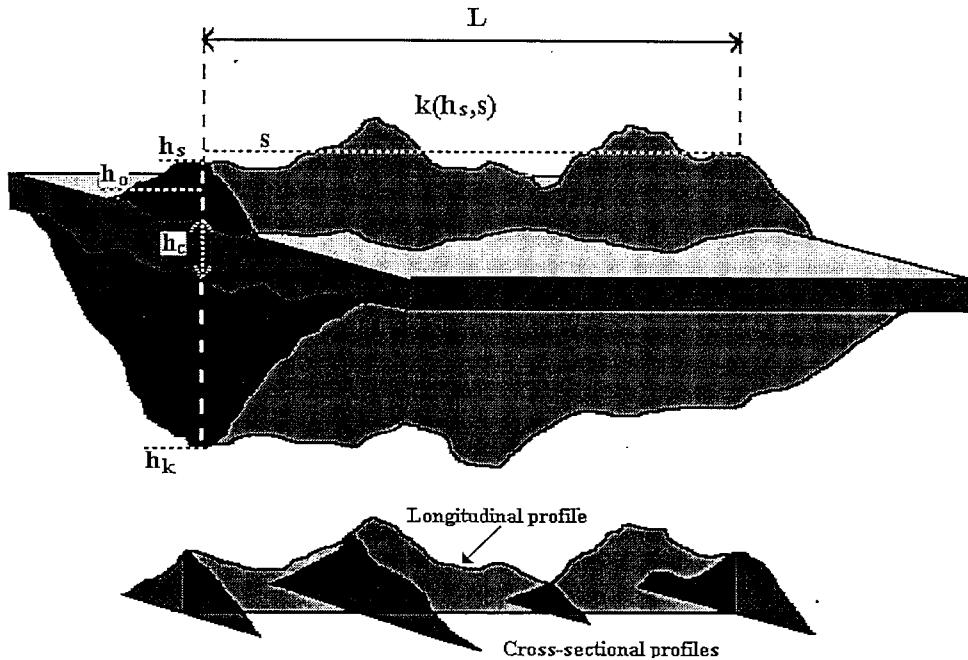
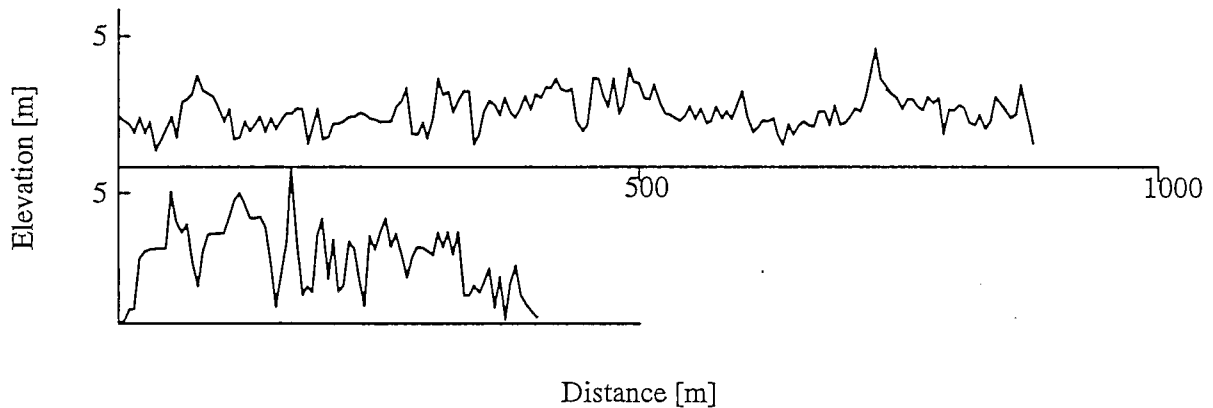


Figure 2.7 . Ridge model. See text for explanations.

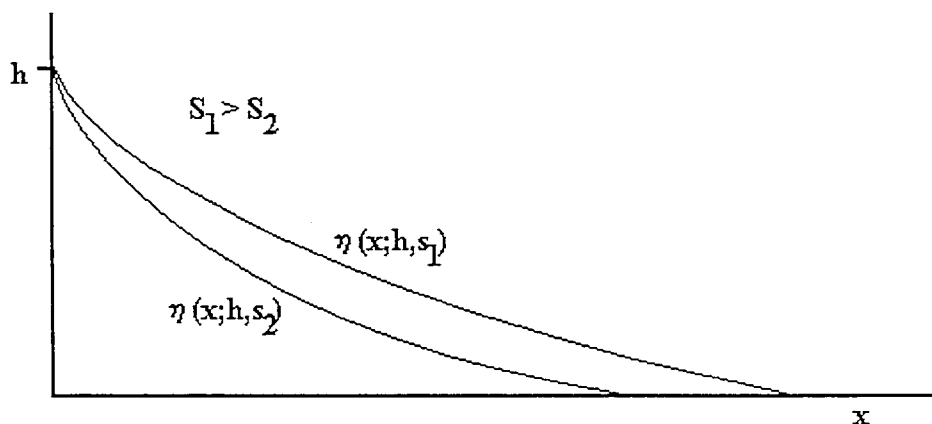


**Figure 2.8.** Longitudinal ridge profiles (from Hibler and Ackley 1975)

For the calculation of ridge link sail volume a model for the link sail shape is required. Instead of assuming a geometric model (a triangle, for example) the following method of obtaining the shape from measurement data is developed. The cross-sectional profile is understood as a statistical average and is given in terms of a cross-sectional shape function (see Figure 2.9)

$$\eta(x; h, s), \quad \eta(0; h, s) = h \quad (2.8)$$

That is, from all links with size  $s$  in a certain area find all locations with crest height  $h$  and determine the average of corresponding cross-sectional profiles.



**Figure 2.9.** Shape function

The dependence on  $s$  takes into account that a cross section with height  $h$  from a large ridge is usually broader than a cross-section with equal height from a smaller ridge.

The ridge link shape function is understood as the average cross sectional shape along the ridge link

$$\eta(x; s) = \int_0^{\infty} k(h, s) \eta(x; h, s) dh \quad (2.9)$$

The average volume of the link sail per unit length is

$$V_s(s) = 2 \int_0^{\infty} \eta(x; s) dx \quad (2.10)$$

The cross-sectional shape function can be obtained from measurements of cross-sectional profiles by a laser profilometer (Lensu 1995). Isostatic equilibrium can be assumed to hold over a typical ridge link length  $L$  so that the keel volume is obtained from the ice and water densities  $\rho_i$  and  $\rho_w$  as

$$V_k = V_s \frac{\rho_i}{\rho_w - \rho_i} \quad (2.11)$$

The keel dimensions are then obtained from a keel shape function, either available from submarine keel profile measurements or assumed. In a simplified model the keel is assumed to have a triangular profile with width/depth ratio from 4 to 5. As the sail slopes are usually steeper than keel slopes, the keel depth / sail height ratio is less than the isostatic volume ratio  $V_k/V_s$ , or typically from 5 to 6.

### 2.5.3 Sail and keel structure

The strength of a ridge is determined by the thickness of the consolidated layer and the cohesion of the unconsolidated ice block mass in the sail and keel. Both the rate of thickness increase of the consolidated layer and the cohesion of the block mass depend on the relative void content, or porosity, of the ridge. The porosity, or relative void content, is typically  $v=0.3$ . The thickness of consolidated layer increases as

$$h_c^2(t) = h_c^2(0) + \frac{1}{v} \alpha^2 S \quad (2.12)$$

where  $S$  is coldsum in degree days and the value of  $\alpha$  is about  $0.03 \text{ m}(\text{°C day})^{-1/2}$  (Leppäranta et al. 1995). Asymptotically the thickness of the consolidated layer is  $v^{-1/2}$  times the thickness of the surrounding undeformed ice. Thus the thickness of the consolidated layer can be assumed to equal the level ice thickness during the early freezing period and be about twice the level ice thickness during the late freezing period and melting period.

The Mohr-Coulomb failure criterion is generally used to describe the shear strength of ridge keel, and it is formulated as

$$\tau = \sigma_o \tan \phi + c \quad (2.13)$$

where  $\tau$  is the shear stress on the shear plane,  $\sigma_0$  is the normal stress,  $c$  is the cohesion, and  $\phi$  is the angle of internal friction. Field and model tests indicate that  $\tau$  has values ranging from 1 to 5 kPa, depending on the degree of cohesion (Leppäranta and Hakala 1992).

#### 2.5.4 Distribution of cross-sectional sail heights

The interpretation of data obtained from ridge fields is influenced by two measurement dependent parameters: the measurement footprint and cutoff height. Most surface data has been collected with laser profilometers that measure the distance between ice surface and an aircraft. The aircraft altitude variation has lower frequency than the surface elevation variation and it can be filtered out, leaving the surface profile. From the profiles ridges exceeding certain cutoff value  $h_0$  are identified; the reason is that below the cutoff the ridges cannot be discerned from other local maxima (protruding floes, rubble etc.)

The ridge height data obtained by a profilometer consists thus of cross-sectional heights  $h$ . According to the current understanding they are distributed according to the negative exponential distribution

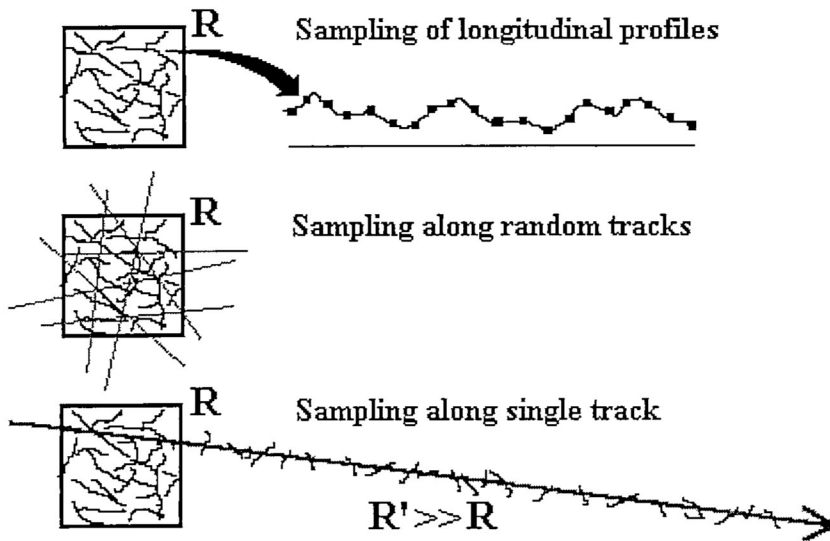
$$f(h) = \frac{1}{\bar{h} - h_0} \exp\left\{-\frac{h - h_0}{\bar{h} - h_0}\right\}. \quad (2.14)$$

The expectation is  $\bar{h}$  and the standard deviation  $\bar{h} - h_0$ . The exponentiality of cross-sectional height distributions has been well confirmed both in the Arctic and in the Baltic (see Lensu 1995b and references therein).

The primary interpretation of  $f(h)$  is as follows. Consider a region  $R$  and let  $l(h)$  be the length of ridge sail crest exceeding  $h$  in  $R$ . Then

$$f(h) = -\frac{1}{l(h_0)} \frac{\partial l(h)}{\partial h}. \quad (2.15)$$

If the ridge field is homogenous (no preferred orientations) there are three possible methods of determining  $f(h)$  (Figure 2.10). First strategy is the measure a sufficient number of longitudinal sail profiles in  $R$  with sufficiently densely spaced measurements. For another possibility consider a track crossing the region  $R$  and count the cross-sectional heights along this track. If the orientation and location of this track is varied randomly a large number of such tracks will sample reliably the distribution  $f(h)$ . However, if the ridge field is homogenous over a larger region  $R'$  this is equivalent to sampling along a linear track across  $R'$  (by a profilometer, for example) if the track is sufficiently long.



**Figure 2.10.** Strategies of determining the distribution of cross-sectional heights for a homogenous ridge field.

### 2.5.5 Distribution of ridge link sizes

To obtain the distribution of ridge link sizes from the distribution of cross-sectional heights two tasks must be accomplished:

- Extrapolate the distribution  $f(h)$  to values below  $h_0$
- Derive data on the crest height distributions  $k(h, s)$  within a ridge link.

Field observations indicate that the distribution  $k(h, s)$  is defined for all values  $h > 0$  and therefore  $f(h)$  is, too (Lensu 1995b). Thus the ridge link size distribution  $g(s)$  is obtained by inverting the integral

$$f(h) = \int_0^{\infty} g(s) k(h, s) ds. \quad (2.16)$$

Measurements of  $k(h, s)$  from the Baltic indicate that it follows Rayleigh distribution (Lensu 1995b)

$$k(h, s) = \frac{\pi h}{2s^2} \exp\left\{-\frac{\pi}{4s^2} h^2\right\}. \quad (2.17)$$

Then if the exponentiality of (2.14) extrapolates down to zero, the ridge size distribution is

$$g(s) = \frac{2}{\pi \bar{s}} \exp \left\{ -\frac{1}{\pi} \left( \frac{s}{\bar{s}} \right)^2 \right\}, \quad (2.18)$$

(Lensu 1995b). The mean value is  $\bar{s}$  which, by (2.16), is equal to  $\bar{h}$  when  $h_o=0$ . This distribution was first proposed by Hibler et al. (1972) who also derived it from a general statistical argument by assuming that all arrangements of ridge sizes are equally probable as long as the total amount of deformed ice remains the same.

The ridge link size distribution  $g(s)$  (2.18) is defined for all nonnegative  $s$ . However, it is reasonable to assume that the link size has a certain physically based minimum  $s_o$  that is related to the thickness of parent ice from which the blocks in the ridge are formed. Repeating Hibler's the argument, the link size distribution is then

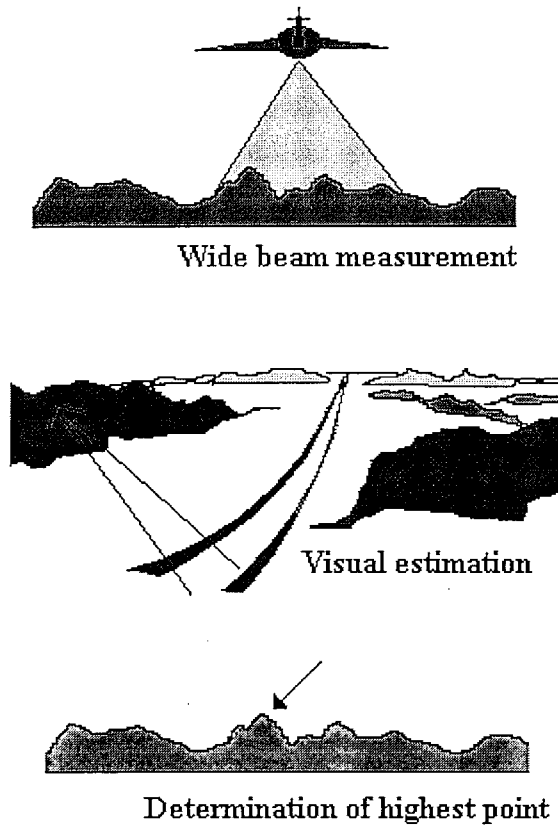
$$g(s) = \frac{2}{\pi (\bar{s} - s_o)} \exp \left\{ -\frac{1}{\pi} \left( \frac{s - s_o}{\bar{s} - s_o} \right)^2 \right\}, \quad s \geq s_o \quad (2.19)$$

The mean value is  $\bar{s}$  which, likewise, is equal to  $\bar{h}$  when  $h_o=0$ . Thus, as no data on  $f(h)$  for very small values of  $h$  exists, it is assumed that the ridge size distribution  $g(s)$  has the form (2.19) and (2.16) is used to obtain the distribution of cross-sectional heights  $f(h)$ .

The ridge link size distribution can be assumed to apply if (Figure 2.11)

- ridge sails are measured by a wide beam instrument recording an extended segment of the sail,
- ridge sizes are estimated visually, or
- the highest peaks of ridges are measured or estimated.

The third possibility follows since the expected highest point of a ridge link is linearly dependent on the ridge size (by 2.16). The numerical value of this factor, however, is not too well known. A theoretical estimate is derived in Section 2.5.8.



**Figure 2.11.** Direct measurements related to ridge link size.

### 2.5.6 Distribution of ridge spacings

Two distribution models have been proposed for ridge spacing along a straight track. One is negative exponential distribution with expectation  $\bar{x}$  (Mock et al. 1972).

$$f_1(x) = \frac{1}{\bar{x}} \exp\left\{-\frac{x}{\bar{x}}\right\}. \quad (2.20)$$

The standard deviation is likewise  $\bar{x}$  and the number of ridges per unit length is  $1/\bar{x}$ . This distribution follows if the formation of new ridges constitutes a spatial Poisson process. Although this assumption of the generative process has a merit of simplicity, the ridge spacing has been in most cases found to obey better a lognormal distribution (Wadhams and Davy 1978)

$$f_2(x) = \frac{1}{\ln \sigma \sqrt{2\pi}} \frac{1}{x} \exp\left\{-\frac{1}{2} \left(\frac{\ln(x/\mu)}{\ln \sigma}\right)^2\right\}. \quad (2.21)$$

This distribution applies if  $\ln(x)$  is normally distributed with expectation  $\ln(\mu)$  and standard deviation  $\ln(\sigma)$ . The parameters  $\mu$  and  $\sigma$  are the geometric mean and

geometric standard deviation of the spacing distribution. In terms of these the other relevant parameters are

$$\text{Expectation } \mu \exp\left(\frac{1}{2} \ln^2 \sigma\right) = \bar{x}$$

$$\text{Variance } \mu^2 \exp(\ln^2 \sigma) (\exp(\ln^2 \sigma) - 1) = \text{VAR}(X) = \text{STD}(X)^2$$

$$\text{Median } \mu$$

$$\text{Length median } \mu \exp(\ln^2 \sigma) = \text{LMED}(X)$$

The length median is defined as such spacing length that spacings exceeding it cover half of the total track length. The following relationships are found

$$\frac{\bar{x}}{\mu} = \sqrt{\left(\frac{\text{STD}}{\bar{x}}\right)^2 + 1} = \sqrt{\frac{\text{LMED}}{\mu}} = \frac{\text{LMED}}{\bar{x}} \quad (2.22)$$

As the standard deviation is usually larger than the expectation for ridge spacing distributions, it follows that the median of the distribution is considerably smaller than the mean spacing and the length median considerably larger than it. This is the main difference to the negative exponential distribution the median of which is  $\sim 0.7\bar{x}$ . It is seen that if the median/mean ratio decreases the (length median)/mean ratio increases.

Typical values of  $\bar{x}/\mu$  for the Baltic Sea are from 3-10 and typical medians 20-100 m. It follows that a ship with a typical length of 100 m frequently encounters several ridges at the same time and that the basic unit for estimating ridge loads is rather a group, or cluster, of several ridges (Lensu 1995). A thumb rule in the Baltic is that if the number of encounters with a single ridge is  $N$  then the number of encounters with two ridges at the same time is  $N/2$ , with three ridges  $N/4$  and with  $k$  ridges  $N/2^{k-1}$  where the maximum value of  $k$  is about 10 (Lensu 1995). Typical length median in the Baltic is 1-2 km.

The parameters of the lognormal spacing distribution can be estimated if, in addition to the ridge density, either the median or length median is available. Other possibilities exist; analogically to the case of floe sizes (section 2.4) the length weighted mean, defined analogically to (6), is of the order of typical longer spacing, defined by subjective estimation. This relationship, however, should be studied experimentally in order to find out the optimal way to parameterise a ridge field from few visual observations.

### 2.5.7 Extrapolation of ridge density

The ridge densities or ridge spacing distributions are usually based data sets with a cutoff height  $h_o$  and measured along a straight track. Thus

$$\bar{x} = \bar{x}(h_o) \quad (2.23)$$



These data sets consist of cross-sectional heights sampled from ridge links. However, ridge spacings are meaningfully defined for ridge links only. If the track crosses a link above a trough with zero sail elevation the ridge appears not to exist although this is clearly not the case. Since shallow sail segments are expected to be most numerous the measured ridge densities are considerably smaller than what actually exists. Also very large ridge links have a nonzero probability to be left out from the spacing distribution because they can contain sail segments below the cutoff height. This probability for a ridge link size  $s$  is given by

$$\int_0^{h_0} k(h; s) dh \quad (2.24)$$

It is evident that the exponential cross-sectional height distribution (2.14) can to some extent be extrapolated downwards. However, extrapolation to zero raises the ridge densities to unrealistic values. On the other hand, field observations of individual ridges show that of distribution  $k(h, s)$  extends down to zero and so does  $f(h)$ , as defined by integral (2.16). This supports the form (2.19) for the ridge size distribution  $g(s)$  with  $s_0 > 0$  since assuming  $s_0 = 0$  would produce the exponential  $f(h)$  down to zero. The distribution of cross-sectional heights is thus

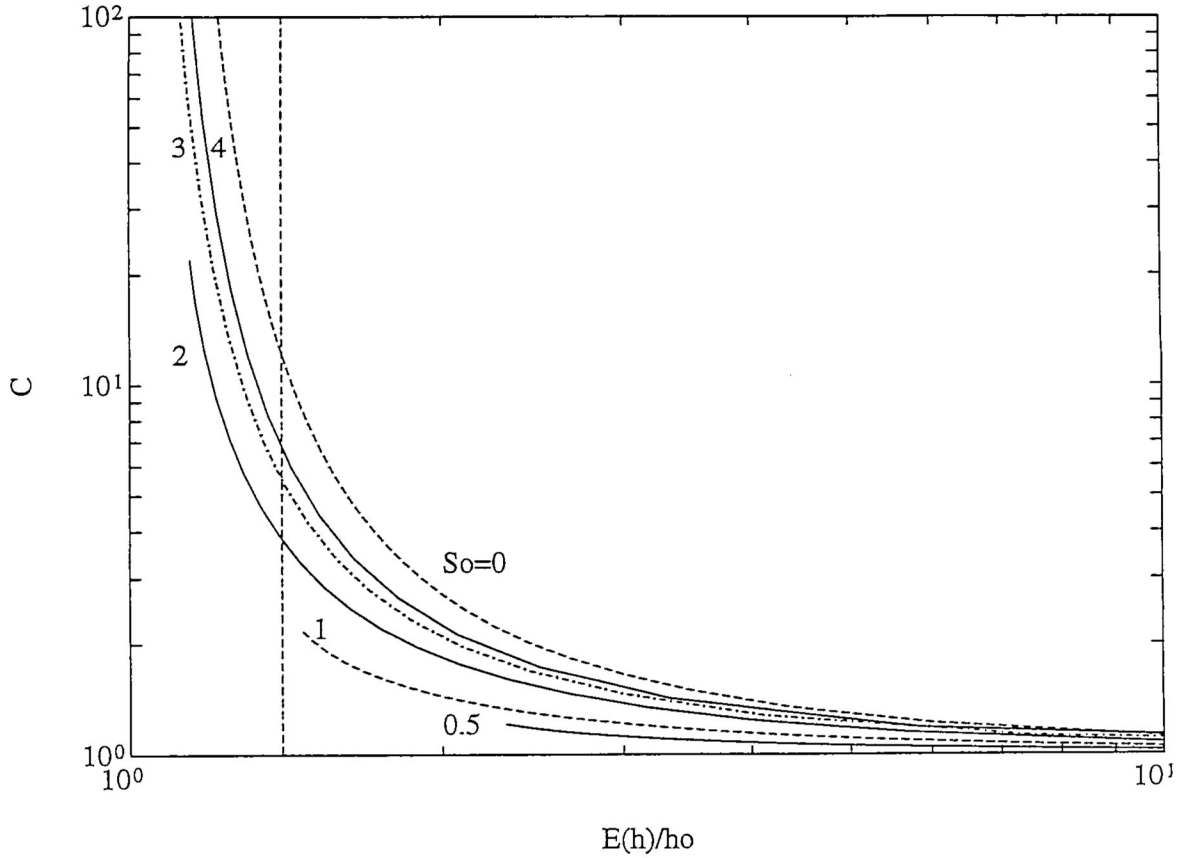
$$f(h) = \int_{s_0}^{\infty} \frac{2}{\pi (\bar{s} - s_0)} \exp \left\{ -\frac{1}{\pi} \left( \frac{s - s_0}{\bar{s} - s_0} \right)^2 \right\} k(h, s) ds \quad (2.25)$$

The integral (2.25) with  $k(h, s)$  given in (2.17) can be solved numerically for  $f(h)$ . The solution is asymptotically exponential while the relative amount of shallow ridges is smaller than that calculated from the exponential  $f(h)$ .

The ridge density is obtained from the measured mean ridge spacing as

$$D = C(s_0, h_0, \bar{h}) \frac{1}{\bar{x}(h_0)} \quad (2.26)$$

where the factor  $C$  is a function of ratios  $h_0/s_0$  and  $\bar{h}/h_0$ . However, little is known what the value  $s_0$  should be. A possible choice is to assume that  $s_0$  equals block thickness in the ridge so that in the ridge sail would consist at least of one layer of blocks in the average. The factor  $C$  is given in Figure 2.12 for different ratios  $h_0/s_0$  and  $\bar{h}/h_0$ .



**Figure 2.12.** The ridge density extrapolation factor  $C$  for different values of ratio  $h_o/s_o$ . The vertical line corresponds to the value  $\bar{h}/h_o=1.4$ , a value typical for ridge sail measurements in the Baltic.

### 2.5.8 Extremal statistics

It is desirable to have probabilities of the occurrence of very large ridges to be used in transit analyses. For a random sample of  $n$  cross sectional ridge heights the maximum ridge height  $h_{\max}$  in the sample has the cumulative distribution

$$F_n(h_{\max}) = \{F(h_{\max})\}^n, \quad (2.27)$$

where  $F(h)$  is the cumulative distribution of  $f(h)$ , (2.14). The sample consists usually of  $n$  ridges on a track segment. The distribution is asymptotically ( $n \rightarrow \infty$ ) of the Gumbel I double exponential type (Ang and Tang 1984)

$$F_n(h_{\max}) = \exp\{-n \exp\{(h_{\max} - h_o)/(\bar{h} - h_o)\}\} \quad (2.28)$$

and the expected maximum for  $n$  ridges exceeding the cutoff  $h_o$  is

$$EXP(F_n^{\alpha}) = h_o + (\bar{h} - h_o)(\ln n + \gamma) = h_o + (\bar{h} - h_o)(\ln ld + \gamma) \quad (2.29)$$

where  $l$  is traversed distance, ridge density (number of ridges per km) and  $\gamma$  Euler's constant ( $\sim 0.58$ ).

As explained in section (2.5.4) the distribution  $f(h)$  can also be interpreted to refer to all ridges within in a certain area. The number  $n$  in the sampling can be related with the area  $A$  as follows. Consider a ridge sail segment containing the highest ridge sail point of a certain area. The sail height variation has two components: primary, following from the elevation of blocks, and secondary, following from the slopes of the blocks. The latter is superposed on the first and is not considered to truly belong to the height variation. Therefore the longitudinal ridge sail profile can be idealised as a step curve by replacing the upper surface of each tilted block in the crest by a horizontal line with the same mean elevation. The average step length is the scale in which the sail height is meaningful to resolve longitudinally, and for random arrangement of block angles is  $\Delta l = (2/\pi)(\kappa+1)b$  where  $b$  is block thickness and  $\kappa$  average block diameter/thickness ratio. Thus for a random arrangement of ridge directions

$$n \approx 1000 \frac{\pi}{2} \frac{d A}{\Delta l} = 1000 \frac{\pi^2}{4} \frac{d A}{b(\kappa+1)} \quad (2.30)$$

where  $b$  is in meters,  $d$  ridges/km and  $A$  in  $\text{km}^2$ . Using this value for  $n$  an estimate for the highest ridge sail point within  $A$  is obtained. In the Baltic the calculated maximum sail heights are in a good agreement with observations also in basinwide scale.

The estimate (2.30) can also be used for the expected highest point of a ridge link with length  $L$ . For the Rayleigh distribution (2.19) the distribution of maximum values in samples of  $n$  values is likewise of double exponential type and with the expected value

$$EXP(K_n^{as}) = s \frac{1}{\sqrt{\pi}} \left( 2\sqrt{\ln n} + \frac{\gamma}{\sqrt{\ln n}} \right) \quad (2.31)$$

where  $s$  is ridge link size and  $\gamma$  Euler's constant ( $\sim 0.58$ ) (Ang and Tang 1984). Here

$$n \approx \frac{\pi}{2} \frac{L}{b(\kappa+1)}. \quad (2.32)$$

This estimate is in a good agreement with observations from the Baltic.

For ridge link size the asymptotic distribution of the extremes can be derived easily by noting that (2.19) is the restriction of normal distribution to values  $s > s_0$ . Consider  $n$  ridges the size of which is distributed according to (2.19). Modifying the results from Ang and Tang (1984) the asymptotic distribution is

$$G_n^{as}(s_{\max}) = \exp\{-\exp\{-\alpha_n(s_{\max} - u_n)\}\} \quad (2.33)$$

where

$$\alpha_n = \sqrt{\frac{2}{\pi}} \frac{1}{\bar{s} - s_o} \sqrt{2 \ln n}$$

$$u_n = s_o + \sqrt{\frac{\pi}{2}} (\bar{s} - s_o) \left( \sqrt{2 \ln n} - \frac{\ln \ln n + \ln 4\pi}{2\sqrt{2 \ln n}} + \frac{\ln 2 - \ln C_o}{\sqrt{2 \ln n}} \right) \quad (2.34)$$

The expected value is

$$EXP(G_n^w) = u_n + \frac{0.577}{\alpha_n} = s_o + \frac{\sqrt{\pi}}{2} \frac{(\bar{s} - s_o)}{\sqrt{\ln n}} \left( \ln \frac{n^2}{C_o \sqrt{\pi \ln n}} + 0.577 \right) \quad (2.35)$$

For a certain area  $A$  the value  $n$  is estimated as

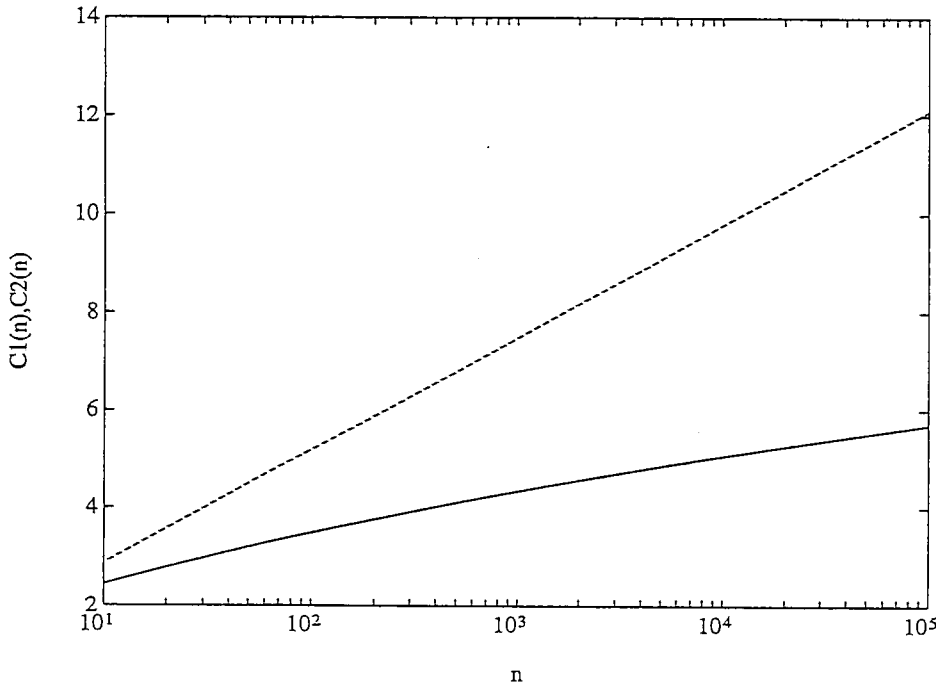
$$n \approx 1000 \frac{\pi}{2} \frac{dA}{L} \quad (2.36)$$

where  $L$  is the length of ridge links. The expected maximal size of ridge links increases with  $n$  much slower than the expected maximal cross-sectional height. Writing (2.29) and (2.35) as

$$EXP(F_n^w) = h_0 + (\bar{h} - h_0) C_1(n)$$

$$EXP(G_n^w) = s_o + (\bar{s} - s_o) C_2(n) \quad (2.37)$$

the factors  $C_1$  and  $C_2$  are given in Figure 2.13 for values of  $n$  less than 100 000.



**Figure 2.13.** The factors for estimating extremal ridge heights

## 2.6. LEADS

While floe size and ridges reflect the history of the stresses experienced by the ice cover and are not expected to change during short time periods leads are transient features reflecting the instantaneous and local state of strain and persist typically at most few days. Power law has been found to apply to lead width (Wadhams 1992),

$$P(w) \propto w^{-\rho} \quad (2.38)$$

where  $P(w)$  is the probability that the lead along a linear track is wider than  $w$ . For leads wider than 100 m values around 1.5 for  $\rho$  have been found. Typically leads (minimum width 1 m) occupy 1-5% of the area of the Arctic ice cover in winter so that the ice concentration is seldom 100%. Leads and ridges tend to occur together; it has been found that lead frequency is high in heavily ridged areas of the Arctic (Wadhams 1981, 1990a).

## 2.7. DYNAMICS

For navigational purposes the most important dynamic characteristics of the ice cover is whether the ice is diverging or converging. Divergence creates leads and relieves ice pressure, facilitating navigation. Convergence closes leads and channels and can create hazardously high pressures against the ship's hull. The areas of convergence and ice pressure are typically elongated features and could be described similarly to leads, but this possibility has not been seized yet.

The values of pressure within an ice sheet is reported to be typically 10-80 kN/m (Coon et al. 1977, Doronin and Kheisin 1977). The pressure in an ice sheet seems to increase the ice resistance of ships navigating independently and is a very dominating factor when ships are proceeding behind an icebreaker. Also the loads on ship sides are high if the ship is stuck. The limit value of ice pressure within the ice pack is given by the force required to initiate ridging of ice. These values are usually less than compressive or buckling strength of ice, about 100 kN/m even for multi-year ice (Parmerter and Coon 1973). Much higher loads can be experienced by a ship in a closing lead or channel.

The dynamic ice models predict the ice motion in typical scale of 100 km. However, the stresses and strains of the model scale are not mirrored in the local scale of ship/ice interaction. Rather in the model cell of 100x100 km can be found a velocity distribution and distribution of local areas of convergence and divergence. This kind of data can be obtained, for example, from SAR images but has thus far not been incorporated to operative descriptions of ice conditions. The main reason is that the relations between ice model scale phenomena and local scale phenomena are not well known. As these become better established the incorporation of the small scale variation in the dynamical state to the ice cover parameterisation becomes feasible.

### 3. ICE CONDITIONS ALONG THE NORTHERN SEA ROUTE

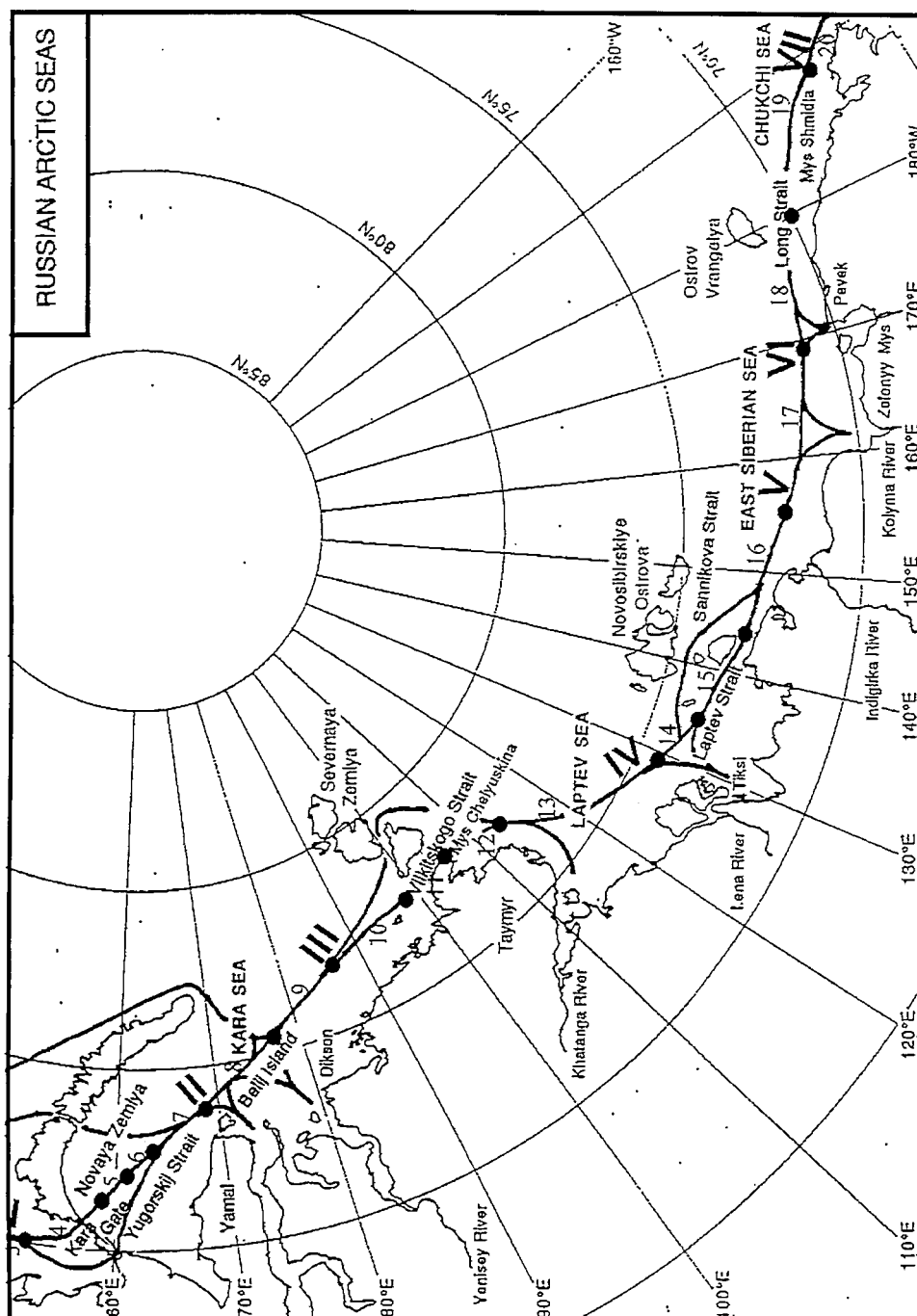
#### 3.1. GEOGRAPHY OF THE AREA

The North East Passage is a historical and geographical term for the sea route joining the Atlantic Ocean and Pacific Ocean through the Siberian coastal sea areas. The Northern Sea Route, NSR, is a Russian administrative term for a part of the route between Novaya Zemlja and the Bering Strait. The area along the route which is ice bound during the winter extends from the island of Kolguev in the west to about latitude 58° in the Bering strait and has the total length of 3200 nautical miles.

The NSR is shown in Figure 3.1 with subdivision into seven segments. The segments are given in Table 3.1. The segments may be further subdivided into 20 segments which are used when more specific ice information is available.

**Table 3.1.** The subdivision of the NSR.

Segment number	Route subdivision	Segment name	End point in west End point in east	Length [nm]	Total Length [nm]
I	1-4	Pechora Sea	Kolguev Island Yugorskij Strait, West	180	180
	4	Yugorskij Strait		30	210
II	4-7	Kara Sea, West	Yugorskij Strait, East Belij Island	320	530
III	8-10	Kara Sea, East	Belij Island Vilkitskovo Strait, West	540	1070
	11-12	Vilkitskovo Strait		90	1160
IV	12-15	Laptev Sea	Vilkitskovo Strait, East Sannikova Strait, West	580	1740
	15	Sannikova Strait		80	1820
V	16-17	East Siberian Sea, West	Sannikova Strait, East Kolyma River	440	2260
VI	17-18	East Siberian Sea, East	Kolyma River Long strait, West	310	2570
	18-19	Long Strait		100	2670
VII	19-20	Chuckhi Sea	Long strait, East Bering Strait, West	390	3060
	20	Bering Strait		140	3200



**Figure 3.1 .** The NSR and its subdivision.

The shipping routes presented in Fig. 3.1 go mainly through the straits mentioned in Table 3.2. even though some alternative routes exist as indicated in Figure 3.1. The ice conditions, especially concerning ice ridges, can be more severe in the straits than in the more open sea areas. The main ports along the NSR are listed in Table 3.2.

**Table 3.2.** Main ports along the NSR.

Port	Geographical area	Location	Depth [m]
Murmansk	Kola Peninsula	68° N 38° E	12
Archangelsk	White Sea	65° N 40° E	8
Narjan Mar	Pechora Sea	68° N 53° E	5
Novyy Port	Ob Bay	67° N 72° E	6
Dikson	Yenisey Bay	71° N 80° E	9
Tiksi	East of Lena River	72° N 129° E	7
Pevek	Chaunskaya Bay	70° N 170° E	13

### 3.2. HYDROGRAPHIC CONDITIONS

The Russian arctic seas are very shallow as shown in Figure 3.2. This applies especially to the Pechora, Laptev and East Siberian seas. The shallowness influences currents and ice types. Frequently occurring features in the shallow sea areas is stamukhas or grounded ridges the ice volume of which the pileup due to the subsequent ice movement may have increased. A stamukha zone exists in front of a shallow coast line when the currents are towards the shore. The stamukhas appear usually around the 20 m isopleth.

The winds and currents cause convergence in the ice field resulting into ice ridge formation and ship loads due to compression. The currents in the Russian Arctic are mainly weak with speeds below 0.25 m/s; the main currents are shown in Figure 3.3. In the straits the currents may be more rapid and they run from west to east with the exception of Litke current trough the Kara Gate. Tidal variation is also small, typically 0.5-1 m, except in the bays (maximum tide is 7 m in the White Sea). However, in shallow sea areas the tidal currents may be of the order of 0.2 m/s.



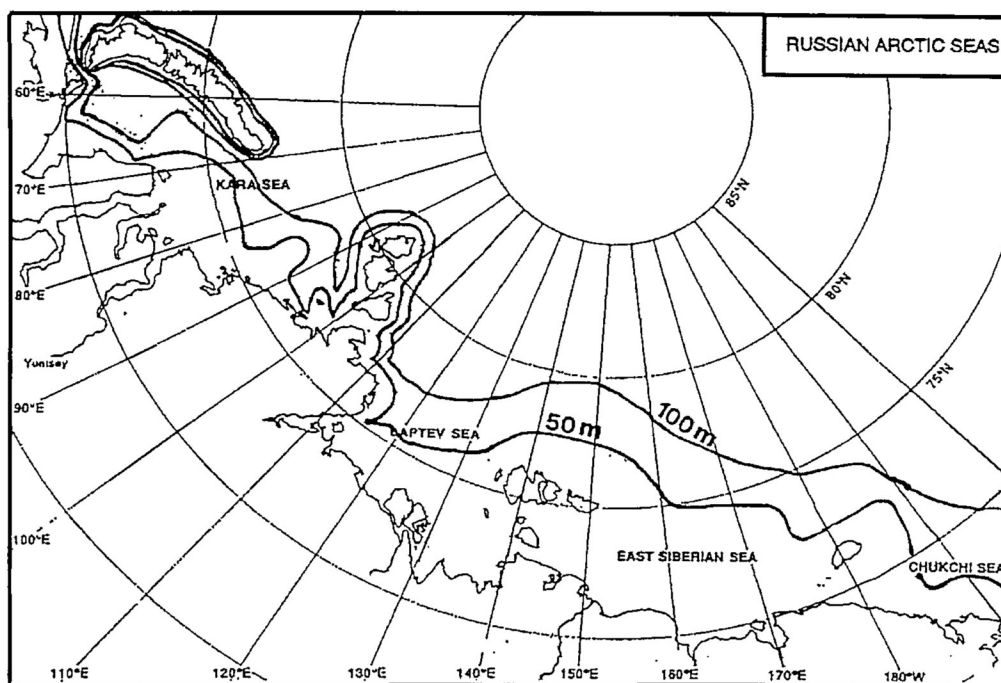


Figure 3.2. Isopleths of the Siberian seas.

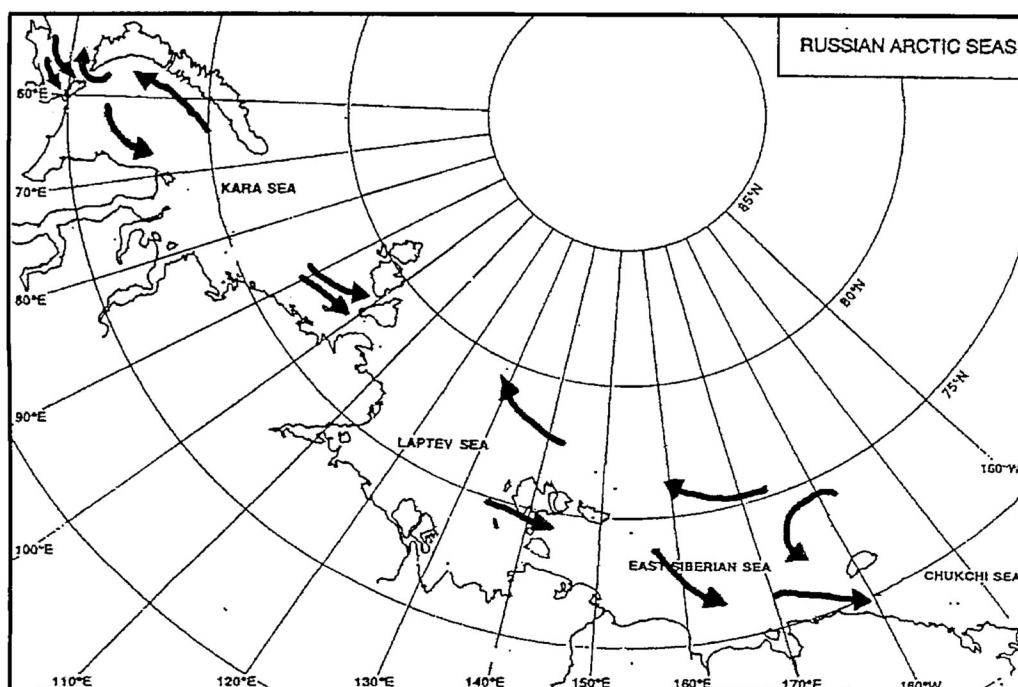


Figure 3.3. Main currents of the Siberian seas.

Winds are more important driving forces of the ice motion and dominate the short term ice motion. The prevailing strong winds are southerly during winter and northerly during summer (Table 3.3). The most common winds are also strongest. The general effect of winds along the NSR is to force ice into the straits from the sea on the western side of the strait.

**Table 3.3.** Distribution of wind directions along the NSR.

	Belij Island				Tiksi				Ambartsik (Pevek)			
	Jan	Apr	Jul	Oct	Jan	Apr	Jul	Oct	Jan	Apr	Jul	Oct
Direction	S	SE	NE	NE	SW	SW	NE	SW	SW	SW	NE	SW
Probability	28	15	23	16	38	18	30	30	51	25	31	34
Probability of > 16 m/s	4	3	0	4	8	2	0	3	10	2	0	3

### 3.3. THE SELECTED PARAMETERISATION

The selected parameterisation of ice conditions is explained in Table 3.4. Data on three kinds of ice conditions are included as far as it has been available, that is, the average, severe and mild ice conditions. Roughly, one year out of ten is very mild and then it is possible to navigate the entire route in open water during late summer. Two out of every ten years are severe, whereas the remaining seven have average or moderate ice conditions (Sackinger 1992)

More detailed interannual variation of ice concentration can be found in Appendix 2. In the annual cycle three rough phases can be defined. The freezing phase begins in September-October and lasts until May when the maximum ice thicknesses are attained. The thawing phase when the ice cover melts and decays but the concentrations are still high lasts from May to July. The ice flow phase from June to September-October is characterized by low concentrations and dispersed ice fields.

**Table 3.4.** The selected parameterisation.

Parameter		Unit	Explanations and references
Coldsum	Average	°Cday	Average cold sum of nearest coastal weather station
concentration	Aver. First-year	1/10	Concentration of first-year ice in average ice conditions
	Aver. Multi-year	1/10	Concentration of multi-year ice in average ice conditions
	Minimum	1/10	Concentration when ice conditions are mild
	Maximum	1/10	Concentration when ice conditions are severe
Level ice thickness	Maximum	cm	Thickness calculated from the coldsum assuming severe conditions

Ice thickness	Average	cm	Ice thickness, average ice conditions, April and September (Romanov 1993)
	Minimum	cm	Ice thickness, mild ice conditions, April and September (Romanov 1993)
	Maximum	cm	Ice thickness, severe ice conditions, April and September (Romanov 1993)
Pressure		0, 1 or 2	Estimate based on prevailing wind and current directions
Floe size	Average	m	Typical floe size in average ice conditions (Romanov 1993)
Ridge size	Average	cm	Mean ridge size in average ridging conditions (Romanov 1993)
	Maximum	cm	Mean ridge size in severe ridging conditions (Romanov 1993)
Max. ridge size	obs/estimated	m	Maximum ridge size given by Romanov (1993) and calculated by (2.33)
Ridge density	aver/min/max	1/km	Ridge density in average/mild/severe ridging conditions (Romanov 1993)

#### Explanations:

*The data.* The data has been collected from available sources and comprises that given in Riska and Salmela (1994) but updated and extended with additional sources. However, relevant data on NSR ice conditions stored in Russia, especially in AARI, vastly exceeds the coverage of the data used in this report. It includes, for example, 13000 measurements on ice thickness during 1937-1991, data on lead sizes and directions, on fast ice and flaw lead positions, and on floe size distributions together with along route databases on relevant ice characteristics. This data will be later at least partially available, see Baskin et al. (1995 IWP 26) for the contents and Bretskin et al. (1995) for the availability of the data, and Vefnsmo and Løvås (1994, IWP 35) for the implementation of the data into the INSROP information system.

*Cold sums.* The temperature data is from monthly overviews from five weather stations located along the NSR. The data is from the period 1967-1981. The temperature distributions are given in Appendix 1. The other source for temperature data is Arctic Ocean Atlas (1980). The coldsums are calculated starting from the date when first ice starts to form, which information is obtained from the Arctic pilots (Department of the Navy 1970)

*Concentration.* The ice concentration values are based on satellite observations, mainly NOAA, and on the Russian atlas (Arctic Ocean Atlas 1980). The detailed concentration statistics given in Appendix 2 are modified from Courseaux and Kerebel (1992) which data is based on satellite images.

*Level ice thickness.* The level ice thicknesses are calculated from the coldsums by (2.2) adjusted so that the maximum level ice thicknesses reported in Romanov (1991) are obtained correctly.

*Ice thickness.* This is understood to contain deformed ice types also. The values are from the morphological ice atlas of Romanov (1993).

*Pressure.* The pressure index is defined as follows:

- 0 winds and currents are away from the shoreline and the ice field diverges
- 1 either wind or current but not both is towards the shoreline
- 2 both wind and current are towards the shoreline

This index is not to be confused with the Russian gradation of ice pressure ('balls').

*Floes.* The floe sizes are diameters in a dominant floe category. Visually estimated floe areas are usually of the order of area weighted mean area (2.6) from which the other parameters can be estimated.

*Ridges.* It is not usually apparent from sources reporting sail heights and spacings what formations are counted as ridges and how is their height defined. Since most data from the Russian Arctic is from ice observations made in the field and from ships, it is assumed that the reference is to ridge links and the height values are mean sail heights or ridge sizes defined in Section 2.5. Thus the sizes are assumed to be distributed according to (2.19) in which case the expected maximum ridge size is given by (2.33). Not cutoff height is assumed. The ridge densities are assumed to be based on visual observations so that no extrapolation of ridge density is needed.

The ridge heights may be thought to apply throughout the season.

*Multi-year ice.* The partial concentrations of multi-year ice have been derived from above sources. This data is very summarising.

### 3.4. THE ICE DATA MATRICES

#### 3.4.1. Area I, Pechora sea

Long term measurements between 1882 and 1934 from Pechora Bay support the thickness value in Table 3.5 (mild winter 0.9 m, severe winter 1.15 m, Iurev 1935)

**Table 3.5.** The ice conditions in the Pechora Sea (Area I)

		I	II	III	IV	V	VI	VII	VIII	IX	X	XI	XII
Coldsum		1030	1500	2000	2270	2360	-	-	-	-	10	220	650
concentration	Aver. First-year					6	3	1	0	0	0	-	-
	Aver. Multi-year	0	0	0	0	0	0	0	0	0	0	0	0
	Minimum					0	0	0	0	0	0		
	Maximum					9	5	1	0	0	0		

Level ice thick.	Maximum	70	90	110	120	120	80	40	0	0	0	30	50
Ice thickness	Average				70					0			
	Minimum				0					0			
	Maximum				120					70			
Pressure		2	1	0	1	1	1	0	-	-	-	0	2
Floe size	Average				500								
Ridge size	Average				100								
	Maximum												
Max. ridge size	Estimated												
Ridge density	aver./min./max												

### 3.4.2 Area II, Western Kara Sea

The main reasons to divide Kara Sea into two parts is the possibility to encounter multi-year ice in the eastern Kara Sea and the strong temperature difference. The freeze-up data for the Western Kara Sea is mid-October. The multi-year coverages are from Anderson et al (1985) and Anderson (1987); these values appear high but no other data is available. The incursion of multi-year ice in summer is possible by the southwesterly current along the eastern coast of Novaya Zemlja (Naval Oceanography Command 1986, Sanderson 1988)

**Table 3.6.** Ice conditions in the Western Kara Sea.

		I	II	III	IV	V	VI	VII	VIII	IX	X	XI	XII
Coldsum		1450	2010	2690	3110	3320	-	-	-	-	60	360	830
concentration	Aver. First-year	10	10	9	8	5	7	4	1	0	1	8	10
	Aver. Multi-year	0	0	1	1	4	1	0	0	0	1	0	0
	Minimum					5	2	1	0	0	0		
	Maximum					10	10	7	3	2	2		
Level ice thick.	Maximum	90	110	130	140	150	120	90	60	30	10	40	60
Ice thickness	Average				100					30			
	Minimum				30					0			
	Maximum				180					70			
Pressure		0	0	0	0	1	2	2	2	1	1	1	0
Floe size	Average				500								
Ridge size	Average				125								
	Maximum				250								
Max. ridge size	Obs./estimated				5/4								
Ridge density	aver./min./max				2/0/3								

### 3.4.3 Area III, Eastern Kara Sea

The freeze-up date for the eastern Kara Sea is taken to be beginning of the October. The information about multi-year ice is scarce. A journey report gives a multi-year ice thickness of 3-4 m (Judge 1958).

**Table 3.7.** Ice conditions in the Eastern Kara Sea

		I	II	III	IV	V	VI	VII	VIII	IX	X	XI	XII
Coldsum		2280	2950	2750	4320	4600	-	-	-	-	220	760	1470
concentration	Aver. First-year	10	10	10	10	9	7	6	4	3	6	9	10
	Aver. Multi-year												
	Minimum					8	3	1	0	0	1		
	Maximum					10	10	8	7	7	8		
Level ice thick.	Maximum	120	140	160	170	180	150	120	90	70	30	60	90
Ice thickness	Average				120					70			
	Minimum				60					0			
	Maximum				280					180			
Pressure		0	0	0	0	1	1	1	1	1	0	0	0
Floe size	Average				500								
Ridge size	Average				150								
	Maximum				250								
Max. ridge size	Obs./estimated				7/6								
Ridge density	aver./min./max				2/0/3								

### 3.4.4 Area IV, Laptev Sea

The ice conditions in Laptev Sea are dominated by two so-called ice massifs. These are quite stable areas of summer ice (Zubov 1945, Barnett 1991). One is the Taimyr massif north and north-east from the Taimyr peninsula and the other is Yansky massif located in the Yanski Bay. If the winds are towards the shore these massifs can block the Vilkitskovo or Sannikova Straits.

Laptev Sea is very shallow with an extensive continental shelf. Most of the area where ships navigate is less than 50 m deep, see Fig 3.2. The sea is shallower than 25 m south of 75°N. This produces a large area of shore fast ice which may extend 500 km from the shoreline. Because winter winds are southerly, ice forming beyond the fast ice zone is pushed north forming very wide leads. The ridge heights do not apply to the fast ice zone and it is possible that in wintertime only the Western Laptev Sea is ridged. Keel depth of stamukas have been measured and average value and maximum value of 10 and 22 m respectively have been found (Gorbunov 1979). In summertime

ridge formation is dependent on the motion of ice massifs. Additional descriptive data on the winter conditions can be found in Nikolaeva and Shesterikov (1976).

The freeze-up data for the Laptev Sea is mid-October even though the temperatures get low well before that. The reason for the late freezing date is the warm water from the rivers combined with the shallowness of the sea.

**Table 3.8.** The ice conditions in Laptev Sea

		I	II	III	IV	V	VI	VII	VIII	IX	X	XI	XII
Coldsum		2620	3460	4330	4930	5210	-	-	-	-	150	830	1690
concentration	Aver. First-year	10	10	9	9	9	5	6	3	1	6	9	10
	Aver. Multi-year	0	0	1	1	0	3	0	0	1	1	0	0
	Minimum					8	4	2	0	0	4		
	Maximum					10	10	9	9	9	10		
Level ice thick.	Maximum	130	150	180	190	200	170	140	110	70	20	70	100
Ice thickness	Average				200					70			
	Minimum				120					0			
	Maximum				240					180			
Pressure		0	0	0	0	0	2	0	0	0	0	0	0
Floe size	Average				1000								
Ridge size	Average				150								
	Maximum				250								
Max. ridge size	Obs./estimated				5/6								
Ridge density	aver./min./max				3/1/5								

### 3.4.5 Area V, western East Siberian Sea

In the western part of East Siberian sea a dominant feature is the Novosibirskij ice massif which is located just east of the New Siberian Islands. The ice is seldom totally absent from this sea area since the prevailing wind direction during summer is northerly. The freeze-up starts in the beginning of October.

**Table 3.9.** The ice conditions in western East Siberian Sea

		I	II	III	IV	V	VI	VII	VIII	IX	X	XI	XII
Coldsum		2470	3580	4420	4990	5260	-	-	-	-	310	940	1810
Concentration	Aver. First-year	9	9	8	8	8	7	6	3	2	5	8	9
	Aver. Multi-year	1	1	2	2	2	1	0	1	2	3	2	1

	Minimum					9	6	4	1	0	6		
	Maximum					10	10	8	6	9	10		
Level ice thick.	Maximum	150	170	190	200	210	170	130	100	70	40	80	110
Ice thickness	Average				220					70			
	Minimum				120					0			
	Maximum				280					180			
Pressure		0	0	0	0	0	1	1	1	0	0	0	0
Floe size	Average				200								
Ridge size	Average				150								
	Maximum				200								
Max. ridge size	Obs./estimated				6/5								
Ridge density	aver./min./max				3/1/10								

### 3.4.6. Area VI, eastern East Siberian Sea

In the eastern part of East Siberian Sea there is one ice massif, the Ayonskij Massif, located west from Vrangeli Island. It usually stays away from the shore due to currents but is sometimes pushed to the coast around Pevek. Then the 3 m thick multi-year ice causes severe problems for shipping (Barr and Wilson 1985). The ice is nearly always present due to northerly winds during the summer. The ridging is more heavy than in the western part of East Siberian Sea. The freeze-up starts in the beginning of October.

**Table 3.10.** The ice conditions in the eastern East Siberian Sea

		I	II	III	IV	V	VI	VII	VIII	IX	X	XI	XII
Coldsum		2490	3280	4050	4590	4840	-	-	-	-	310	880	1660
concentration	Aver. First-year	8	8	7	8	8	8	7	3	2	4	7	8
	Aver. Multi-year	2	2	3	2	1	1	0	1	3	4	3	2
	Minimum					9	7	4	1	0	5		
	Maximum					10	10	8	6	9	10		
Level ice thick.	Maximum	140	160	180	200	200	160	130	100	70	40	70	110
Ice thickness	Average				240					70			
	Minimum				120					0			
	Maximum				320					180			
Pressure		1	1	1	0	0	0	0	0	1	2	2	2
Floe size	Average				400								
Ridge size	Average				200								
	Maximum				250								
Max. ridge size	Obs./estimated				7/7								
Ridge density	aver./min./max				3/2/10								



### 3.4.7 Area VII, Chukchi Sea

The Chukchi Sea is already influenced by the Pacific Ocean. There is a relatively warm current flowing from the Pacific which turns, however, first east and joins the Polar Gyre. A dominant feature is the Wrangel ice massif which in winter is pushed against the coast by the prevailing northerly winds, making navigation difficult. This is also reflected by the heavy ridging, the ridge sizes and densities being larger than in any other route segment of the NSR. Freeze-up starts in the beginning of October.

**Table 3.11.** The ice conditions in the Chukchi Sea.

		I	II	III	IV	V	VI	VII	VIII	IX	X	XI	XII
Coldsum		1820	2460	3140	3590	3780	-	-	-	-	160	550	1130
concentration	Aver. First-year	9	9	8	7	4	3	2	2	1	3	6	10
	Aver. Multi-year	1	1	2	2	4	2	1	0	1	0	1	0
	Minimum					5	2	1	0	1	1		
	Maximum					10	10	6	3	6	8		
Level ice thick.	Maximum	100	120	140	160	160	130	110	90	70	20	50	80
Ice thickness	Average				180					70			
	Minimum				120					0			
	Maximum				240					180			
Pressure		2	2	2	2	2	1	1	0	0	1	2	2
Floe size	Average				400								
Ridge size	Average				200								
	Maximum				250								
Max. ridge size	Obs./estimated				7/8								
Ridge density	aver./min./max				5/3/10								

## 3. 5. DATA SUMMARIES

The data matrices (Tables 3.5-3.11) are too detailed to give insight about the transiting of whole NSR. For this purposes certain data summaries are presented .

The following data (Table 3.12) has been extracted from a morphological ice Atlas compiled on the basis of Russian observations (Romanov 1993). The observation period extends from 1948 to 1988 and the observations consist of seaborne, airborne and drifting station data. In the mapping the Arctic sea areas were divided into 100x100 km squares and the values are average values in each square. The expected values are averages over the observation period and give thus the ice conditions of a normal ice season. The minimum and maximum values are those of the observation period and refer to conditions during a mild and severe ice season respectively.

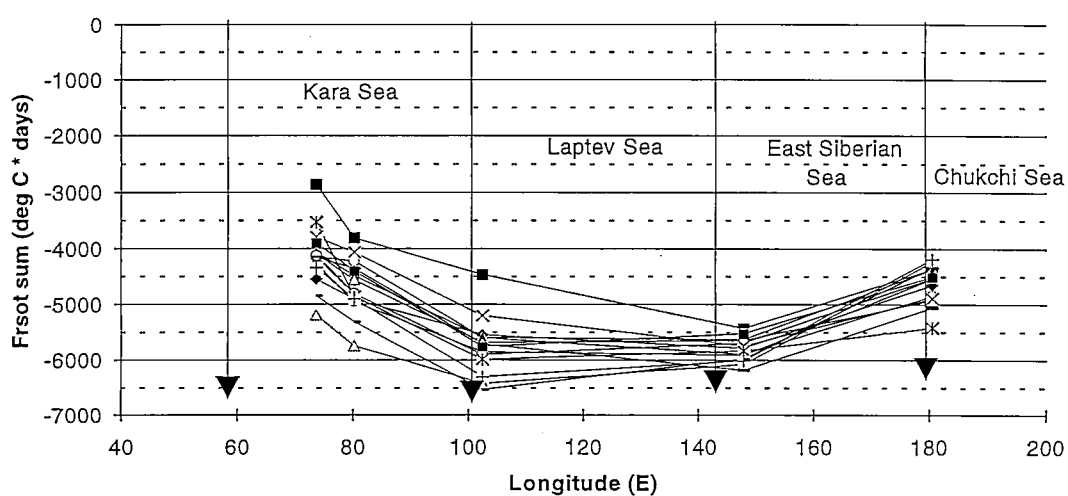
**Table 3.12.** NSR Ice conditions according to Romanov (1993). When two values are given these refer to western and eastern part of the sea area.

	I	II	III	IV	V	VI	VII
Expected mean ice thickness in April [cm]	30-70	70-100	100-120	90-120 180-240	180-240	180-240	120-180 70-120
Minimum mean ice thickness in April [cm]	0	30-60	60-120	30-120 120-180	120-180	120-180	120-180
Maximum mean ice thickness in April [cm]	30-120	120-180	180-240 240-280	180-240	240-280	240-320	180-240 120-180
Expected partial concentrations of first and multi-year ice in April [1/10]	10/0	10/0	10/0	10/0	9/1-10/0	7/3-9/1	7/3-9/1
Partial concentrations in April: minimum multi-year concentration [1/10]	10/0	10/0	10/0	10/0	10/0	10/0	10/0
Partial concentrations in April: maximum multi-year concentration [1/10]		9/1	9/1	7/3 9/1	4/6	4/6	3/7
Expected mean ice thickness in August-September [cm]	0	0-30	30-70 70	70 30-70	30-70	30-70	30-70
Minimum mean ice thickness in August-September [cm]	0	0	0 0-30	0	0	0	0
Maximum mean ice thickness in August-September [cm]	0-70	0-70	70-120 120-180	120-180	120-180	120-180	120-180
Expected ice concentration in August-September [1/10]	0	0-3	0-6 4-8	1-6 1-3	1-3	4-6	0-3
Minimum ice concentration in August-September [1/10]	0	0	0	0	0	0	0
Maximum ice concentration in August-September [1/10]	0	4-8	4-10 10	10 4-10	7-8	10	7-8
Expected mean floe size in April [m]	<500	<500	<500	500-1000	<200	200-400	200-400
Maximum mean floe size in April [m]	<500	<500	<500	1000-2000	<500	500-1000	500-1000
Maximum observed floe size in April km <sup>2</sup>	<1	<1	<1 1-3	<1	<1 1-3	<1	1-3
Expected ridge density in April [1/km]	-	<3	<3	<3	<3	<3	4-5
Minimum ridge density in April [1/km]	0	0	0	1	1	2	3
Maximum ridge density in April [1/km]	0	3	3	4-5	10	10	10

Expected mean ridge height in April [cm]		125	125-150	125-150 100	100 100- 150	150-200	200
Maximum mean ridge height in April [cm]		150-250	200-250	200-250 200	150-200	200-250	200-250
Maximum ridge height in April [m]		4-6	4-7	3-5	2-3 4-6	4-7	5-7

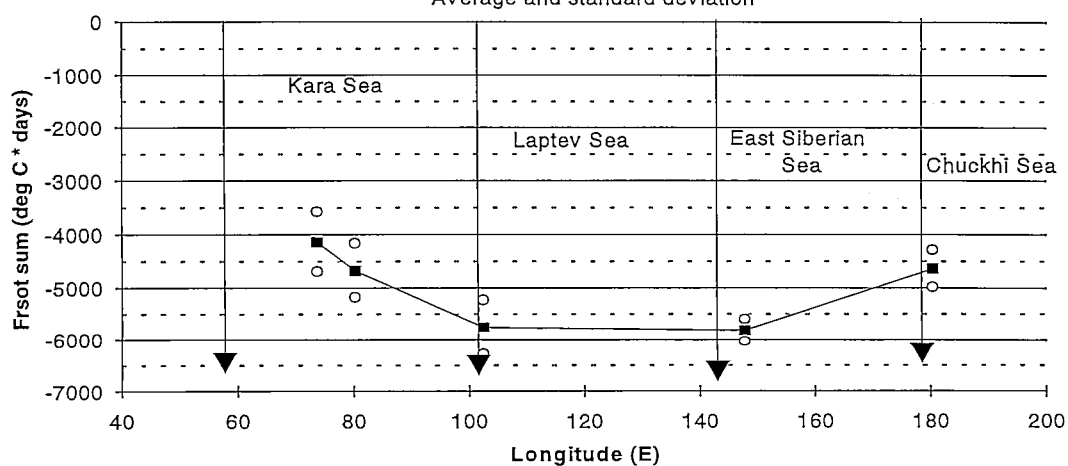
The isotherms along the NSR run, especially during winter, in North-South direction. Climate gets colder when proceeding eastwards until the Laptev sea after which it warms up again. This effect is clearly seen from Fig 3.4.

#### NSR Frost sum, 1968-81



#### Average frost sum, 1968-81

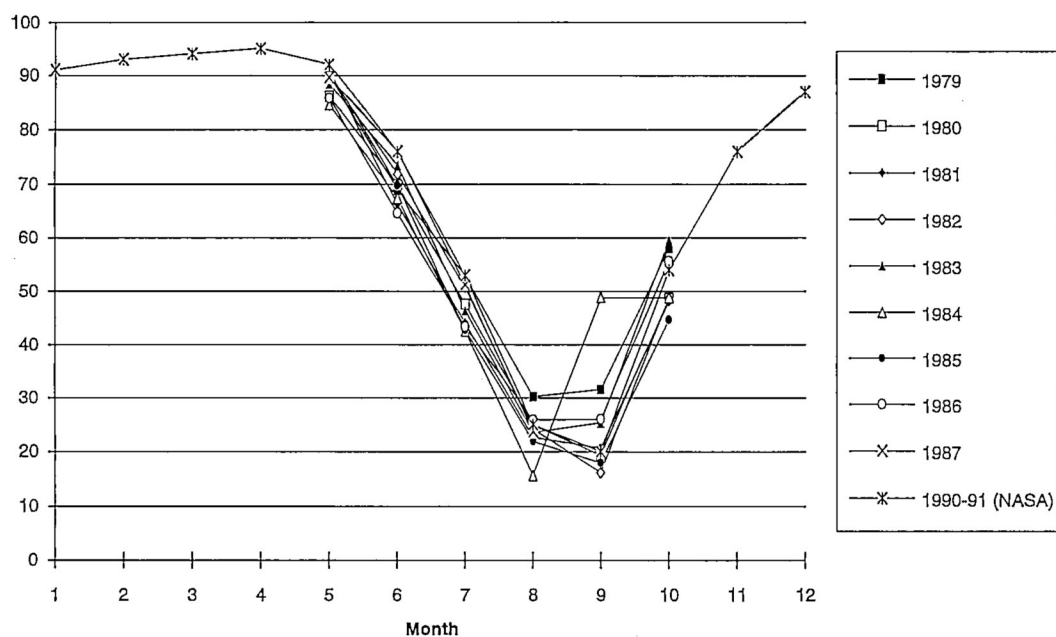
Average and standard deviation



**Figure 3.4.** The cumulative temperature based on monthly mean temperatures of five coastal weather stations and the average value and standard deviation of the cumulative temperature.

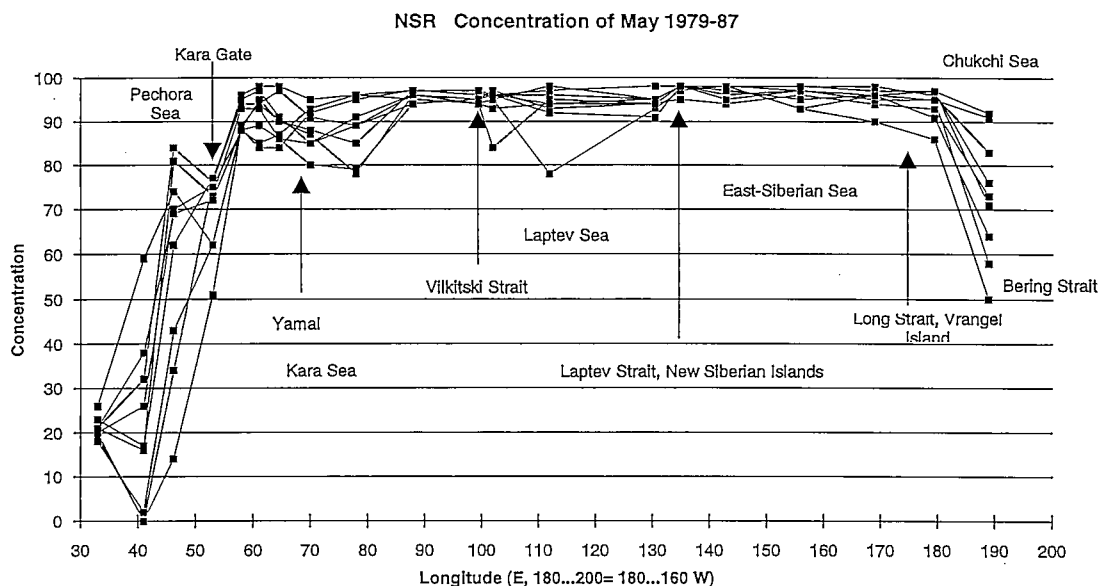
The monthly average ice coverage for the whole NSR is shown in Figure 3.5. In comparison with the sectionwise concentrations (Appendix 2) the variation is much smaller.

NSR Monthly average ice concentration (1979-87 French data compared to 90-91 NASA data)

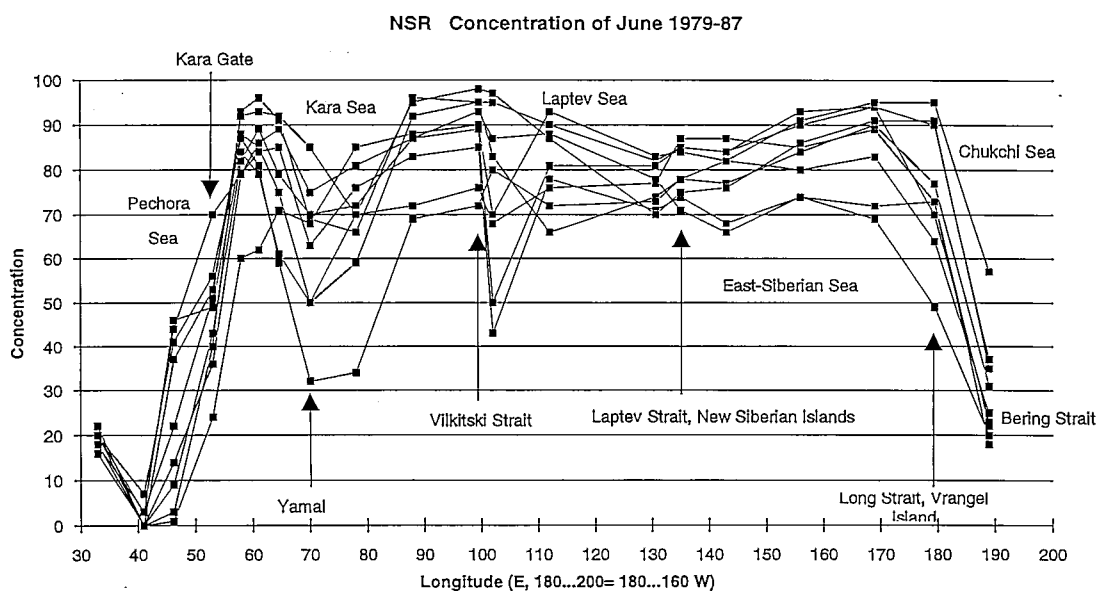


**Figure 3.5.** The monthly average ice coverage along the whole NSR (Courseaux and Kerebel 1992).

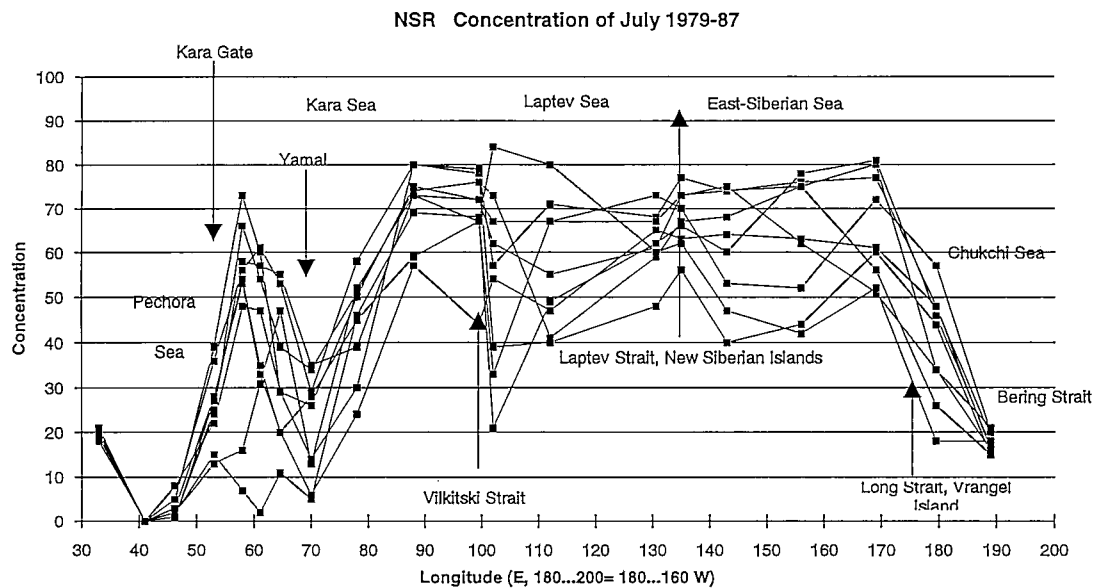
Yearly concentration profiles along the NSR for May-October are given in Figure 3.6.



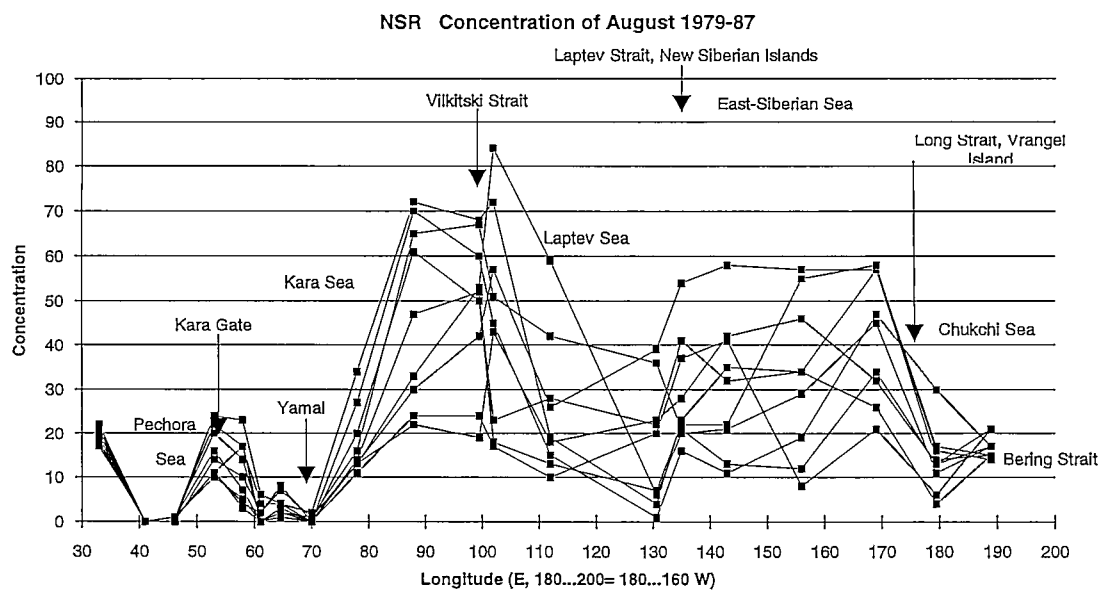
**Figure 3.6 a.** NSR ice concentration in May.



**Figure 3.6 b.** NSR ice concentration in June.



**Figure 3.6 c.** NSR ice concentration in July.



**Figure 3.6 d.** NSR concentration in August.

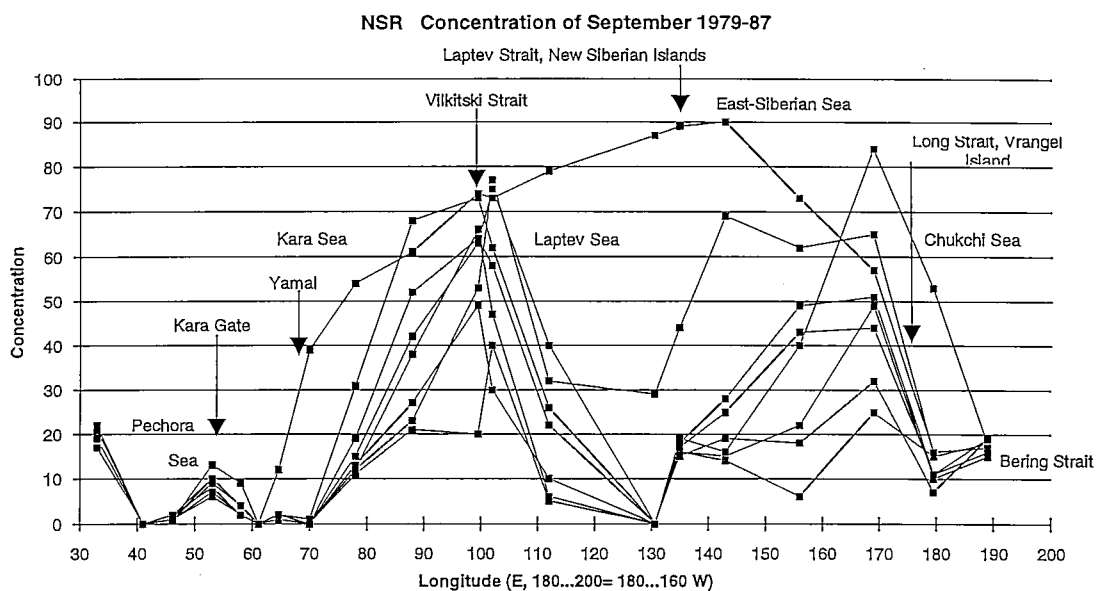


Figure 3.6 e. NSR ice concentration in September.

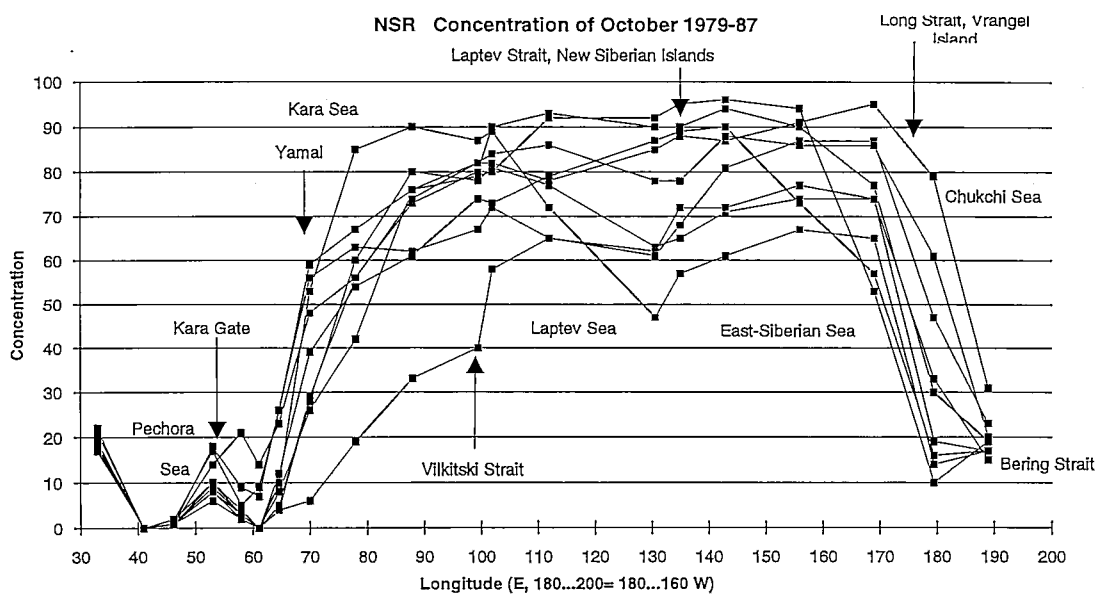


Figure 3.6 f. NSR ice concentration in October.

## 4. SHIP TRANSIT ALONG THE NSR

### 4.1 TRANSIT MODELLING

The target of ship ice transit modelling is to determine the transit times and the energy consumption when a ship navigates through a certain route in the prevailing ice conditions. The first question to be settled is whether the navigation is feasible at all. It might be that the ship, even with icebreaker escort, cannot manage the conditions. The other question is what are the seasons the ship can manage independently and when icebreaker escort is needed.

The transit simulation is done determining the average speed of the ship in the ice conditions prevailing. This may be done by just determining the ice resistance and thrust and equating these obtaining the speed. This is possible only if the conditions are uniform. This is not the case in an ice ridge field where the ship slows down when she encounters ridges and then accelerates after the ridges. The determination of the average speed requires a time step simulation of the ship progress through a ridge field. This simulation requires knowledge about the instantaneous ice resistance and thrust. If resistance is greater than thrust, ship decelerates consuming her inertia in penetrating the ridges. An example of this kind of full transit simulation models is presented in La Prairie & al. (1995).

Most of the transit simulation models are based on blind navigation where the ship proceeds through the ridge field on a straight route. In reality the ship seeks easier conditions and even if the route becomes longer the transit speed gets higher. The determination of speed increase through active navigation requires knowledge about the two dimensional properties of ice surface. These properties could include so called connectedness of the level ice patches in the ridge field. Only empirical results exists, however, about the influence of active navigation through ridge fields.

Another problem in the transit simulation is that the ridges are located randomly in the ridge field. Thus the transit analysis requires a Monte Carlo simulation of the ridge field and then transit simulation through it. This way the statistics of transit speeds is determined. This must finally be related to the ridge statistics. This work is just beginning at the Helsinki University of Technology and thus no results exists as yet.

The transit speed calculation is done here, in view of the short comings of the present knowledge, using an equivalent ice thickness. This is the average thickness of all the deformed ice. If the ridge sail height to keel depth ratio is assumed to be 5, and  $\phi$ ,  $s$  and  $d$  are the slope angle of the keel, ridge sail size and the ridge density respectively, then the equivalent ice thickness is

$$h_{eq} = \frac{(5s)^2}{\tan \phi} d \quad (4.1)$$



The resistance in the ridge field is now calculated by modelling the field as a channel with a thickness equal to the equivalent thickness calculated using the above formula. The channel ice resistance is (Malmberg 1983, Riska 1995)

$$R_{ch} = C_1 h_{eq} T (0.18 B + h_{eq} \tan \phi \cos \alpha) (\mu \cos \alpha + \sin \phi \sin \alpha) + C_2 h_{eq} T L_{pp} \quad (4.2)$$

The values of the constants are  $C_1 = 7.4 \text{ kN/m}^3$  and  $C_2 = 103 \text{ N/m}^3$ ; and the ship particulars are ship's beam  $B$ , ship's draft  $T$ , ship length between perpendiculars  $L_{pp}$ , bow stem angle  $\phi$ , bow waterline entrance angle  $\alpha$  and ice/ship coefficient of friction  $\mu$ .

The first term in this equation accounts for the ridge breaking resistance from the bow and the second for the resistance from the sides and the bottom. The speed dependence in channel transit comes from the superposition principle in which the open water resistance accounts for the speed dependence.

In addition to the resistance due to deformed ice a level ice component exists. Level ice is considered to have uniform thickness and properties. This report uses the method of Lindqvist, as modified by Riska (1996) to calculate the resistance due to level ice. The first term in the following formula accounts for the resistance of the bow region, the second for the resistance along the midbody:

$$R_i = C_1 + C_2 v \quad (4.3)$$

where

$$C_1 = f_1 \frac{1}{2 \frac{T}{B} + 1} B L_{par} h_i + (1 + 0.021 \phi) (f_2 B h_i^2 + f_3 L_{bow} h_i^2 + f_4 B L_{bow} h_i) \quad (4.4)$$

$$C_2 = (1 + 0.063 \phi) (g_1 h_i^{1.5} + g_2 B h_i) + g_3 h_i (1 + 1.2 \frac{T}{B}) \frac{B^2}{\sqrt{L}} \quad (4.5)$$

where  $v$  is ship, speed and  $h_i$  level ice thickness. The constants have the values  $f_1 = 0.23 \text{ kN/m}^3$ ,  $f_2 = 4.58 \text{ kN/m}^3$ ,  $f_3 = 1.47 \text{ kN/m}^3$ ,  $f_4 = 0.29 \text{ kN/m}^3$ ,  $g_1 = 18.9 \text{ kN/(m/sm}^{1.5})$ ,  $g_2 = 0.67 \text{ kN/(m/sm}^2)$  and  $g_3 = 1.55 \text{ kN/(m/sm}^{2.5})$ .

The total open water resistance,  $R_{ow}$ , is calculated as the sum of the following components (Holtrop and Mennen 1984)

- frictional resistance due to wetted surface area
- form resistance due to ship's shape
- viscous drag of appendages
- wave making and breaking resistance
- resistance of a bulbous bow (can be negative)
- a model-ship correlation allowance to account for resistance equations derived from model data

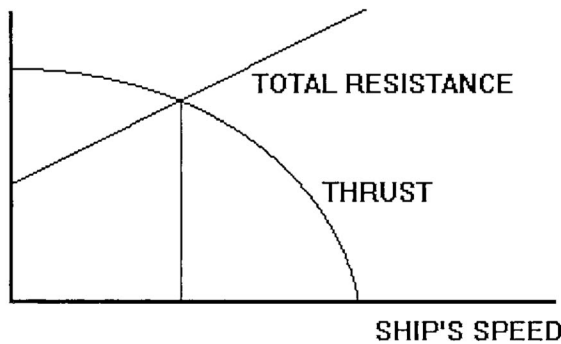
Ships designed for ice conditions usually do not have bulbous bows. The appendage resistances are likewise a minor component. Therefore these two are left out from the resistance equations. For detailed equations see Holtrop and Mennen (1984).

## 4.2 SHIP'S SPEED IN THE NSR SEA AREAS

The ice conditions in the seven sea areas of the NSR are modelled as level ice on top of an ice channel. The ships total resistance is thus

$$R_{\text{tot}} = R_{\text{ch}} + R_i + R_{\text{ow}} \quad (4.6)$$

To determine the ship's speed through each of the sea areas during each month of the year, the total resistance and thrust are calculated for each speed from zero to the ships open water speed, using an increment of 0.1 m/s. The ship's speed in the sea area is the speed at which the total resistance and the ship's thrust are within one percent of each other. Fig. 4.1 illustrates how the total resistance and thrust converge to give the ship speed. A Norilsk type of merchant vessel (SA-15) is used throughout the calculations as an example ship.



**Figure 4.1.** Determination of the ship's speed.

Using the level ice resistance equations, the maximum level ice that the SA-15 can transverse unescorted is 1.3 m. Therefore, the ship can not proceed through many of the sea areas during the winter months without icebreaker assistance. The resistance and speed of the ship following an icebreaker is calculated by assuming that the effect of the icebreaker is to break up the consolidated layer, thereby increasing the channel thickness by the level ice thickness, and removing the level ice resistance component from the total resistance calculations. Since these speeds are larger than the unescorted speeds and channel resistance is speed independent, the open water resistance must also be included in these icebreaker assisted resistance calculations. Thus

$$R_{\text{tot}} (\text{icebreaker assisted}) = R_{\text{ch}} + R_{\text{ow}} \quad (4.7)$$

The speed through the ridge field is then calculated in the same manner as for the unescorted ship i.e. the total resistance and thrust are calculated for a range of speeds, until they converge to within one percent.

### 4.3 THE TRANSIT RESULTS

Following are the transit speed data matrices for each of the seven sea areas (Tables 4.1 - 4.7). The ice concentration value is the sum of the average first and multi-year concentrations, given in section 3.4 of this report. The concentrations for November to April in the Pechora Sea have been estimated, since no actual data was available for these months in this sea. It is felt that these are the worst case estimates.

The average level ice thickness was assumed to be 90% of the maximum thickness, since maximum thickness is the only data available. The average ridge heights given in section 3.4 are given only for the months with the worst ice conditions in each sea area. Other months were scaled according to the level ice thicknesses, to obtain average ridge heights throughout the year.

Shaded speed cells in the data matrices indicate that the values are calculated assuming icebreaker assistance. If a month has two speeds, the ship may proceed without icebreaker assistance but the speed is calculated for both situations as explained below.

The following are the months in which icebreaker assistance is required for the SA-15 ship, listed by sea area:

- Sea Area I - never needs icebreaker assistance
- Sea Area II - March, April, May
- Sea Area III - January, February, March, April, May, June
- Sea Area IV - January, February, March, April, May, June, July
- Sea Area V - January, February, March, April, May, June
- Sea Area VI - January, February, March, April, May, June, July
- Sea Area VII - February, March, April, May, June

In addition, during several of the months immediately before and after these months requiring icebreaker assistance, the ship is able to proceed, but at a slow rate and at an increased risk of damage. In these cases, although not essential, icebreaker assistance would be greatly beneficial. For these months, all the following calculations have been done for both cases - transit with and without icebreaker assistance. The months during which icebreaker assistance is greatly beneficial although not absolutely necessary are:

- Sea Area II - February, June
- Sea Area III - July, December
- Sea Area IV - December
- Sea Area V - July, December

Sea Area VI - December  
Sea Area VII - January, July

The length of each sea area is given in table 3.1. Note that the lengths of the straights are included with the sea area immediately above that straight in the table. Using the concentrations given in Tables 4.1 - 4.7, the open water and ice lengths were calculated and the average transit time for the entire NSR has been calculated for each month. The results can be seen in Table 4.8 and are illustrated graphically in Fig. 4.2. In Table 4.8, several cells contain two values. The first value is the transit time with extensive icebreaker assistance, the second is with icebreaker assistance only when absolutely necessary. When observing Fig. 4.2, it is important to note that the values from December to July assume that there is icebreaker assistance. This explains why these transit times are not necessarily higher than the values calculated for the summer months.

When completing the damage probability analysis, the transit time only while the ship is in ice is used. Figures 4.3 and 4.4 show graphically the calculated ice transit times for each sea area for each month throughout the year. In any month which has two values for Ni, one value is with icebreaker assistance, and one is without. These are the months during which icebreaker assistance is not essential, but is very beneficial, as previously discussed.

As can be seen from the graphs, October has the shortest total transit time both in ice and in open water. The longest transit time occurs in either April or May.

**Table 4.1.** Sea Area I, Pechora sea

	Jan	Feb	Mar	Apr	May	Jun	Jul	Aug	Sept	Oct	Nov	Dec
Ice concentration	8	8	8	8	6	3	1	0	0	0	4	8
Level ice thickness	65	80	100	110	110	70	35	0	0	0	25	45
Ridge density (1/km)	2	2	2	2	2	2	2	2	2	2	2	2
Ridge height (cm)	60	70	90	100	100	65	30	0	0	0	25	40
Consol. layer (m)		1	1	1	1	1	1	1	1	1	1	1
Speed (m/s)	3,7	2,7	1,4	0,9	0,9	3,3	6	ow	ow	ow	6,7	5,2

**Table 4.2.** Sea Area II, Western Kara Sea

	Jan	Feb	Mar	Apr	May	Jun	Jul	Aug	Sept	Oct	Nov	Dec
Ice concentration	10	10	10	9	9	8	4	1	0	2	8	10
Level ice thickness	80	100	115	125	135	110	80	55	25	10	35	55
Ridge density (1/km)	2	2	2	2	2	2	2	2	2	2	2	2
Ridge height (cm)	75	95	105	115	125	100	75	50	25	10	30	50
Consol. layer (m)	1	1	1	1	1	1	1	1	1	1	1	1
Speed (m/s)	2,7	6,5	6,3	6,2	6	6,4	2,7	4,4	3,7	8	6	4,4
Speed (m/s)		1,4				0,9						

**Table 4.3.** Sea Area III, Eastern Kara Sea

	Jan	Feb	Mar	Apr	May	Jun	Jul	Aug	Sept	Oct	Nov	Dec
Ice concentration	10	10	10	10	9	7	6	4	3	6	9	10
Level ice thickness	110	125	145	155	160	135	110	80	65	25	55	80
Ridge density (1/km)	2	2	2	2	2	2	2	2	2	2	2	2
Ridge height (cm)	105	120	135	145	150	125	105	75	60	25	50	75
Consol. layer (m)	1	1		1	1	1	1	1	1	1	1	1
Speed (m/s)	6,3	6,1	5,9	5,7	5,6	6	6,3	2,7	3,7	6,7	4,4	6,7
Speed (m/s)							0,9					2,7

**Table 4.4.** Sea Area IV, Laptev Sea

	Jan	Feb	Mar	Apr	May	Jun	Jul	Aug	Sept	Oct	Nov	Dec
Ice concentration	10	10	10	10	9	8	6	3	2	7	9	10
Level ice thickness	115	135	160	170	180	155	125	100	65	20	65	90
Ridge density (1/km)	3	3	3	3	3	3	3	3	3	3	3	3
Ridge height (cm)	95	115	135	140	150	130	105	85	55	15	55	75
Consol. layer (m)	1	1	1	1	1	1	1	1	1	1	1	1
Speed (m/s)	6,3	6	5,5	5,4	5,1	5,6	6,1	1,4	3,7	7,2	3,7	6,6
Speed (m/s)												2

**Table 4.5.** Sea Area V, Western East Siberian Sea

	Jan	Feb	Mar	Apr	May	Jun	Jul	Aug	Sept	Oct	Nov	Dec
Ice concentration	10	10	10	10	10	8	6	4	4	8	10	10
Level ice thickness	135	155	170	180	190	155	115	90	65	35	70	100
Ridge density (1/km)	3	3	3	3	3	3	3	3	3	3	3	3
Ridge height (cm)	105	125	135	140	150	125	90	70	50	30	55	80
Consol. layer (m)	1	1	1	1	1	1	1	1	1	1	1	1
Speed (m/s)	6	5,7	5,4	5,2	5	5,7	6,3	2	3,7	5,9	3,3	6,5
Speed (m/s)							0,6					1,4

**Table 4.6.** Area VI, Eastern East Siberian Sea

	Jan	Feb	Mar	Apr	May	Jun	Jul	Aug	Sept	Oct	Nov	Dec
Ice concentration	10	10	10	10	9	9	7	4	5	8	10	10
Level ice thickness	125	145	160	180	180	145	115	90	65	35	65	100
Ridge density (1/km)	3	3	3	3	3	3	3	3	3	3	3	3
Ridge height (cm)	140	160	180	200	200	160	130	100	70	40	70	110
Consol. layer (m)	1	1	1	1	1	1	1	1	1	1	1	1
Speed (m/s)	5,9	5,5	5,1	4,6	4,6	5,5	6,1	2	3,6	5,9	3,6	6,4
Speed (m/s)												1,3

**Table 4.7.** Area VII, Chukchi Sea

	Jan	Feb	Mar	Apr	May	Jun	Jul	Aug	Sept	Oct	Nov	Dec
Ice concentration	10	10	10	9	8	5	3	2	2	3	7	10
Level ice thickness	90	110	125	145	145	120	100	80	65	20	45	70
Ridge density (1/km)	5	5	5	5	5	5	5	5	5	5	5	5
Ridge height (cm)	125	150	170	200	200	165	140	110	90	30	60	95
Consol. layer (m)	1	1	1	1	1	1	1	1	1	1	1	1
Speed (m/s)	6,2	5,7	5,2	4,2	4,2	5,3	5,9	2,4	3,5	7,1	5,1	3,1
Speed (m/s)	1,7						1					

**Table 4.8.** Transit times for the entire NSR (days).

	Jan	Feb	Mar	Apr	May	Jun	Jul	Aug	Sept	Oct	Nov	Dec
Sea Area I OW	0,1	0,1	0,1	0,1	0,2	0,4	0,5	0,5	0,5	0,5	0,3	0,1
Ice	1	1,3	2,6	4	3	0,4	0,1	0	0	0	0,3	0,7
Sea Area II OW	0	0	0	0,1	0,1	0,2 / 6,1	0,5	0,7	0,8	0,6	0,2	0
Ice	2,5	1,1 / 4,9	1,1	1	1	0,9	1	0,2	0	0,2	0,9	1,6
Sea Area III OW	0	0	0	0	0,2	0,5	0,6	0,9	1,1	0,6	0,2	0
Ice	2,1	2,2	2,3	2,4	2,2	1,6	1,3 / 9	2	1,1	1,2	2,8	2,0 / 5,0
Sea Area IV OW	0	0	0	0	0,2	0,3	0,7	1,1	1,3	0,5	0,2	0
Ice	2,3	2,4	2,6	2,6	2,5	2	1,4	3	0,8	1,4	3,4	2,1 / 7,1
Sea Area V OW	0	0	0	0	0	0,2	0,4	0,7	0,7	0,2	0	0
Ice	1,6	1,7	1,8	1,8	1,9	1,3	0,9 / 9,4	1,9	1	1,3	2,9	1,5 / 6,7
Sea Area VI OW	0	0	0	0	0,1	0,1	0,3	0,6	0,5	0,2	0	0
Ice	1,5	1,6	1,7	1,9	1,7	1,4	1	1,8	1,2	1,2	2,4	1,4 / 6,8
Sea Area VII OW	0	0	0	0,1	0,3	0,7	0,9	1	1	0,9	0,4	0
Ice	1,8 / 6,7	2	2,2	2,4	2,2	1,1	0,6 / 3,4	1	0,7	0,5	1,6	3,7
Total N <sub>I</sub> (days)	12,9 / 17,8	12,4 / 16,2	14,4	16,4	15,6	11,1 / 17	10,2 / 29,2	15,4	10,7	9,3	15,6	13,1 / 31,7

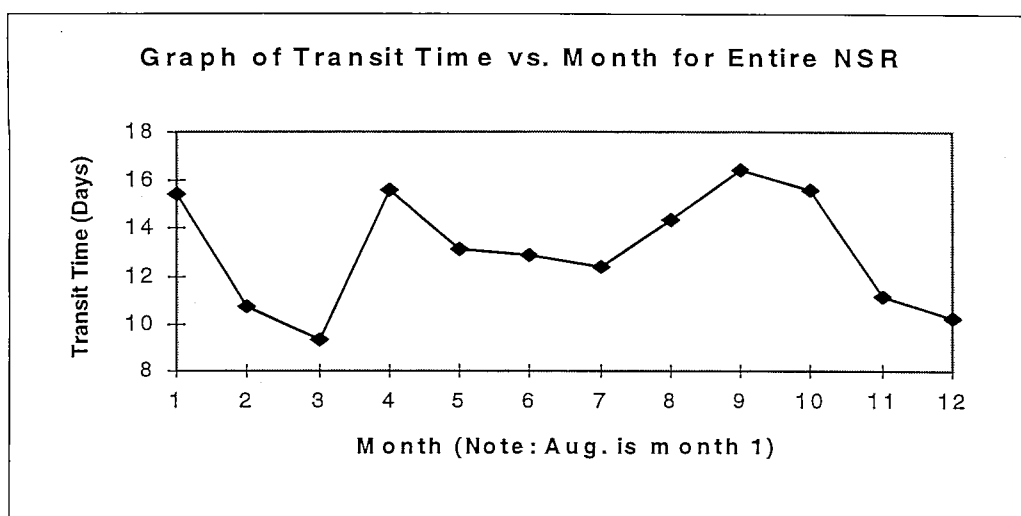


Figure 4.2. Transit times for the entire NSR

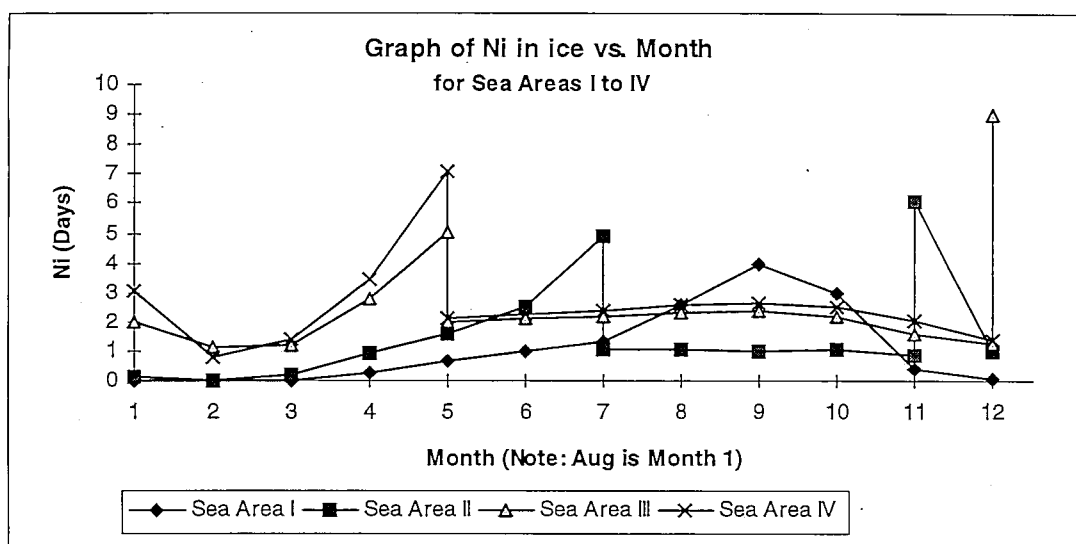
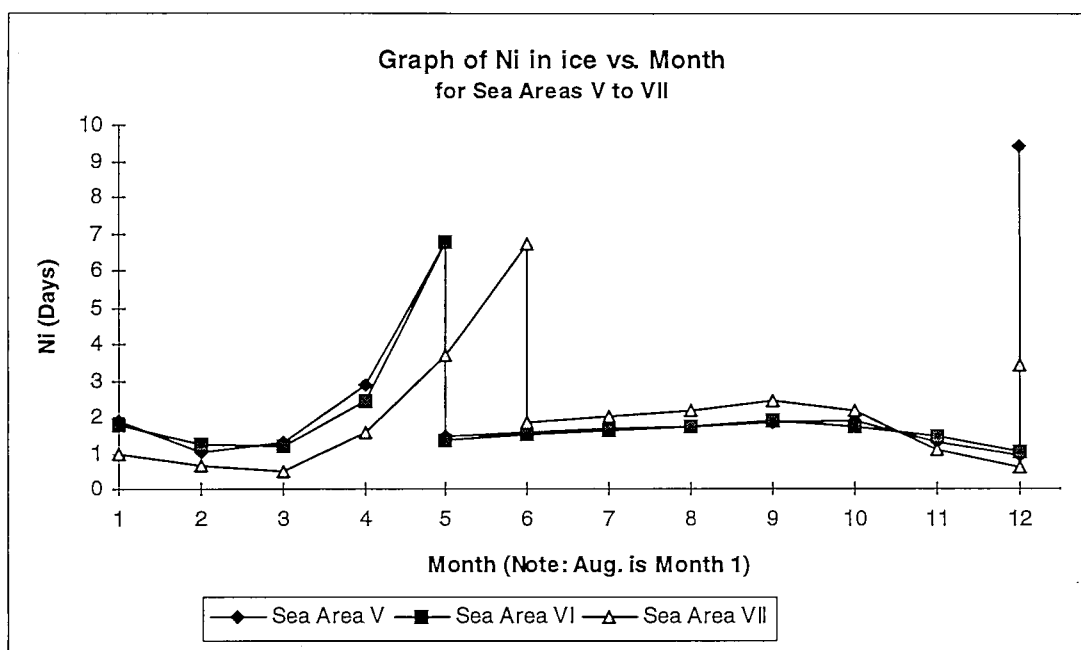


Figure 4.3. Monthly transit times for different sea areas.



**Figure 4.4.** Monthly transit times for different sea areas.



## **5. SHIP SAFETY ALONG THE NSR**

### **5.1. DESCRIPTION OF THE APPROACH APPLIED**

#### **5.1.1. General description**

The probabilistic analysis of structural safety requires evaluation of statistical characteristics for the ice loads and strength of the structure. The structural behaviour can be studied on the basis of established methods from structural mechanics, but the evaluation of ice loads is more problematic.

The following long term approach for the determination of maximum ice loads aims to relate the load level with the main ship parameters and the prevailing ice conditions on various parts of the NSR. A semi-empirical approach for estimation of long term ice loads, which relies partly on full scale measurements and partly on the analysis of the ice edge failure process (Kujala 1994), is applied. Ice thickness is the main variable used to specify the prevailing ice conditions. The effects of ridges on the load level is included by specifying an equivalent level ice thickness for a ridged ice field.

The basic idea behind the equivalent ice thickness is to find an equivalent average ice thickness of ridged ice which gives the same load level as encountered by a ship when it navigates in ice conditions with varying amounts of level and ridged ice. A statistical ice load model developed for calculation of ice induced loads on ships navigating in specific ice conditions (Kujala 1994) is used to determine the equivalent ice thickness of a ridged ice field.

The relation between equivalent ice thickness and ice loads encountered by a ship is defined semi-empirically. A database of annual ice induced loads on various sea areas is gathered by full scale measurements and the statistical characteristics of the measured loads are related to the winter maximum equivalent ice thickness of the sea area under consideration. By conducting the measurements during several winters, the relationship between ice load level and winter maximum equivalent ice thickness can be established by regression analysis.

#### **5.1.2. Formulations for the long term loads**

The long term measurements onboard MS Kemira formed the basic database and the general applicability of the method was tested by calculating long term loads for MS Arcturus and comparing the obtained distribution with the measured long term results onboard this ship. The load on one frame at bow, midship, and aftship were studied throughout the long term analysis. In the database the maximum ice load values measured on various sea areas operated by the ship during one winter formed a basic sample of data. A number of these samples were then gathered by conducting measurements during several winters. The automatic measuring system onboard the studied ship was programmed to gather 12 hour maximum values. After each winter the measured maximum values were analysed and divided into various sea areas based on the ship's time schedule and route in ice during each voyage.

The method used for the evaluation of the long term ice load statistics is based on the assumption that the measured 12 hour maximum values during one winter on each sea area can be related to the winter maximum equivalent ice thickness,  $h_e$ , of this sea area. The empirical studies conducted (Kujala 1991) have shown that the best correlation between measured winter maximum load values and prevailing ice conditions is obtained when the equivalent ice thickness is used to describe the annual ice conditions instead of parameters such as the maximum ice extent, fast or pack ice thickness. Thereafter the long term ice loads can be calculated based on the long term statistics of  $h_e$ .

Fig. 5.1 illustrates schematically the calculation procedure to obtain the long term cumulative distribution function for ice loads on each sea area. The measured 12 hour maximum values for ice load is denoted by  $w$  and the collection of them

$\{w_n\}, n=1, \dots, N$ . The mean value of the measured maxima,  $E[w_n] = \bar{w}$ , during one winter on a specific sea area is taken as piece-wise linearly related to the  $h_e$  of the sea area (Kujala et al. 1994):

$$\begin{aligned} \bar{w} &= k_i h_e & h_e &\leq h_{\max} ; \\ \bar{w} &= k_i h_{\max} + k_a (h_e - h_{\max}) & h_e &\geq h_{\max} . \end{aligned} \quad (5.1)$$

where the subscript  $i$  is for independent navigation in solid ice and  $a$  is for navigation in a broken ice field either independently or with icebreaker assistance. For the damage risk analysis calculations which follow,  $h_{\max}$  for the SA-15 ship is taken to be 1.3 m, as calculated in section 4.1.6 of this report. The linearity is divided into two groups because the process of the highest load events in ice is different with independent navigation in solid ice and with navigation in the broken ice field as is discussed in section 5.1.3. In addition, the division of Eq. 5.1 into two categories enables the consideration of the effect of ship's maximum ice breaking capability,  $h_{\max}$ , on the encountered load level. The coefficient of variation,  $k$ , of the maxima  $\{w_n\}$  is assumed to be independent of  $h_e$ :

$$k = \frac{\sqrt{\text{var}[w_n]}}{\bar{w}}. \quad (5.2)$$

where  $\text{var}[w_n]$  is the variance of  $\{w_n\}$ . The coefficients  $k_i, k_a$  and  $k$  are determined empirically for the bow, midship, and aftship frames for the instrumented ship based on the measured maxima during several winters on various sea areas with varying  $h_e$ . The values are then modified according to bow angles of the project ship, see Kujala (1994). The values of  $k_i, k_a$  and  $k$  for the SA-15 ship are given in Table 5.1. The coefficients  $k_i$  and  $k_a$  for any other ice-strengthened ship are obtained using two ship parameters: maximum ice breaking capability,  $h_{\max}$ , and normal frame angle,  $\beta_n$ , as is discussed in sections 5.1.3 and 5.1.4.

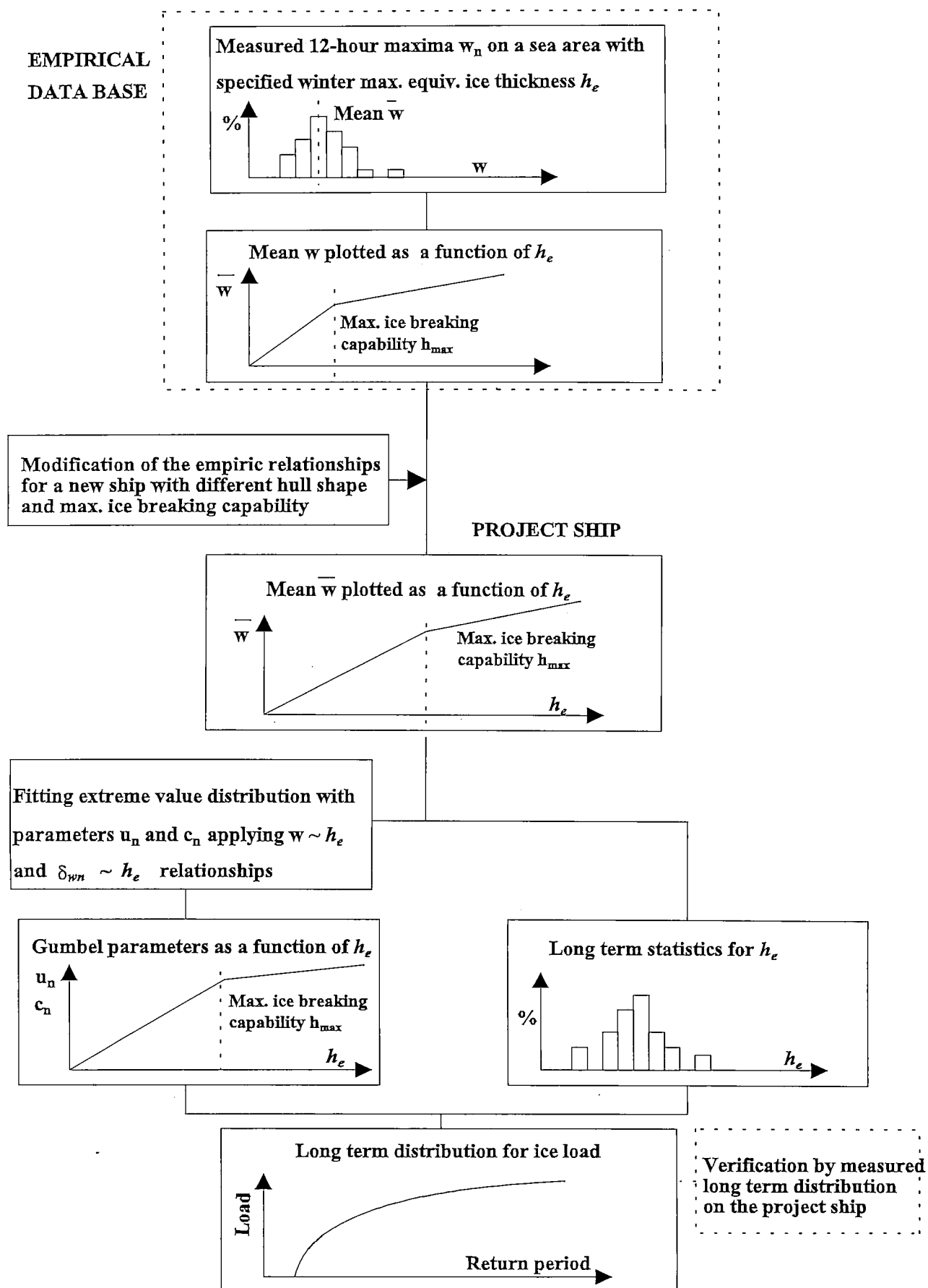


Figure 5.1. The calculation procedure to obtain lifetime ice loads for each sea area

**Table 5.1** The obtained values for the coefficients  $k_i$ ,  $k_a$  and  $k_\delta$  on various parts of the ship

	$k_i$ [kN/m]	$k_a$ [kN/m]	$k_\delta$
Bow	274	99	0.61
Midship	111	111	0.66
Aftship	146	146	0.66

When the mean and coefficient of variation for the maxima are specified, an extreme value probability distribution can be fitted on the data. The long term measurements have indicated that Gumbel I asymptotic extreme value distribution fits well on the measured extreme values (Kujala 1994). Gumbel I has the following cumulative distribution function:

$$F_a(w/h_e) = e^{-e^{-\frac{1}{c_n}(w-u_n)}} \quad (5.3)$$

where the parameters  $c_n$  and  $u_n$  are related to the mean and coefficient of variation of the maxima (Ochi 1990):

$$c_n = \frac{\bar{w} k}{\pi / \sqrt{6}} \quad (5.4)$$

$$u_n = \bar{w} - \gamma c_n = \bar{w} (1 - \gamma \frac{\sqrt{6}}{\pi} k) \quad (5.5)$$

where  $\gamma$  is Euler's constant, 0.577. The annual cumulative distribution function given in Eq. 5.3 is defined as conditional because the parameters are related to  $h_e$ . The long term cumulative distribution function for each sea area can then be obtained by integrating over the long term statistics of  $h_e$ :

$$F(w) = \int_0^{\infty} F_a(w/h_e) f(h_e) dh_e \quad (5.6)$$

where  $f(h_e)$  is the statistical distribution function for the  $h_e$ , which is taken to be normally distributed, with coefficient of variation for each sea area given in Table 5.2 (Kujala 1995). Because of the lack of detail of ice conditions on the NSR, the coefficient of variation of each sea area is a very difficult quantity to determine. As long as the range of values integrated over is large enough, the coefficient of variation has very little effect on the results.  $F(w)$  is determined for each month in each sea area on the NSR.

**Table 5.2** - Coefficient of Variation for each Sea Area

Sea Area	Coefficient of Variation (%)
I Pechora Sea	6
II Western Kara Sea	6
III Eastern Kara Sea	6
IV Laptev Sea	5.6
V Western East Siberia Sea	2.2
VI Eastern East Siberia Sea	2.2
VII Chukchi Sea	4.6

The final lifetime cumulative distribution function for ice loads is then the weighted sum of the cumulative distributions on each sea area:

$$F_l(w_n) = \sum_{i=1}^t a_i (F_i(w))^{2N_i} \quad (5.7)$$

where  $t$  is the number of sea areas and  $a_i$  is the relative distance of ice navigation in each sea area. The proper way to calculate the parameter  $a_i$  is to estimate the relative number of load events on each sea area, but this is not possible at present because of the limited knowledge of the ice navigation and ice breaking process in various ice conditions.  $N_i$  in equation 5.7 is the time (in days) that the ship navigates in ice in the  $i^{\text{th}}$  sea area, calculated from the length of the sea area, the ice concentration as well as the speed in ice (calculated in chapter 4).

The cumulative long term distributions are usually plotted as a function of return period, which is defined as the number of observations required to achieve a certain load level. The number of observations can be changed to a time scale by noting that the time between observations is a half day so that the return period in days  $T(w)$  is:

$$T(w) = \frac{0.5}{1 - F_l(w)} \quad (5.8)$$

### 5.1.3. Effect of the maximum ice breaking capability

In addition to the ice conditions and ice edge failure process, ship performance in ice is an important factor affecting the level of ice loads encountered by a ship. The ship's speed in solid ice is a function of ice thickness. The decrease of ship's speed as a function of level ice thickness is approximated for the load calculations as a line shown schematically in Fig. 5.2. This is an approximate calculation method, but the calculated examples on various ships (Kujala and Sundell 1992) indicate a good correspondence with full scale observations of ship's average speed as a function of ice thickness.

Noting the maximum open water speed as  $v_{ow}$  and the maximum level ice breaking capability as  $h_{max}$ , ship's speed,  $v_i$ , in level ice field with ice thickness,  $h_i$ , can be described as:

$$\begin{aligned} v_i &= v_{ow} \left(1 - \frac{h_i}{h_{max}}\right) , \quad h_i \leq h_{max} ; \\ v_i &= 0 , \quad h_i \geq h_{max} . \end{aligned} \quad (5.9)$$

Ship's speed in a ridged ice field is a more complicated problem. As reviewed by Daley and Riska (1992) the ship-ridge interaction mechanics is poorly understood. The navigation in a ridged field can be continuous movement or movement by ramming through the ridges. In this work the resistance in a ridged field is idealised by assuming that the thickness of the consolidated layer determines the speed of a ship in a ridged field. This means that the maximum level ice breaking capability defined in Fig. 5.2 is also applied in a ridged field when the thickness of the consolidated layer forms the level ice thickness.

The semi-empirical long term approach defined by Eq. 5.1 includes the effect of  $h_{max}$  by dividing the empirical data base in two categories. This is done as the ship can not navigate independently in a solid ice thickness thicker than  $h_{max}$  and needs icebreaker assistance. This decreases the number of ice impacts at the bow of the ship following the icebreaker, which again can be assumed to affect the relationship between maximum loads and level ice thickness.

#### 5.1.4. Effect of ship hull shape

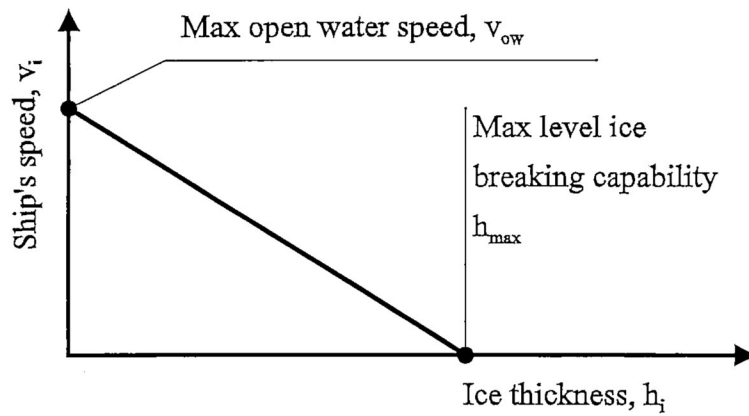
The ship-ice interaction is assumed to initiate by crushing of ice at the contact. The penetration of the ship into ice by crushing continues until the ice cover breaks either due to macroscopic shearing or bending failure. Fig. 5.3 illustrates this failure process. The ice load increases as long as the crushing area increases before the macroscopic bending or shear failure. The normal frame angle,  $\beta_n$ , is an important parameter in the process. The normal frame angle is a function of the waterline angle and frame angle of the hull area under consideration. The failure processes are shown schematically for  $\beta_n = 0$  and  $\beta_n > 0$  in Fig. 5.3.

In the statistical model developed the parameters used are level ice thickness, ship's speed, ship hull shape, ice crushing strength and ice flexural strength. Applying the statistical ice load model the effect of the normal frame angle can be studied. Fig. 5.4 illustrates the calculated load on a frame as a function of the normal frame angle with ice thickness as a parameter. In the long term approach, the effect of  $\beta_n$  is taken into account using the equation:

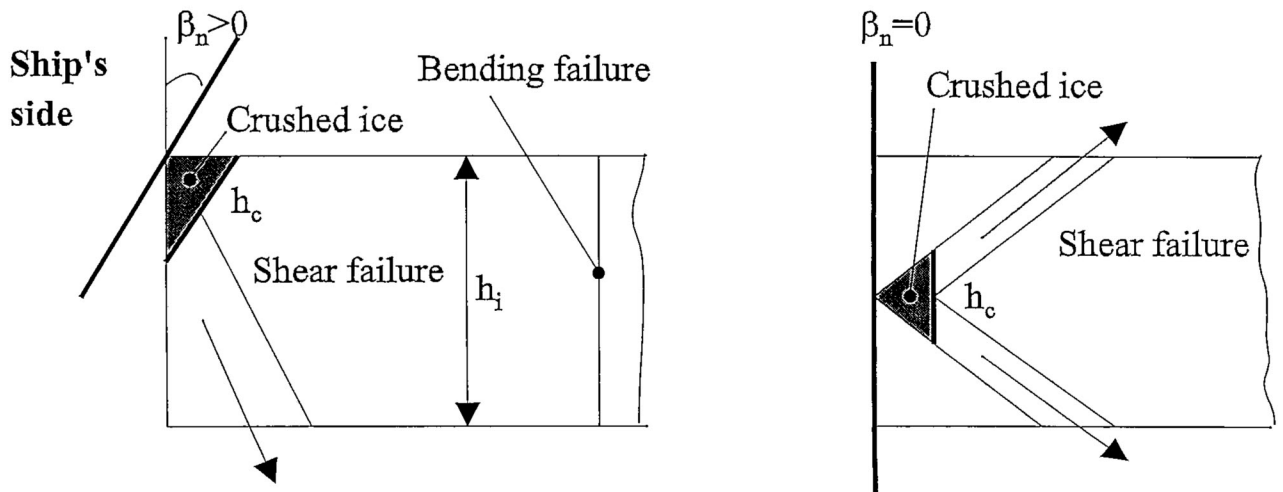
$$k_i^p = b_1 \left( \frac{\beta_n}{\beta_n^p} \right)^{b_2} k_i \quad (5.10)$$

where the superscript p is for definition of the coefficient  $k_i$  for the new, project ship. Eq. 5.10 is the same for the coefficient  $k_a$ . The coefficient of variation  $k_g$  is assumed to be independent of the frame angle. The following numerical values are found for

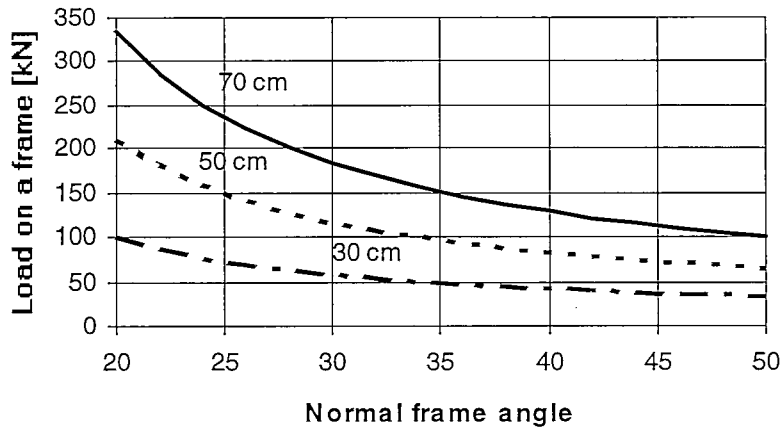
the coefficients  $b_1$  and  $b_2$  by regression analysis to fit the calculated ice load curves given in Fig. 5.4:  $b_1=1.01$ ,  $b_2=1.46$ . These values are valid when the bending failure determines the peak load values. With small  $\beta_n$  values ( $< \sim 12^\circ$ ) the coefficients  $k_i$  and  $k_a$  can be taken as constant.



**Figure. 5.2.** Schematic presentation of the decrease of ship's speed as a function of ice thickness



**Figure. 5.3.** Idealisation of the ice edge failure process.



**Figure. 5.4.** The load on one frame as a function of the normal frame angle with ice thickness as a parameter. The probability level is  $p=0.001$  and coefficient of variation for ice thickness is 0 (Kujala 1994).

### 5.1.5. Evaluation of failure probability for the frames

For statistically independent load and strength distributions, the failure probability can be obtained from the equation

$$P_f = 1 - \int_{-\infty}^{\infty} f_R(w) F_l(w) dw \quad (5.11)$$

where  $f_R(w)$  is the statistical distribution for the strength of the structure and  $F_l(w)$  is determined by Eq. 5.7. Due to the lack of information relating to the statistical distribution for the strength of the structure, it has been assumed in this analysis to be fixed. Therefore it is a Dirac delta function, so equation 5.11 becomes

$$P_f = 1 - \int_{-\infty}^{\infty} \delta(w - m_R) F_l(w) dw = 1 - F_l(m_R)$$

The first yield and ultimate strength of the frames are typical limit states used for ice-strengthened frames in the probabilistic failure analysis. Only the first yield limit state is used in the subsequent calculations. The load giving the first yield for a frame can be calculated with the formula

$$m_{R_y} = \frac{W_z m_t \sigma_y}{L} \quad (5.12)$$



where  $W_z$  is the section modulus of the frame,  $\sigma_y$  is the yield strength,  $L$  is the span of the frame and  $m_t$  is a factor to take into account the end conditions of the frame (Ice rules 1985).

$$m_t = \frac{7 \times 5.7}{7 - 5 \left( \frac{h_c}{L} \right)} \quad (5.13)$$

where  $h_c$  is the load height, assumed to be  $0.2h_l$  at the bow and  $0.6h_l$  at the mid and aftships for the SA-15. This theory works for one sea area, but must be modified when calculating the damage probability over several sea areas, each with a different  $h_c$ . Therefore, in the calculations which follow,  $h_c$  was assumed to be 0.2 (for bow) or 0.6 (mid and aftship) of 0.5 x the maximum  $h_c$  for the entire route. For the SA-15 ship,  $L=1.175$ m and the section modulus requirements for ULA class are 1013, 288 and 403 cm<sup>3</sup> for the bow, midship and aftship respectively and similarly for the UL class 438, 157 and 159cm<sup>3</sup> (Riska, 1992). The yield strength of a normal steel is assumed to be 290 MPa.

The ultimate strength  $R_u$ , for a frame can be obtained by calculating the force required to form a plastic hinge mechanism. For a typical ice-strengthened frame the load required to reach the ultimate strength is about 1.6 time higher than the load required for the first yield (Kujala 1991).

## 5.2. APPLICATION TO THE NSR

The long term statistics from the Baltic is extrapolated to correspond to the ice conditions in the NSR as similar data bases are not available for the NSR. In this approach, multi-year ice in the NSR has been treated as first year ice and the coefficient of variation for the ice thicknesses in different sea areas of the NSR have been estimated from those of the Baltic Sea. These assumptions are quite strong and thus some validation is required. This may be given by damage statistics.

In the period between 1954 and 1990 a total number of 800 damages have been reported on the NSR (Lenskiy 1992, see also Kjerstad 1994, IWP 14). The damages can be categorised to have occurred in the following ice conditions:

- Ice pressure (no impact)
- Ice impact when sailing unescorted
- Ice impact when following an icebreaker
- Damage due to pressure from an icebreaker when towed
- Damage caused by an icebreaker trying to free a trapped ship

The relative percentages of ice damages for bow, midship and stern was 67,23 and 10 respectively.

**Table 5.2.** Percentage of 800 ice accidents on different sections of different routes of the NSR (Lenskiy, 1992)

Route	Section of route	Percentage of accidents
Novaja Zemlya - Jenisey ports	Novaja Zemlya - Beliy Island	28
	Beliy Island - Dikson	46
	Dikson - C.Sopochhnaya Karga	17
	C.Sopochhnaya Karga - Dudinga	9
Dikson - Tiksi	Dikson - West Vilkitskovo Strait	18
	Vilkitskovo Strait	38
	East Vilkitskovo Strait - Tiksi	52
Tiks - Pevek	Tiksi - Indigirka (Laptev Strait)	15
	Tiksi - Indigirka (Sannikova strait)	46
	Indigirka - Pevek	39
Pevek - Bering Strait	Pevek - Cape Billings	30
	Cape Billings - Cape Schmidta	53
	Cape Shcmidta - Bering Strait	17

Since the early seventies the navigation season has been extended. For October-December the numbers of ice damages for ULA, UL, L1 and L3 cargo ships have been 5,11,12, and 1 respectively (Lenskiy, 1992). These figures may be used as a reference for the following analysis.

### 5.3. RESULTS OF THE DAMAGE PROBABILITY CALCULATIONS

Table 5.3 contains the damage probability data and results for the SA-15 ULA class ship in the bow region. The calculations are done for the entire NSR for each month, calculated by sea area. Similar tables for each of the ULA class midship and aftship regions as well as the UL class bow, midship and aftship can be found in Appendix 3. Figures 5.5 to 5.7 show the probability of damage for each month for each sea area for the ULA class ship at the bow, and for the UL class ship at aftship, which is has the highest probability of damage of all cases studied.

Tables 5.4 and 5.5 show the results of the damage probability analysis for one transit through the entire for NSR during each month of the year. Table 5.4 contains the probabilities of damage with extensive icebreaker assistance whereas table 5.5 assumes icebreaker assistance only when the ship cannot proceed without it.

Figures 5.8 to 5.11 show graphically the probability of damage vs. month for the UL and ULA class ships, both with extensive icebreaker assistance as well as icebreaker assistance only when absolutely necessary. Probabilities of less than  $10^{-8}$  have been omitted from the graphs, as the risk in these months is for all practical purposes zero.

From these results, it can be seen that the probability of damage of the ULA class is up to an order of four magnitudes less than that of the UL class. These results also show that icebreaker assistance reduces the probability of damage considerably. The best example of this is with the UL class aftship in July. The probability of damage for an aftship frame decreases from 0.409 without icebreaker assistance to 0.158 with icebreaker assistance. These graphs also show that the probability of a ship being damaged during a transit of the NSR is the highest during the month of May. The probability is the lowest during the month of October for the UL class, but is zero from August to December for a SA-15 ship in the ULA class.

	Jan	Feb	Mar	April	May	June	July	Aug	Sept	Oct	Nov	Dec
	I	II	III	IV	V	VI	VII	VIII	IX	X	XI	XII
h <sub>e</sub> (m)	0,68	0,84	1,06	1,17	1,17	0,74	0,36	0	0	0	0,25	0,46
N <sub>i</sub> (days)	0,97	1,33	2,57	4,00	3,00	0,41	0,08	0,00	0,00	0,00	0,27	0,69
a <sub>i</sub>	0,053	0,053	0,053	0,055	0,045	0,028	0,013	0,000	0,000	0,000	0,031	0,053
m <sub>vy</sub> (kN)	1641,66	1641,66	1641,66	1641,66	1641,66	1641,66	1641,66	1641,66	1641,66	1641,66	1641,66	1641,66
P	0	0	0	0	0	0	0	0	0	0	0	0
h <sub>e</sub> (m)	0,84	1,06	1,24	1,35	1,47	1,17	0,84	0,57	0,25	0,1	0,36	0,57
N <sub>i</sub> (days)	2,54	4,90	1,09	1,00	1,03	6,10	1,02	0,16	0,00	0,17	0,91	1,56
a <sub>i</sub>	0,101	0,101	0,101	0,094	0,103	0,113	0,078	0,034	0,000	0,037	0,094	0,101
m <sub>vy</sub> (kN)	1641,66	1641,66	1641,66	1641,66	1641,66	1641,66	1641,66	1641,66	1641,66	1641,66	1641,66	1641,66
P	0	0	0	0,000128	0,000399	0	0	0	0	0	0	0
P esc.	0	0	0	0	0	0	0	0	0	0	0	0
h <sub>e</sub> (m)	1,19	1,36	1,58	1,71	1,76	1,47	1,19	0,84	0,68	0,25	0,57	0,84
N <sub>i</sub> (days)	2,14	2,21	2,29	2,37	2,17	1,58	9,00	2,00	1,09	1,21	2,76	5,00
a <sub>i</sub>	0,199	0,199	0,199	0,205	0,202	0,194	1,29	0,272	0,234	0,217	0,208	2,02
m <sub>vy</sub> (kN)	1641,66	1641,66	1641,66	1641,66	1641,66	1641,66	1641,66	1641,66	1641,66	1641,66	1641,66	1641,66
P	0	0,000333	0,001509	0,002498	0,002671	0,000612	0	0	0	0	0	0
P esc.	0	0	0	0	0	0	0	0	0	0	0	0
h <sub>e</sub> (m)	1,27	1,5	1,81	1,94	2,05	1,75	1,39	1,09	0,69	0,2	0,69	0,97
N <sub>i</sub> (days)	2,25	2,36	2,57	2,62	2,50	2,02	1,39	3,03	0,76	1,38	3,44	7,07
a <sub>i</sub>	0,209	0,209	0,209	0,215	0,212	0,232	0,242	0,213	0,163	0,265	0,218	2,14
m <sub>vy</sub> (kN)	1641,66	1641,66	1641,66	1641,66	1641,66	1641,66	1641,66	1641,66	1641,66	1641,66	1641,66	1641,66
P	0	0,001074	0,003645	0,005208	0,006399	0,002406	0,0003	0	0	0	0	0
P esc.	0	0	0	0	0	0	0	0	0	0	0	0

Table 5.3. Damage probabilities for SA-15 ULA class ship in the bow region.

	Jan I	Feb II	Mar III	April IV	May V	June VI	July VII	Aug VIII	Sept IX	Oct X	Nov XI	Dec XII
$h_a$ (m)	1,5	1,74	1,92	2,05	2,17	2,17	1,25	0,97	0,68	0,36	0,74	1,09
$N_t$ (days)	1,57	1,65	1,75	1,81	1,89	1,32	9,43	1,89	1,02	1,28	2,86	6,74
Sea Area V							0,90					1,45
$a_i$	0,139	0,139	0,139	0,143	0,157	0,155	0,162	0,190	0,218	0,202	0,162	0,139
$m_{IV}$ (kN)	1641,66	1641,66	1641,66	1641,66	1641,66	1641,66	1641,66	1641,66	1641,66	1641,66	1641,66	1641,66
P	0,000696	0,001873	0,00325	0,004575	0,006126	0,004303	0	0	0	0	0	0
P esc.						0						0
$h_a$ (m)	1,41	1,65	1,84	2,07	2,09	1,65	1,3	0,95	0,7	0,36	0,7	1,11
$N_t$ (days)	1,49	1,60	1,72	1,91	1,72	1,44	1,01	1,76	1,22	1,19	2,44	6,76
Sea Area VI												1,37
$a_i$	0,130	0,130	0,130	0,133	0,131	0,162	0,176	0,177	0,254	0,188	0,151	0,130
$m_{IV}$ (kN)	1641,66	1641,66	1641,66	1641,66	1641,66	1641,66	1641,66	1641,66	1641,66	1641,66	1641,66	1641,66
P	0,000377	0,001341	0,002605	0,005035	0,004732	0,001207	3,69E-05	0	0	0	0	0
P esc.												0
$h_a$ (m)	1,05	1,31	1,5	1,75	1,77	1,44	1,18	0,92	0,73	0,21	0,5	0,8
$N_t$ (days)	6,68	1,99	2,18	2,43	2,16	1,07	3,41	0,95	0,65	0,48	1,56	3,66
Sea Area VII							0,58					
$a_i$	0,168	0,168	0,168	0,155	0,151	0,117	0,097	0,114	0,131	0,091	0,136	0,168
$m_{IV}$ (kN)	1641,66	1641,66	1641,66	1641,66	1641,66	1641,66	1641,66	1641,66	1641,66	1641,66	1641,66	1641,66
P	0	8,84E-05	0,000985	0,002875	0,002714	0,000342	0	0	0	0	0	0
P esc.							0					
P	0,000146	0,000741	0,002019	0,003416	0,003926	0,001579	7,91E-05	0	0	1,11E-16	0	0
P esc.	0,000146	0,000741	0,002019	0,003416	0,003926	0,001579	7,91E-05	0	0	1,11E-16	0	0

Table 5.3. Damage probabilities for SA-15 ULA class ship in the bow region.

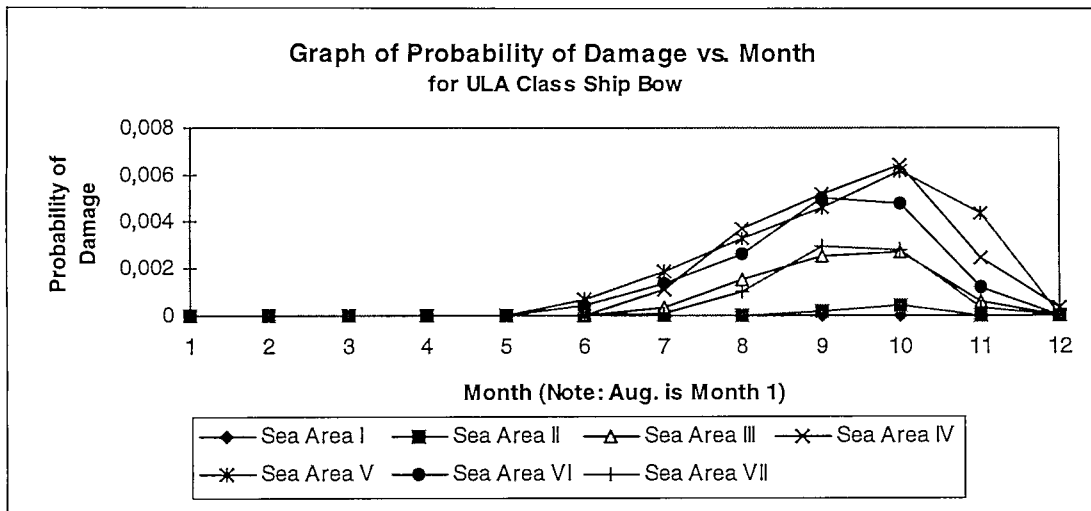


Figure 5.5.

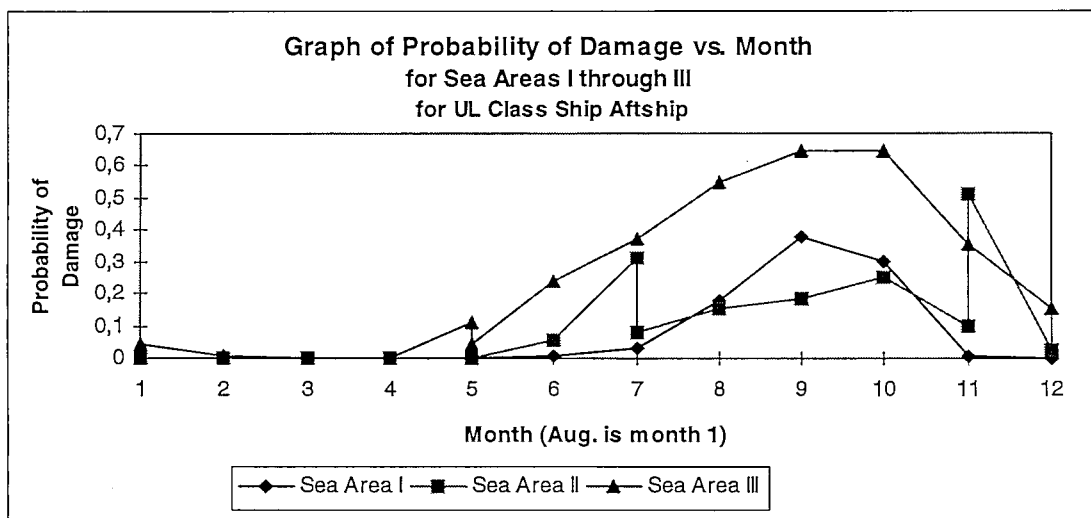


Figure 5.6.

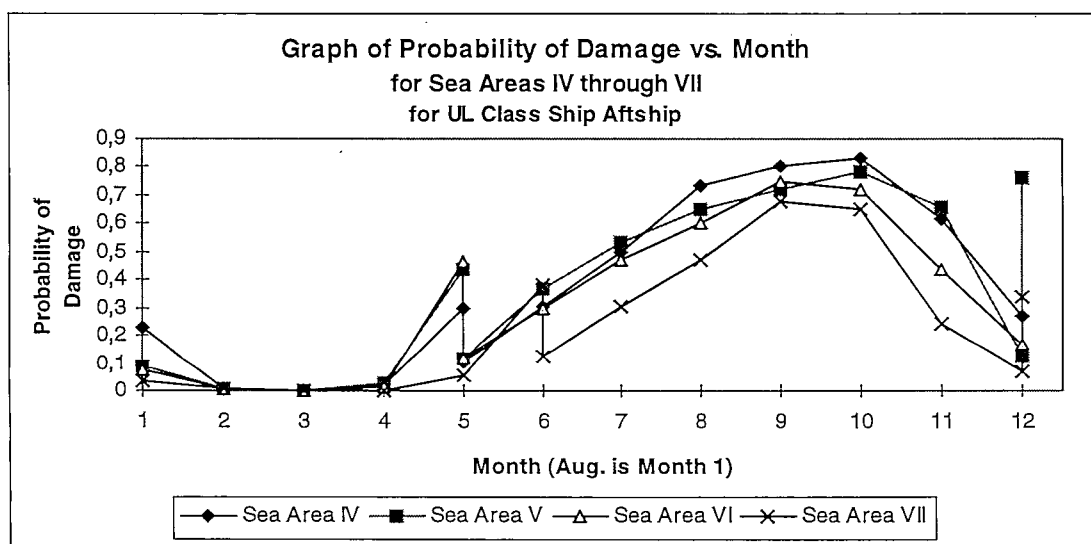


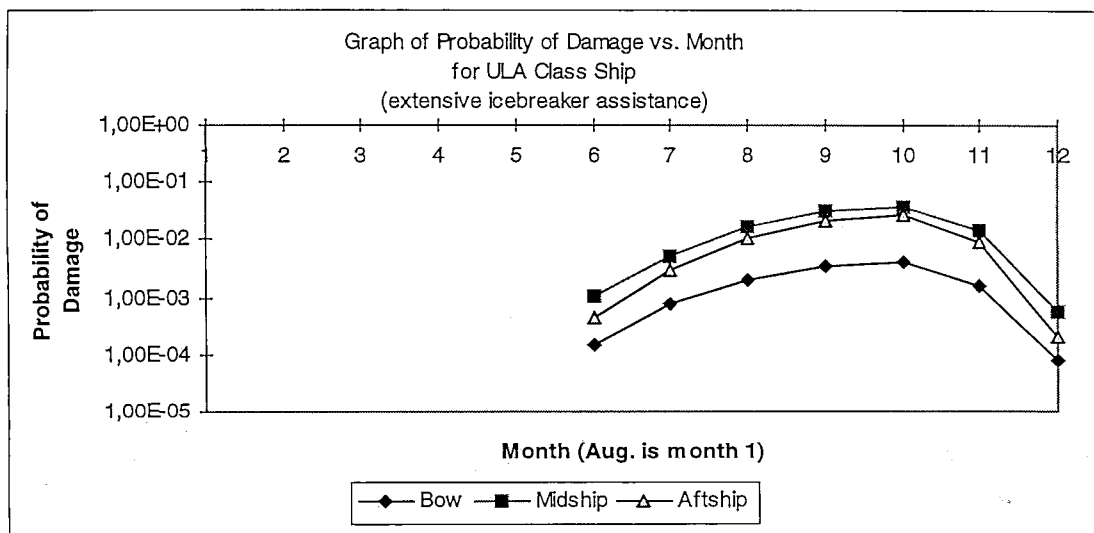
Figure 5.7.

**Table 5.4.** Damage probability for transit with extensive icebreaker assistance.

	ULA Class Bow	ULA Class Midship	ULA Class Aftship	UL Class Bow	UL Class Midship	UL Class Aftship
Aug	0,00E+00	0,00E+00	0,00E+00	6,78E-02	2,31E-02	9,46E-02
Sept	0,00E+00	0,00E+00	0,00E+00	3,16E-03	3,01E-04	6,04E-03
Oct	0,00E+00	0,00E+00	0,00E+00	0,00E+00	0,00E+00	0,00E+00
Nov	0,00E+00	0,00E+00	0,00E+00	6,21E-03	7,68E-04	1,18E-02
Dec	0,00E+00	0,00E+00	0,00E+00	4,95E-02	1,61E-02	7,09E-02
Jan	1,46E-04	1,01E-03	4,31E-04	1,66E-01	8,15E-02	2,28E-01
Feb	7,41E-04	5,28E-03	2,98E-03	2,50E-01	1,67E-01	3,75E-01
March	2,02E-03	1,63E-02	1,05E-02	3,30E-01	2,89E-01	5,36E-01
April	3,42E-03	3,08E-02	2,08E-02	3,97E-01	3,94E-01	6,52E-01
May	3,93E-03	3,73E-02	2,57E-02	3,93E-01	4,12E-01	6,60E-01
June	1,58E-03	1,37E-02	9,10E-03	2,49E-01	2,20E-01	4,22E-01
July	7,91E-05	5,48E-04	1,99E-04	1,18E-01	5,47E-02	1,58E-01

**Table 5.5.** Damage probability for transit with icebreaker assistance only when necessary.

	ULA Class Bow	ULA Class Midship	ULA Class Aftship	UL Class Bow	UL Class Midship	UL Class Aftship
Aug	0,00E+00	0,00E+00	0,00E+00	6,78E-02	2,31E-02	9,46E-02
Sept	0,00E+00	0,00E+00	0,00E+00	3,16E-03	3,01E-04	6,04E-03
Oct	0,00E+00	0,00E+00	0,00E+00	0,00E+00	0,00E+00	0,00E+00
Nov	0,00E+00	0,00E+00	0,00E+00	6,21E-03	7,68E-04	1,18E-02
Dec	0,00E+00	0,00E+00	0,00E+00	1,60E-01	5,88E-02	2,14E-01
Jan	1,46E-04	1,01E-03	4,31E-04	2,00E-01	9,49E-02	2,72E-01
Feb	7,41E-04	5,28E-03	2,98E-03	2,68E-01	1,74E-01	3,99E-01
March	2,02E-03	1,63E-02	1,05E-02	3,30E-01	2,89E-01	5,36E-01
April	3,42E-03	3,08E-02	2,08E-02	3,97E-01	3,94E-01	6,52E-01
May	3,93E-03	3,73E-02	2,57E-02	3,93E-01	4,12E-01	6,60E-01
June	1,58E-03	1,37E-02	9,10E-03	2,88E-01	2,38E-01	4,68E-01
July	7,91E-05	7,67E-04	1,99E-04	3,38E-01	1,69E-01	4,09E-01

**Figure 5.8.**

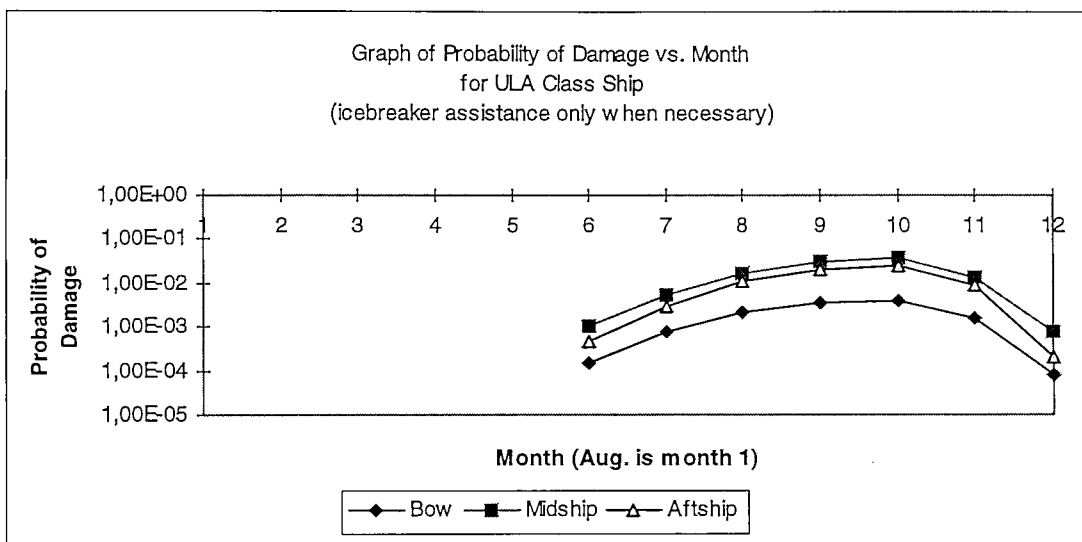


Figure 5.9.

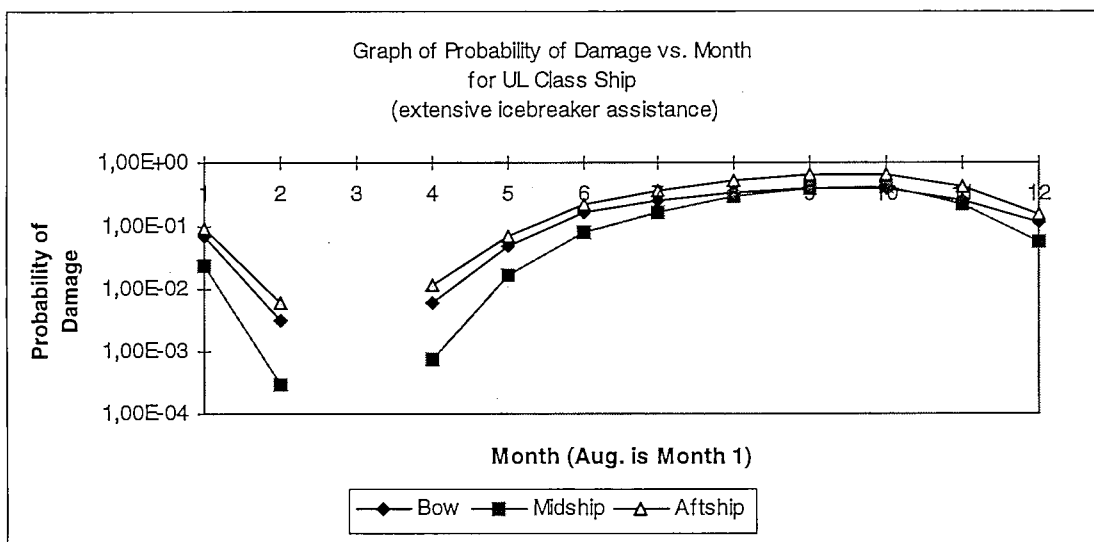


Figure 5.10.

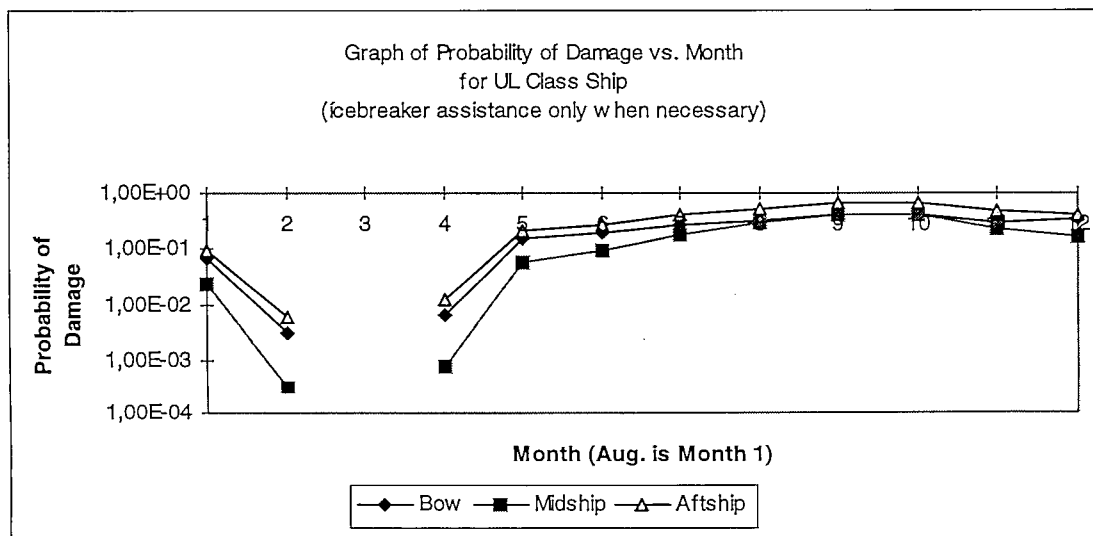


Figure 5.11.



## 6. CONCLUSION

It is exceptional that the NSR can be transited without encountering any ice. This introduces to the navigation a basic uncertainty which has two main components: the transit times cannot be exactly defined and a ship runs a certain risk of ice damage. What can be theoretically attained by modelling are probabilities of transit times and damages. How realistic the calculated values are in practice depends partly on the description of ice conditions. This description involves uncertainties on many levels. The severity of ice conditions vary from year to year; this is described by long term statistics. During one ice season the arrangement of the ice cover into different types, each with its particular effect to navigation, is highly variable in space and time; this local variation is addressed by ice charts and ice forecasts. Within a certain region, however small, the ice properties vary. This variation can be described in terms of probability distributions which are the input to calculate the probability distributions for transit times and ice damages.

The objective of this project is to combine the ice conditions and transit and damage calculations. It has been addressed by many other INSROP reports, too. The special feature of the present approach is that it is from the outset based on the parameterisation of the ice cover by distributions: floe size distribution, ice thickness distribution and ice ridge distributions. As such data on the NSR is lacking, the main contribution of the report is on the methodological side rather than on the calculation of operatively applicable transit times and damage probabilities. The theory is running ahead of the data, showing what data should be collected.

The weakest link of the present approach is still the characterisation of ice conditions. The vast data resources of AARI are opening and this will greatly increase the data coverage both in time and space. However, this data is bound to be of conventional type, that is, probabilities of typical thickness, concentration and floe size on a certain area at a certain time. This situation will remain until geophysical ice models and theories of ice cover morphology attain such a maturity and unification that the standardisation, in a way analogical to WMO ice code, of sea ice description in terms of distributions becomes feasible.

The problems of ice codes was addressed in Chapter 3 and outlined how these should be developed. The basic distributions to describe sea ice morphology were given. What distribution models should be used is largely unsettled, due to the sparsity of the data. The theory of ice ridge distributions has attained some convergence towards a limited set of possible models, but not so for floe size and ice thickness distributions. The determination of these should be included to the routine of ice services, especially as ice floe sizes can be quantified semiautomatically from imagery. Also the operational monitoring of ice thickness distribution is becoming reality (Hautaniemi et al. 1994).

Transit calculations for the NSR were reported in Chapter 4. The approach was kept as simple as possible due to the coarseness of the ice cover description. HUT Ship Laboratory has been developing a transit simulation model which describes the ice cover in terms of distributions and gives as an output the probabilities of different

transit times, together with the probability that the ship gets stuck. The ship parameters can be freely chosen. This kind of approach uses Monte Carlo simulation to create the ice conditions and thus gives as an output probability distributions. Before these can be used they must be related to input ice condition distributions. This work is not complete yet. Thus a simpler approach to transit analysis was adopted here. It is based on calculating the average conditions the route using an equivalent rubble ice thickness. The results of the transit calculations for SA-15 class ship are, however, comparable to the reported transit times. Transit time attains a minimum in October and icebreaker assistance, even during the melting season, improves the transit times. From January to July SA-15 cannot proceed through at least one of the sea areas of the NSR without assistance.

The damage probabilities for SA-15 ships strengthened to ULA or UL class ships were calculated in chapter 5. These mirror the seasonal and regional variation in ice conditions and also the transit times. The parameters needed in the calculations were obtained by assuming that the variation in ice thickness follows the same statistics as in the Baltic. These data are lacking from the ice data available. It was found that the damage probability for the SA-15 ship ULA class is up to four magnitudes less than that for the SA-15 in UL class. The highest and lowest damage probabilities occur in during May and October respectively. From August to December the damage probability for the ships in ULA class is virtually zero.

The future development of the approach points towards a simulation package including both transit and damage calculations and accepting any ice conditions and ship parameters as an input. This kind of a system has three distinct applications. Firstly, it can be used as a tool during preliminary phases of ship design. Secondly, given the probabilities of various ice conditions in a certain sea area the simulation package can output the probabilities of transit parameters and damage and answer questions like 'what is the probability that the transit time exceeds n days?'. Finally, used as a tool when a ship is navigating through ice and the ice chart or ice forecast is available, the simulation can estimate the optimal route as a suitable combination of minimal transit time and minimal damage probability or forecast the need of icebreaker assistance in a certain area. Also the probabilities of the time of arrival to the next way point will be obtained. This would mean the real time case-by-case determination of the 'ice regime'.

To attain this, however, a new policy towards the description of ice conditions is required. Presently this is feasible for the third case, ice navigation, as the local properties of ice cover can be derived from satellite images delivered on board in almost real time.

## ACKNOWLEDGEMENTS

The developments in Chapter 2 are based on work done as part of the joint project 'Ice State' by Helsinki University of Technology, Nansen Environmental and Remote Sensing Center, Scott Polar Research Institute, University of Helsinki and University of Iceland, funded by the European Commission through the Marine Science and Technology programme 1994-1998, MAST III (Contract No MAS3-CT95-0006).

## REFERENCES:

- AES 1994. MANICE. Manual of standard procedures for observing and reporting ice conditions. 8th edition. Canada. Atmospheric Environment Service. Ice Services Branch, Ottawa, Ontario, Environment Canada, Ice Centre.
- Anderson, M., Crane, R. and Barry, R. 1985. Characteristics of Arctic Ocean ice determined from SMMR data for 1979. *Adv. Space Res.* 1985, 257-261.
- Anderson, M. 1987. The onset of spring melt in first-year ice regions of the Arctic as determined from scanning multichannel microwave radiometer data for 1979 and 1980. *Journal of Geophysical Research*, 92, pp. 13153-13163.
- Arctic Ocean Atlas 1980. The Soviet Defence Ministry, Leningrad. 1984 p.
- Ang, H-S. and Tang, H. 1984. Probability concepts in engineering, planning and design, vol II. John Wiley and Sons.
- Arctic Ocean Atlas 1980. The Soviet Defence Ministry, Leningrad.
- Barnett, D. 1991. Sea ice distribution in the Soviet Arctic. In: *The Soviet Maritime Arctic*, ed. L. Brigham, Naval Institute Press, Annapolis, USA, pp. 47-62.
- Barr, W. and Wilson, E. 1985. The shipping crisis in the Soviet eastern Arctic at the close of the 1983 Navigation Season. *Arctic* 38/1, pp. 1-17.
- Baskin, A. and 18 others 1995. Content of database. Insrop Working Paper I.4.1. No 26.
- Bovin, A. and 8 others 1995. Planning and risk assessment. Volume 1 - 1993 project work. Insrop Working Paper I.5.5 no 23.
- Bretskin, S. and 9 others 1995. Content of database. Insrop Discussion Paper 1.4.1., 18 April 1995.
- Brovin, A., Frolov, S., Fedyakov, V., Likhomanov, V., Timofeev, O., Stepanov, I., Karavanov, S. and Glebko, Yu. Planning and risk assessment. Volume I - 1993 project work. Insrop Working paper I.5.5, No.23.
- Coon, M., Hall, R. and Pritchard, R. 1977. Prediction of Arctic ice conditions for operations. Offshore technology conference, OTC, Houston, pp. 307-314.
- Courseaux and Kerebel 1992. *Le Passage du Nord-Est. Projet de Fin D'Etudes*, Ecole Militaire de la Flotte, 61. p.
- Daley, C., Riska, K. (1992). Review of ship-ice interaction mechanics. Helsinki University of Technology, Ship Laboratory Report Series M-102.
- Department of the Navy, 1970. *Oceanographic Atlas of the Polar Seas, Part II, Arctic*. Oceanographic Office, Publ. no 705.

Doronin, Y and Kheisin, D. Sea ice. Amerind publishing company, New Delhi, India, 323 p.

Gorbunov, I.U. 1979: Grounded ice hummocks in the southeastern part of the Laptev Sea [in Russian]. Poles-North-76 (scientific results), Part 2, Gidrometeoizdat, Leningrad, pp. 107-110.

Grishchenko, V., Yakshevitch, E., Kostychenko, O., Smirnov, V., Stepanov, V. and Yegorov, L. 1995. Design of information system. Insrop Working Paper I.3.4. No 25.

Hagen, D.L. and Jones, S.J. 1996. Evaluation of the Northern Sea Route using the Ice Regime Shipping Control System. Insrop Working Paper I.2.2. No 32.

Hautaniemi, H., Oksama, M., Multala, J., Leppäranta, M., Riska, K. and Salmela, O. 1994. Airborne electromagnetic mapping of ice thickness in the Baltic Sea. Proc. IAHR Ice Symposium 1994, Vol. 2, p. 530-539. The Norwegian Institute of Technology, Trondheim, Norway.

Hibler, W.D. and Ackley, S.F. 1975. Height variation along sea ice pressure ridges and the probability of finding 'holes' for vehicle crossing. Journal of Terramechanics 12 (3/4), pp. 191-199.

Holtrop, J. and Mennen, G. 1984. A statistical Power Prediction Method. International Shipbuilding Progress.

Ice rules 1985. Finnish-Swedish ice class rules 1985. Board of Navigation. Helsinki. 43 p.

Iurev, B. 1935. Ice conditions and Navigation in the Estuary of the Pechora River [in Russian]. In Uste Reki Pechory, Sevgosmorparokhodstvo, Archangel, pp. 92-104.

Johannessen, O.M., Sandven, S., Kloster, K., Melentyev, V.V. and Bobylev, L. 1996. Ice monitoring by Non-Russia satellite data. Phase II. Pilot demonstration. Insrop Working paper I.4.2, No. 38

Judge, S, 1958. The Kara Sea. Marine Observer, 28/182, pp. 206-209.

Kjerstad, N. (1995). Routing, communication and IT-Customizing, Vol 2. Insrop Working Paper I.1.1. No. 14.

Kujala, P., Results of long-term measurements on board chemical tanker Kemira in the Baltic Sea during the winters 1985 to 1988. *Winter Navigation Research Board. Report 47*. Helsinki, 1989. 55 p. + app. 137 p.

Kujala, P., Safety of ice-strengthened ships in the Baltic Sea. *Royal Institution of Naval Architects. Transactions*. London, 1991, Pp 83-97.

- Kujala, P., Goldstein, R., Osipenko, N. and Danilenko, V. (1991). A ship in compressive ice, preliminary model test results and analysis of the process. Helsinki University of Technology, Ship Laboratory Report Series M
- Kujala, P., Sundell, T. (1992). Performance of ice-strengthened ships in the northern Baltic Sea in winter 1991. Helsinki University of Technology, Ship Laboratory Report Series M-117.
- Kujala, P. 1994. On the statistics of ice load on ship hull in the Baltic. *Acta Polytechnica Scandinavica, Mechanical Engineering Series No. 116*, 98 p.
- Kujala, P., Tuhkuri, J., Varsta, P., Ship-ice contact and design ice loads. Paper presented at *IceTech'94*, March, Calgary, 1994.
- La Prairie, D., Wilhelmson, M., Riska, K. and Petten, J. 1995. A transit simulation model for ships in Baltic ice conditions. First revision of the Ship Laboratory M-series report 200, Helsinki University of Technology.
- Lensu, M 1989. Ice floe distributions. Proceedings of POAC, 10th international conference on port and ocean engineering under arctic conditions, Vol. 1, 354-366.
- Lensu, M 1990. The fractality of sea ice cover. Proceedings of the 10th IAHR ice symposium, Espoo, Finland, Vol. 1, pp. 300-313.
- Lensu, M. 1995. The analysis of laser profilometer data. AEM flights in the Baltic, winter 1994. Helsinki University of Technology, Ship Laboratory Report Series M-195.
- Lensu, M. 1995b. Ridge link distributions. Proceedings of 13th international conference on port and ocean engineering under arctic conditions (POAC'95), Murmansk, Russia. Vol 3 (to appear).
- Lenskiy, L. (1992). Damage statistics on ships sailing the Northern Sea Route. Proceedings of NNF symposium on Arctic Navigation, Tromsø, Norway.
- Leppäranta, M. and Hakala, R. 1992. The structure and strength of first-year ice ridges in the Baltic Sea. *Cold Regions Science and Technology* 20, 295-311.
- Leppäranta, M., Lensu, M., Kosloff, P. and Veitch, B. 1995. The life story of a first year sea ice ridge. *Cold Regions Science and Technology* 23, 279-290.
- Lindqvist, G. ( ). A straightforward method for calculation of ice resistance of ships. Wärtsilä Marine Industries - Arctic Sea Transportation; Helsinki.
- Løset, S. and Vefsnmo, S. 1994. Content of database, planning and risk assesment. Insrop Working paper I.5.1, No. 5.
- Løvås, S.M., Smith, C. and Moe, K.A. (1994). Design and development of information system. Insrop Working paper I.3.1 & II.3.1, No. 4.

Makarov, E. and 6 others 1995. Operational Information on nature conditions. Insrop Working Paper I.2.1, No. 24.

Malmberg, S (1983). On the phenomenon of getting stuck in ice. M.Sc. thesis, Helsinki University of Technology, Espoo.

Matsushita, M. 1985. Fractal viewpoint of fracture and accretion. J. of the Physical Society of Japan 54 (3) 857-860.

Mock, S.J., Hartwell, A.D. and Hibler, W.D., III 1972. Spatial aspects of pressure ridge statistics, J. Geophys. Res. 77 (30) p. 5945-5953.

Mulherin, N., Sodhi, D. and Smallidge, E. 1994. Northern Sea Route and icebreaking technology, an overview of current conditions. US Army Corps of Engineers, June 1994.

Naval Oceanography Command Detachment 1986: Sea Ice Climatic Atlas, Vols. 2 and 3, Asheville, NC NAVAIR 50-1C-541/2.

Nikolaeva, A. and Shesterikov, N. 1976. Method of calculation of ice conditions (on the examples of the Laptev Sea). Amerind Publishing company, New Delhi, India.

Ochi, K.M., Applied Probability and Stochastic Processes in Engineering and Physical Sciences. John Wiley&Sons. New York, 1990. 499 p.

Parmeter, R. and Coon, M. 1973. Mechanical models of ridging in the Arctic sea ice cover. AIDJEX Bulletin 19, pp 59-112.

Poznyak, I.I. and Ionov, B.P., The division of icebreaker resistance into components. *Proc. SNAME STAR Symp.*, Ottawa, 1981.

Riska, K. (1995). Performance requirements for ships in the Baltic. Helsinki University of Technology (to be published).

Riska, K. and Salmela, O. 1994. Description of ice conditions along the North-East Passage. Helsinki University of Technology, Ship Laboratory report series M-192.

Romanov, I. (1991). Ledjanoi Pokrov Arktitseskogo Basseina [Ice cover of the Arctic Basin]. Arctic and Antarctic Institute, Leningrad, 212 p.

Romanov, I. (1993). Atlas of morphometric characteristics of ice and snow in the Arctic basin. St.Petersburg.

WMO 1970/1985. WMO Sea-Ice nomenclature, WMO - No. 259. TP.145. Geneva.

Riska, K. Kujala, P., Goldstein, R. Danilenko, V. and Osipenko, N. (1995). Application of results from 'A ship in compressive ice' research project to ship operability. Helsinki University of Technology and Russian Academy of Sciences.

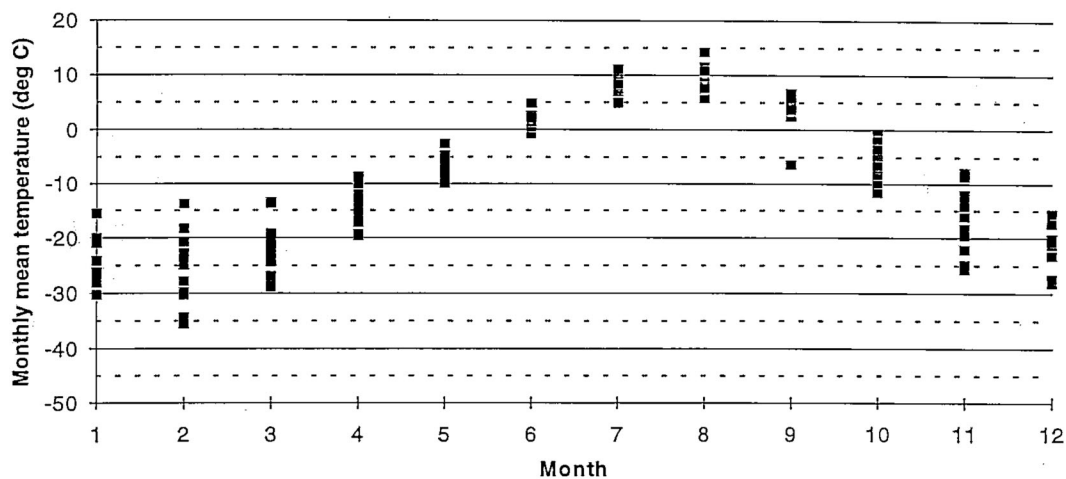
- Sackinger, W.M. (1992). The ice conditions in the eastern part of the Northern Sea route. *International Challenges* 75.
- Sanderson, T. 1986. *Ice mechanics: Risks to Offshore Structures*. Graham and Trotman, London, UK, 253 p.
- Sandven, S. and Kloster, K. 1994. Ice monitoring by Non-Russia satellite data. Phase I. Feasibility study. *Insrop Working paper I.4.2, No. 3*.
- Schneekluth, H. (1987). *Ship design for efficiency and economy*. Butterworth & Co, London.
- Subcommittee 1989. Proposals for the revision of the Arctic shipping pollution prevention regulations. Report of the Sub-committee for Canadian Coast Guard, December 1989, TP 9981.
- Thorndike, A.S., Rothrock, D.A., Maykut, G.A. and Colony, R. (1975). The thickness distribution of sea ice. *J. Geophys. Res.* 80(300): 4501-4513.
- Torrens, Diana L. (1994). Marine insurance for the Northern Sea Route Pilot Study. *Insrop Working paper IV.3.3., No. 1*.
- Wadhams, P. and Davy, T. 1978. On the spacing and draft distributions for pressure ridge keels. *J. Geophys. Res.* 91 C9, 10697-10708.
- Wadhams, P. (1981). Sea ice topography of the Arctic Ocean in the region 70°W to 25°E. *Phil. Trans. Roy. Soc., Lond.* A302 (1464), 45-85, 1981.
- Wadhams, P. (1990). Evidence for thinning of the Arctic ice cover north of Greenland. *Nature, Lond.*, 345, 795-797.
- Wadhams, P. (1992). Sea ice thickness distribution in the Greenland Sea and Eurasian basin, May 1987. *J. Geophys. Res.* 97(C4), 5331-5348.
- Vefnsmo, S., Løvås, S.M., Backlund, A. and Ranki, E. Content of database, planning and risk assesment. Volume 2 - 1994 project work. *Insrop Working paper I.5.1, No. 35*.
- WMO 1985. *WMO Sea-Ice nomenclature*, World Meteorological Organization, Reference publication. WMO/OMM/BMO No. 259.
- Zakharov, V.F., Baskin, A., Alekseyev, G.V. and Buzyev, A.Ya. 1995. Perspective research (1994 project work). *Insrop Discussion Paper I.7.1, 4. August 1995*
- Zubov, N. 1945. *Arctic Ice*. Northern Sea Route Administration, Moscow, USSR. Translated by the U.S. Naval Oceanographic Office, Washington D.C.

## **APPENDIX 1.**

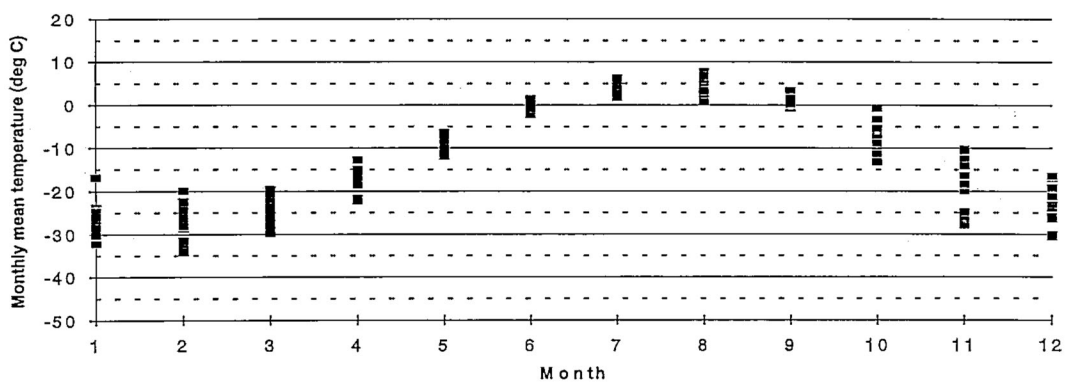
### **Monthly mean temperatures on five weather stations**



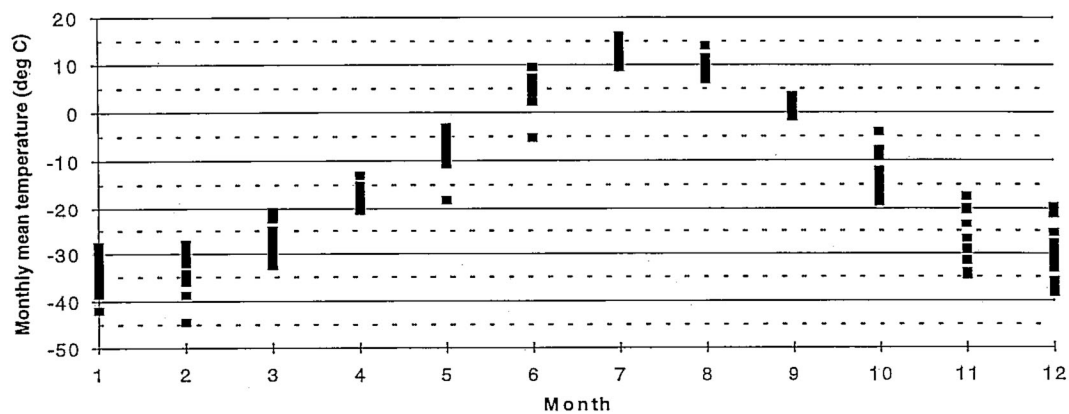
Monthly mean temperature 1967-1981 Mys Kamennii



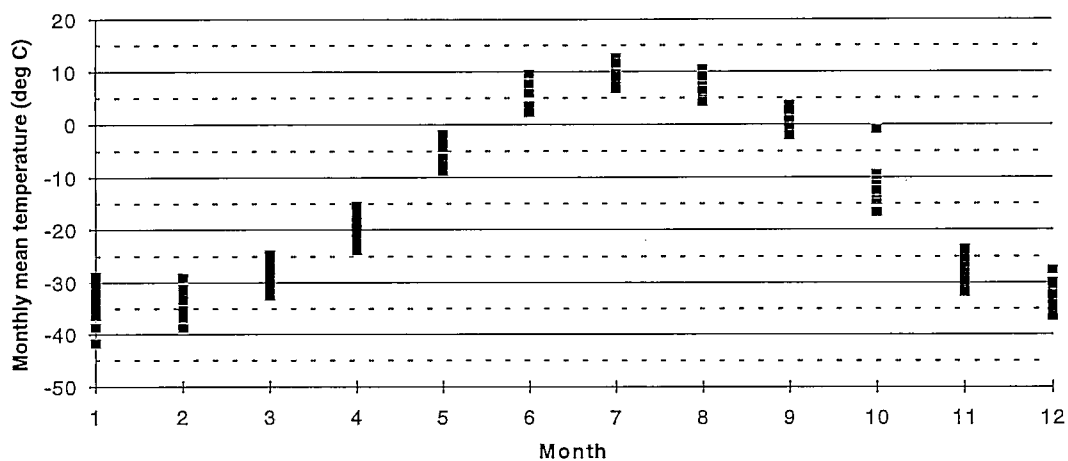
Monthly mean temperature 1967-1981 Ostrov Dikson



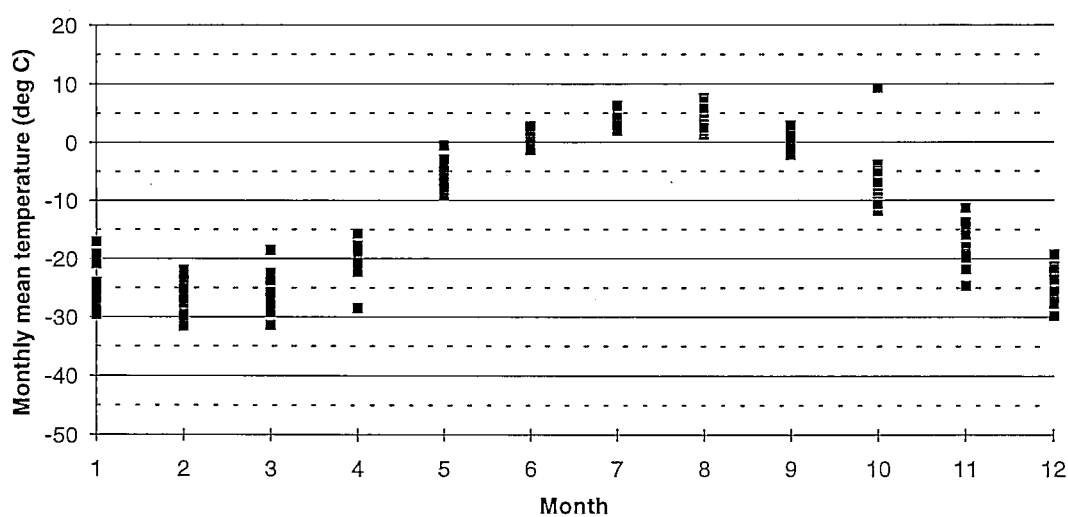
Monthly mean temperature 1967-1981 Hatanga



Monthly mean temperature 1967-1981 Zhokurdah



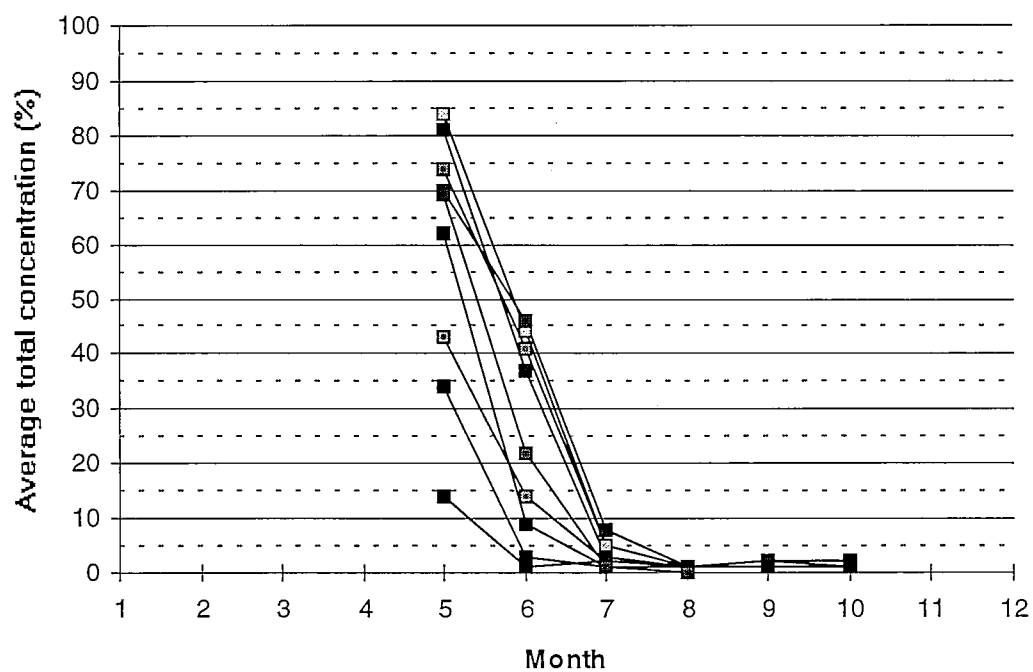
Monthly mean temperature 1967-1981 Mys Shmidt



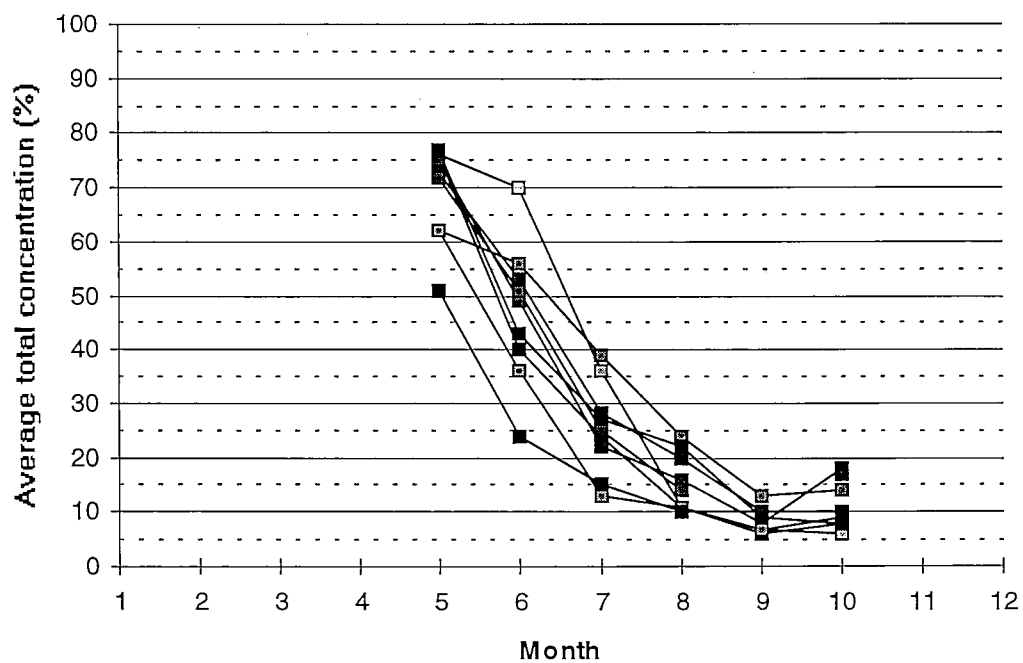
## **APPENDIX 2.**

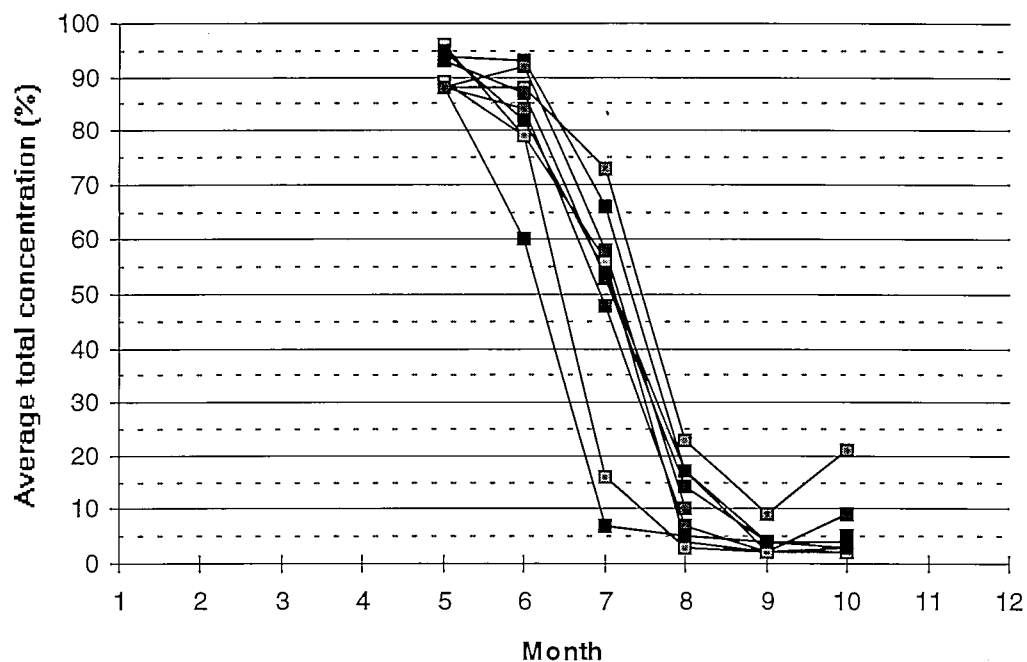
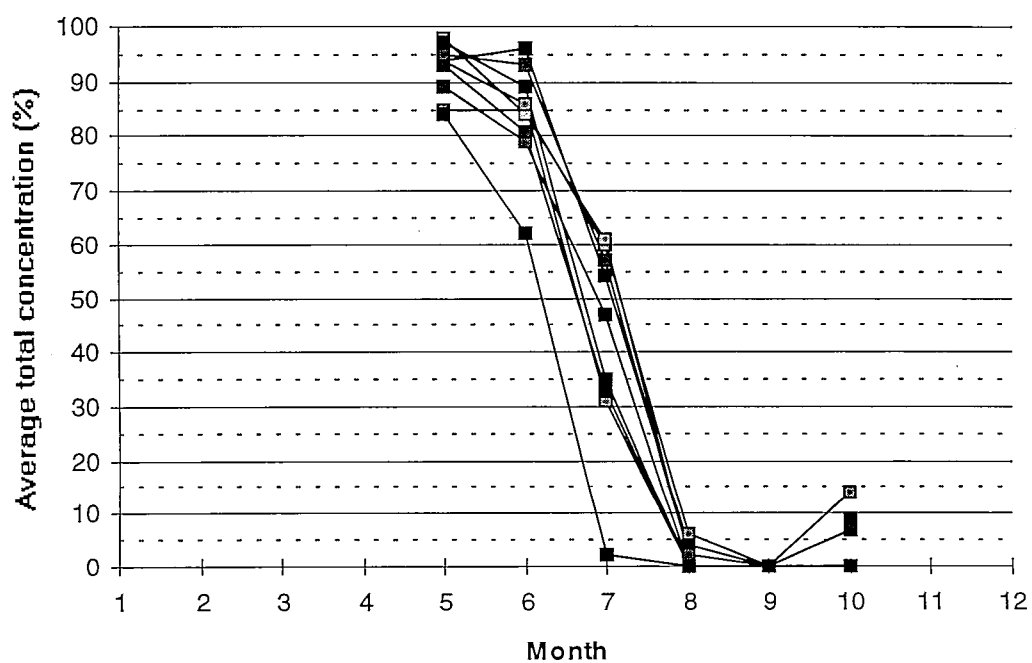
**Sectionwise monthly concentrations along the NSR.**

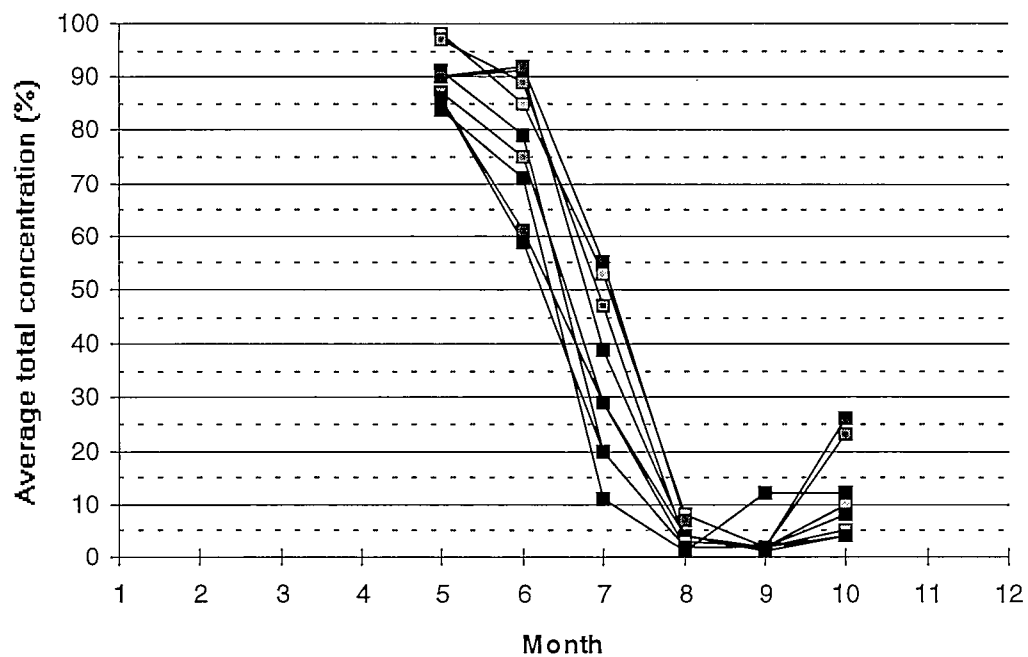
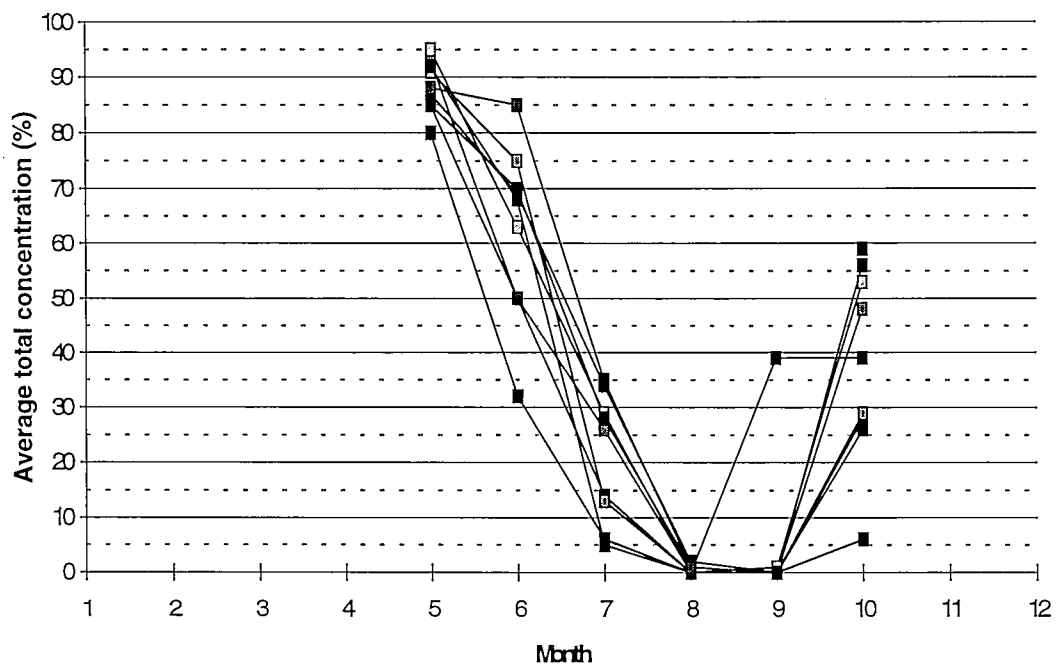
Average total concentration of section 3, 1978-87



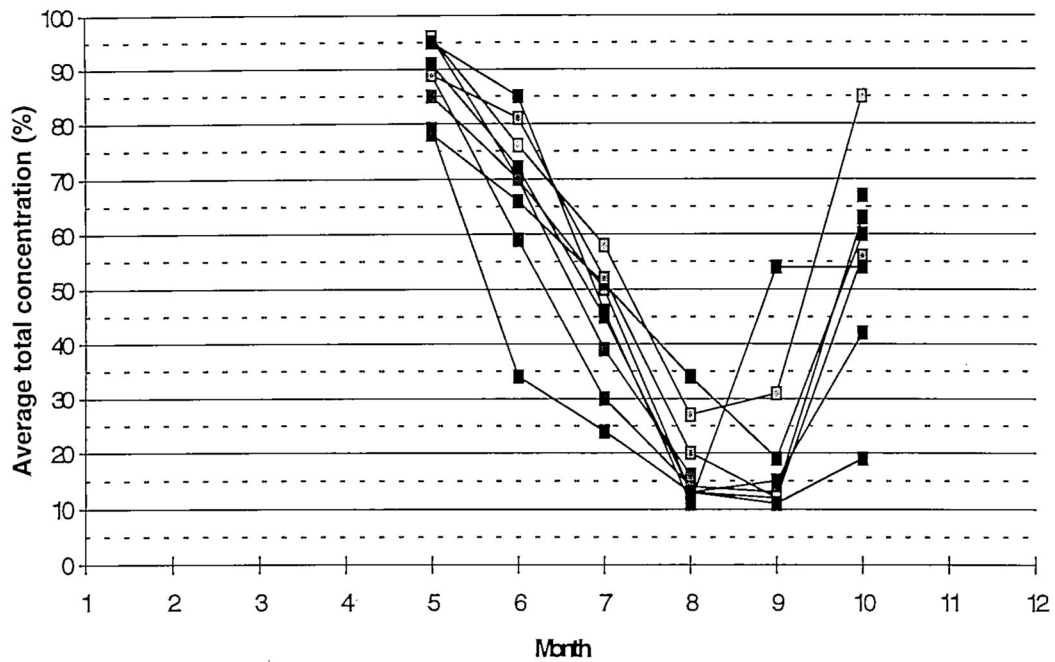
Average total concentration of section 4, 1978-87



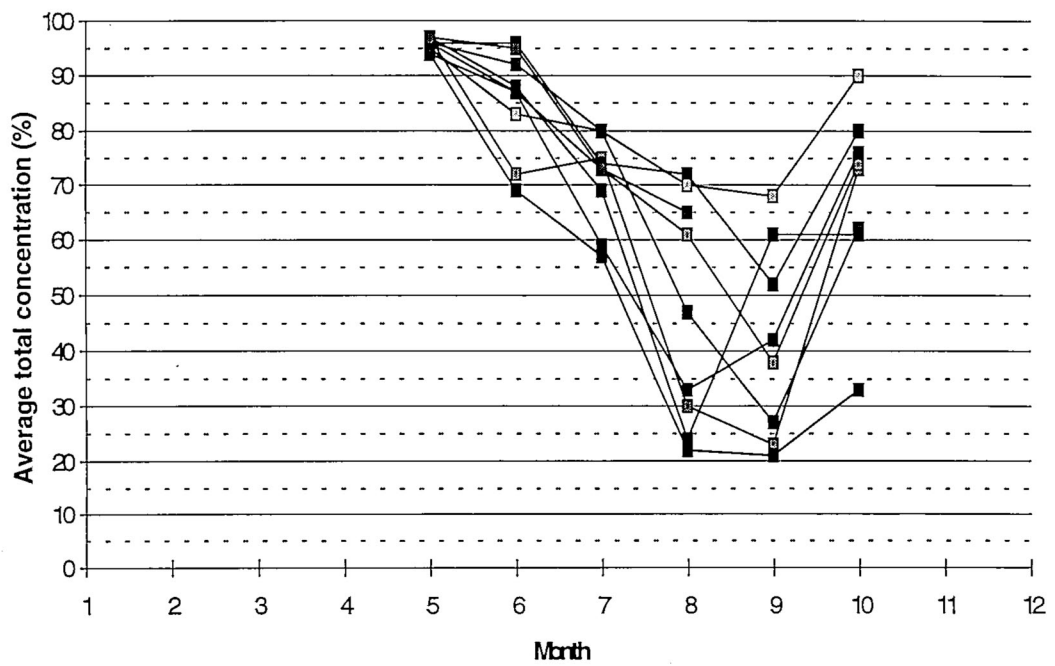
**Average total concentration of section 5, 1978-87****Average total concentration of section 6, 1978-87**

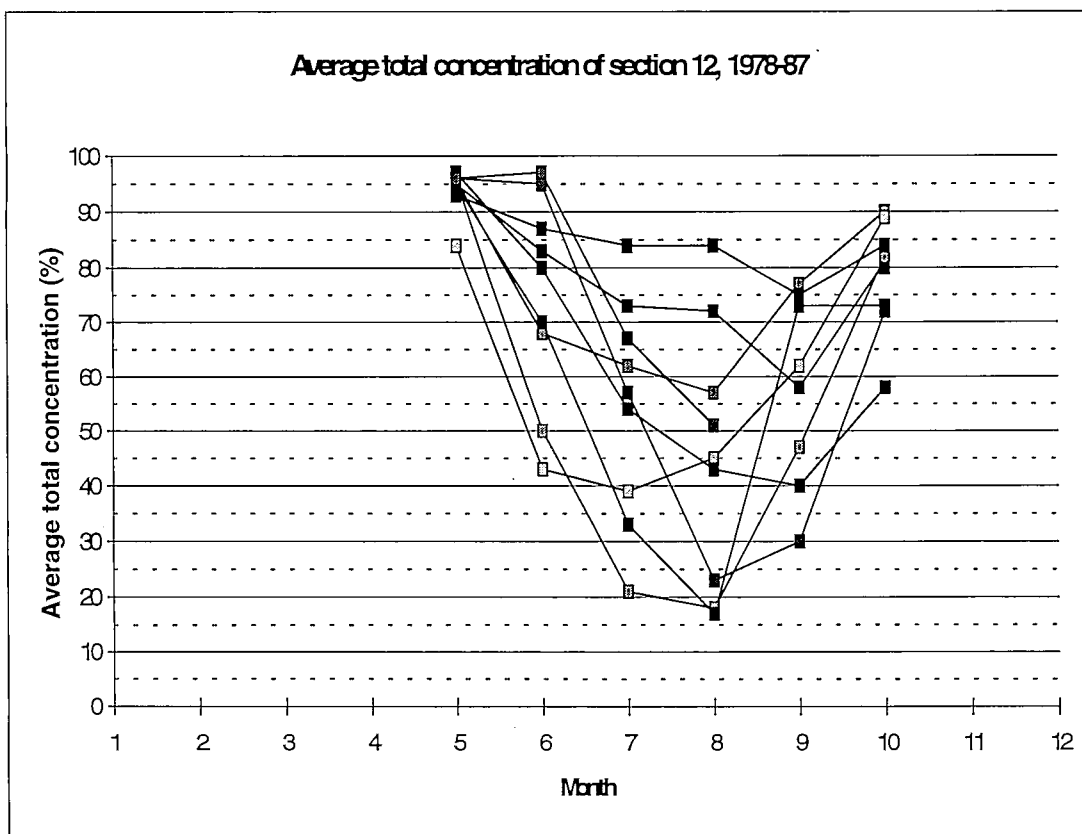
**Average total concentration of section 7, 1978-87****Average total concentration of section 8, 1978-87**

Average total concentration of section 9, 1978-87



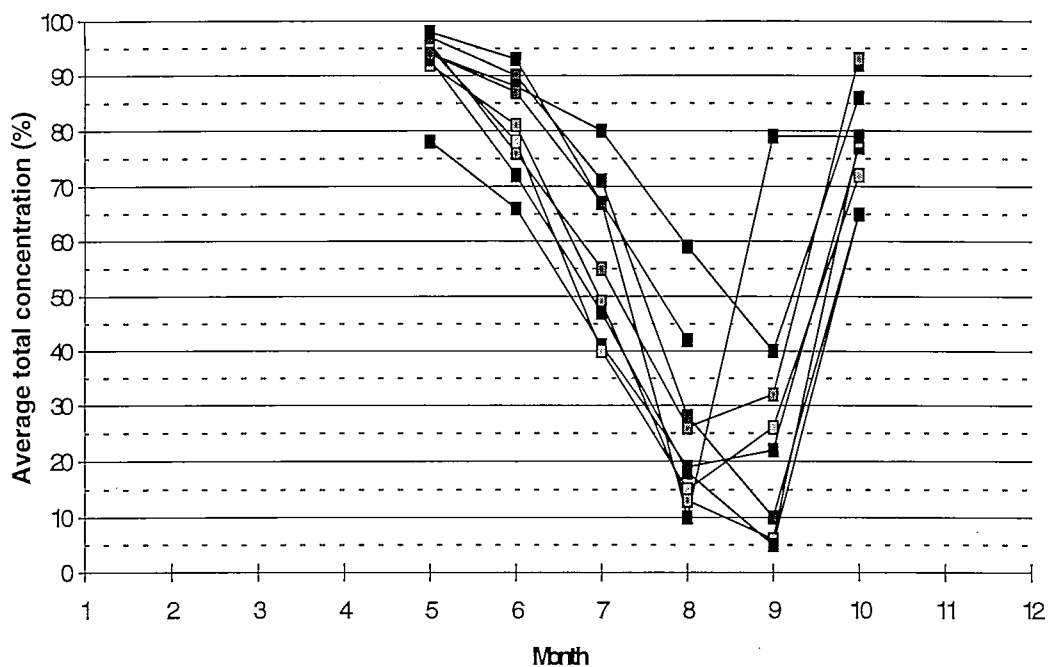
Average total concentration of section 10, 1978-87



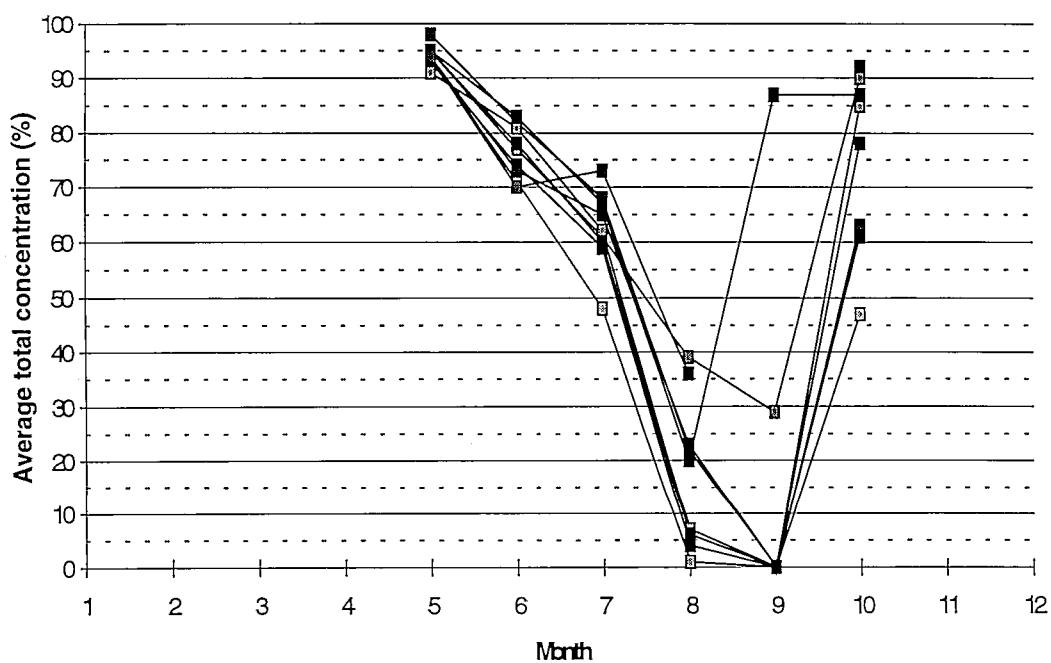


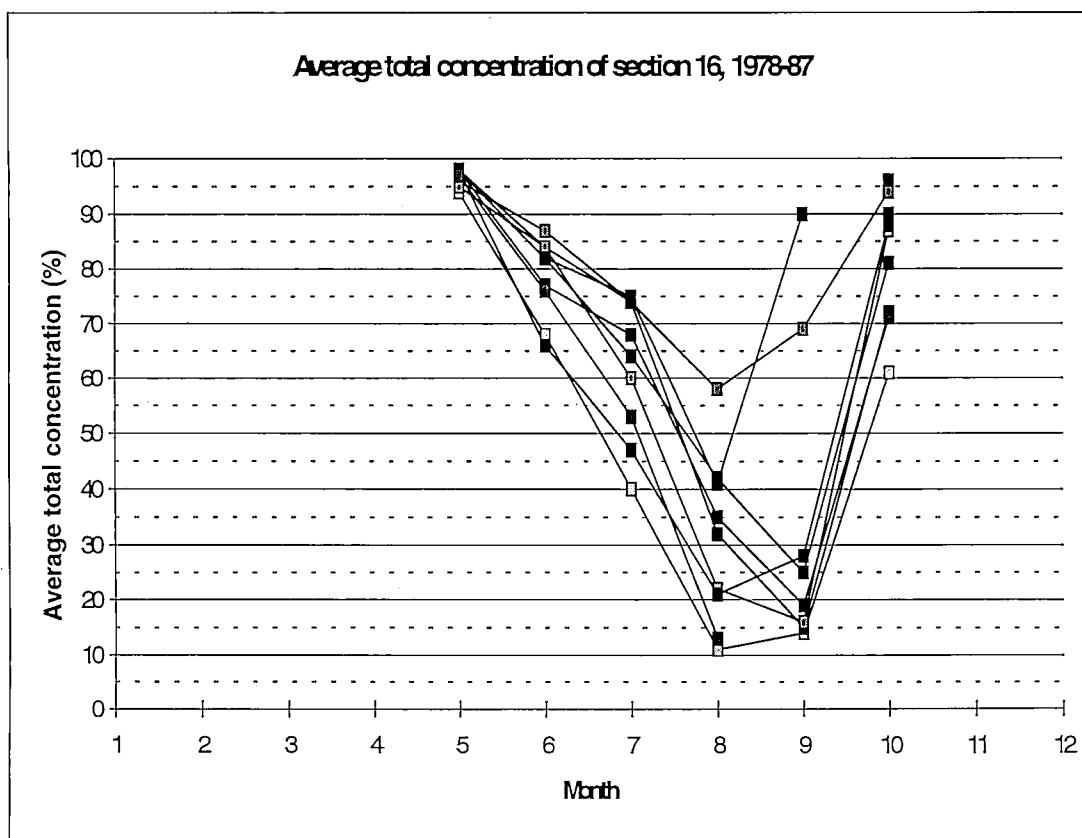
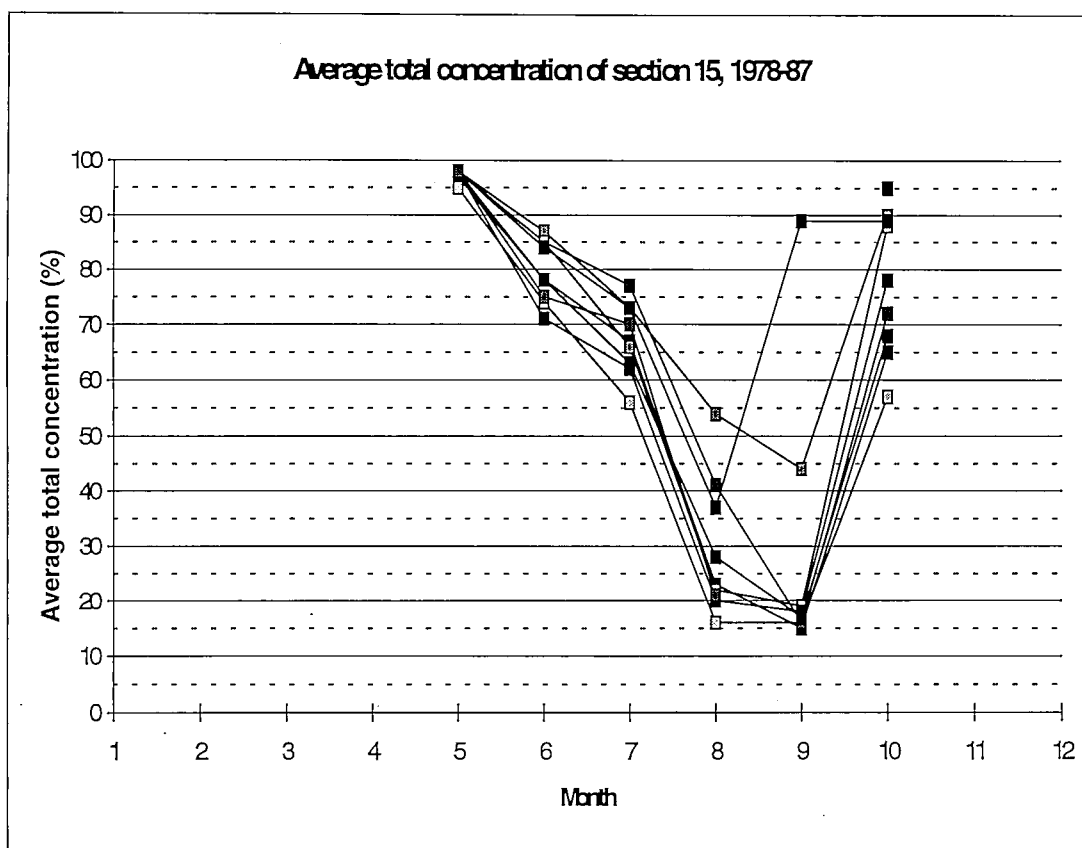


Average total concentration of section 13, 1978-87

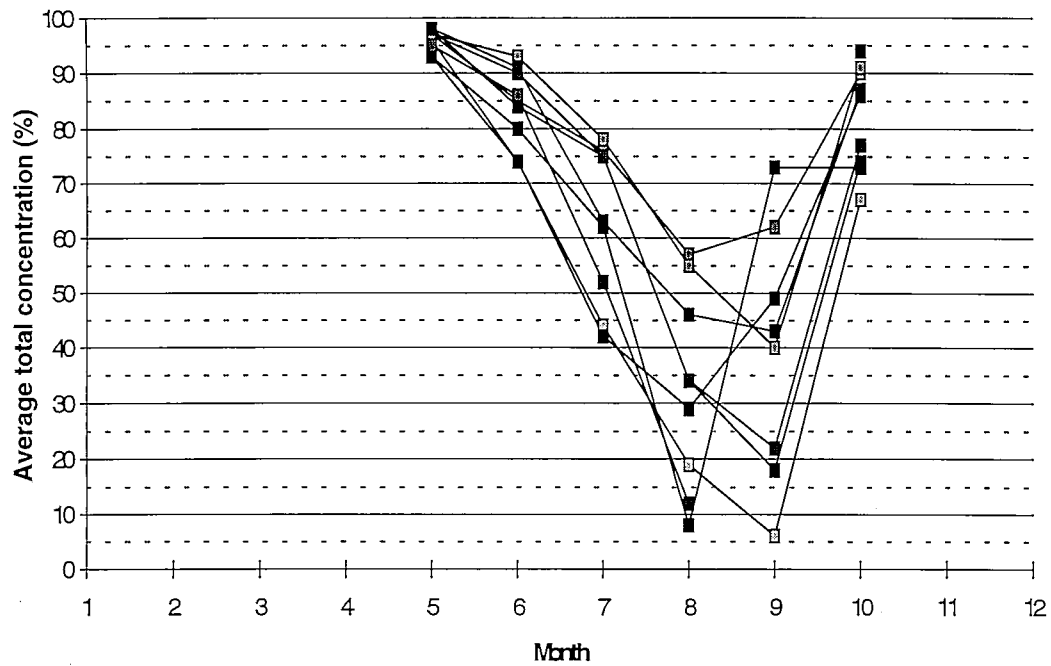


Average total concentration of section 14, 1978-87

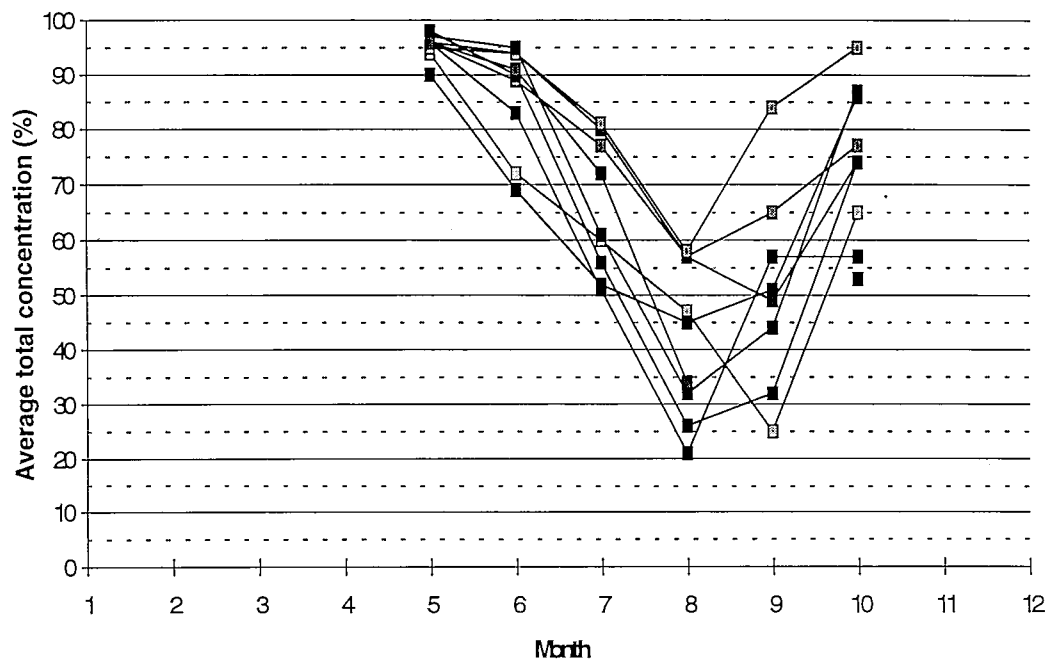


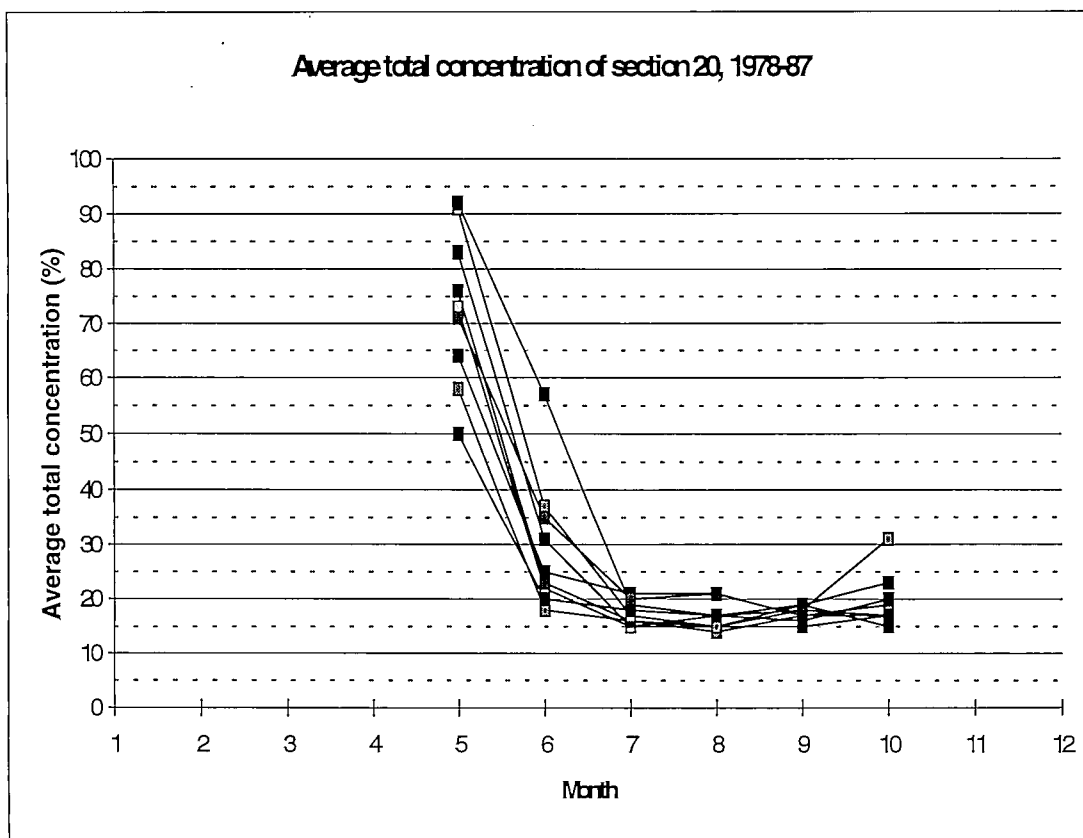
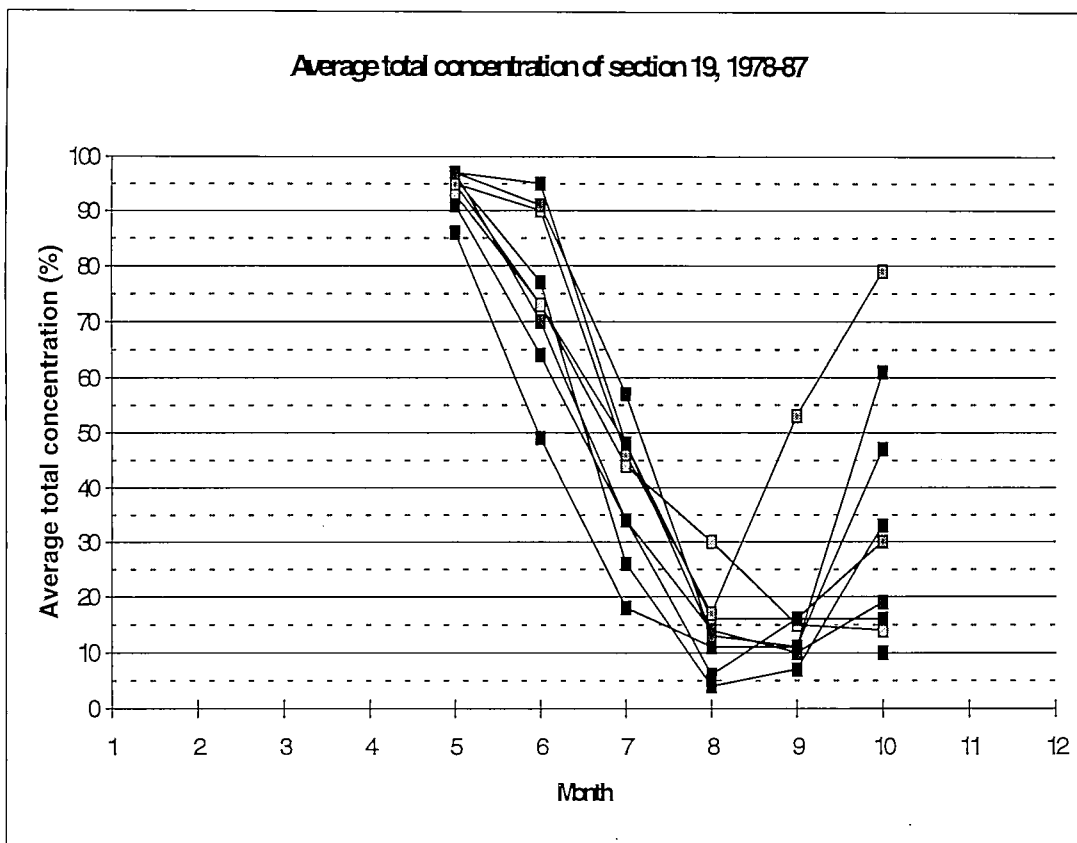


Average total concentration of section 17, 1978-87



Average total concentration of section 18, 1978-87





## **APPENDIX 3.**

### **The damage probability tables**

## UL Bow

	Jan I	Feb II	Mar III	April IV	May V	June VI	July VII	Aug VIII	Sept IX	Oct X	Nov XI	Dec XII
Sea Area I	$h_e$ (m) 0,68 0,97 0,053 709,82 0,002732	0,84 1,33 0,053 709,82 0,01884	1,06 2,57 0,053 709,82 0,13175	1,17 4,00 0,055 709,82 0,298115	1,17 3,00 0,045 709,82 0,233169	0,74 0,41 0,028 709,82 0,002351	0,36 0,08 0,013 709,82 0	0 0,00 0,000 709,82 0	0 0,00 0,000 709,82 0	0 0,00 0,000 709,82 0	0,25 0,27 0,031 709,82 0	0,46 0,69 0,053 709,82 0
Sea Area II	$h_e$ (m) 0,84 2,54 0,101 709,82 0,03558	1,06 4,90 0,101 709,82 0,235931 0,056557	1,24 1,09 0,101 709,82 0,115284	1,35 1,00 0,094 709,82 0,133402	1,47 1,03 0,103 709,82 0,158595	1,17 6,10 0,113 709,82 0,416906 0,073048	0,84 1,02 0,078 709,82 0,014387	0,57 0,16 0,034 709,82 3,58E-05	0,25 0,00 0,000 709,82 0	0,1 0,17 0,037 709,82 0	0,36 0,91 0,094 709,82 0	0,57 1,56 0,101 709,82 0,000358
Sea Area III	$h_e$ (m) 1,19 2,14 0,199 709,82 0,184801	1,36 2,21 0,199 709,82 0,2763	1,58 2,29 0,199 709,82 0,350161	1,71 2,37 0,205 709,82 0,397252	1,76 2,17 0,202 709,82 0,384794	1,47 1,58 0,194 709,82 0,232348	1,19 9,00 1,29 0,231 709,82 0,576058 0,115377	0,84 2,00 0,272 709,82 0,028126	0,68 1,09 0,234 709,82 0,003073	0,25 1,21 0,217 709,82 0	0,57 2,76 0,208 709,82 0,000633	0,84 5,00 2,02 0,199 709,82 0,06884 0,028333
Sea Area IV	$h_e$ (m) 1,27 2,25 0,209 709,82 0,240527	1,5 2,36 0,209 709,82 0,335566	1,81 2,57 0,209 709,82 0,45245	1,94 2,62 0,215 709,82 0,496731	2,05 2,50 0,212 709,82 0,511286	1,75 2,02 0,232 709,82 0,361191	1,39 1,39 0,242 709,82 0,191493	1,09 3,03 0,213 709,82 0,173874	0,69 0,76 0,163 709,82 0,002423	0,2 1,38 0,265 709,82 0	0,69 3,44 0,218 709,82 0,010858	0,97 7,07 2,14 0,209 709,82 0,213841 0,070314

## UL Bow

	Jan I	Feb II	Mar III	April IV	May V	June VI	July VII	Aug VIII	Sept IX	Oct X	Nov XI	Dec XII
$h_e$ (m)	1,5	1,74	1,92	2,05	2,17	2,17	1,25	0,97	0,68	0,36	0,74	1,09
Ni (days) Ni esc.	1,57	1,65	1,75	1,81	1,89	1,32	9,43	1,89	1,02	1,28	2,86	6,74
$a_i$	0,139	0,139	0,139	0,143	0,157	0,155	0,90	0,190	0,218	0,202	0,162	1,45
$m_{IV}$ (kN)	709,82	709,82	709,82	709,82	709,82	709,82	709,82	709,82	709,82	709,82	709,82	709,82
P	0,238364	0,304477	0,362115	0,405264	0,44747	0,340527	0,669685	0,0606	0,00263	0	0,015302	0,340744
P esc.							0,100122					0,08583
$h_e$ (m)	1,41	1,65	1,84	2,07	2,09	1,65	1,3	0,95	0,7	0,36	0,7	1,11
Ni (days) Ni esc.	1,49	1,60	1,72	1,91	1,72	1,44	1,01	1,76	1,22	1,19	2,44	6,76
$a_i$	0,130	0,130	0,130	0,133	0,131	0,162	0,176	0,177	0,254	0,188	0,151	1,37
$m_{IV}$ (kN)	709,82	709,82	709,82	709,82	709,82	709,82	709,82	709,82	709,82	709,82	709,82	709,82
P	0,20884	0,275278	0,338945	0,426581	0,398587	0,251565	0,12788	0,05036	0,00411	0	0,008203	0,367282
P esc.												0,088785
$h_e$ (m)	1,05	1,31	1,5	1,75	1,77	1,44	1,18	0,92	0,73	0,21	0,5	0,8
Ni (days) Ni esc.	6,68	1,99	2,18	2,43	2,16	1,07	3,41	0,95	0,65	0,48	1,56	3,66
$a_i$	1,83	0,168	0,168	0,155	0,151	0,117	0,58	0,114	0,131	0,091	0,136	0,168
$m_{IV}$ (kN)	709,82	709,82	709,82	709,82	709,82	709,82	709,82	709,82	709,82	709,82	709,82	709,82
P	0,292221	0,236601	0,315268	0,416999	0,386449	0,159856	0,267788	0,023174	0,003244	0	0	0,03597
P esc.	0,090416						0,051457					
P	0,200253	0,26803	0,330473	0,396595	0,393432	0,288085	0,337722	0,067777	0,003156	1,11E-16	0,00621	0,159657
P esc.	0,166384	0,249854	0,330473	0,396595	0,393432	0,249375	0,117943	0,067777	0,003156	1,11E-16	0,00621	0,04949





## UL Midship

	Jan	Feb	Mar	April	May	June	July	Aug	Sept	Oct	Nov	Dec
	I	II	III	IV	V	VI	VII	VIII	IX	X	XI	XII
Sea Area V	h <sub>a</sub> (m)	1,5	1,74	1,92	2,05	2,17	1,25	0,97	0,68	0,36	0,74	1,09
	Nl(days)	1,57	1,65	1,75	1,81	1,32	9,43	1,89	1,02	1,28	2,86	6,74
	a <sub>i</sub>						0,90					1,45
	m <sub>ny</sub> (kN)	0,139	0,139	0,139	0,143	0,155	0,162	0,190	0,218	0,202	0,162	0,139
	P	365,52	365,52	365,52	365,52	365,52	365,52	365,52	365,52	365,52	365,52	365,52
	P esc.	0,158507	0,279325	0,386297	0,46549	0,419185	0,355397	0,019185	0,000148	0	0,002537	0,136182
							0,040959					0,031039
Sea Area VI	h <sub>a</sub> (m)	1,41	1,65	1,84	2,07	2,09	1,65	1,3	0,7	0,36	0,7	1,11
	Nl(days)	1,49	1,60	1,72	1,91	1,72	1,44	1,01	1,22	1,19	2,44	6,76
	a <sub>i</sub>											1,37
	m <sub>ny</sub> (kN)	0,129829	0,129829	0,129829	0,13342	0,13141	0,162269	0,17575	0,253713	0,188181	0,150625	0,129829
	P	365,52	365,52	365,52	365,52	365,52	365,52	365,52	365,52	365,52	365,52	365,52
	P esc.	0,117003	0,227996	0,340779	0,493403	0,467629	0,207758	0,055653	0,000422	0	0,000845	0,150949
												0,032692
Sea Area VII	h <sub>a</sub> (m)	1,05	1,31	1,5	1,75	1,77	1,44	1,18	0,73	0,21	0,5	0,8
	Nl(days)	6,68	1,99	2,18	2,43	2,16	1,07	3,41	0,65	0,48	1,56	3,66
	a <sub>i</sub>	1,83						0,58				
	m <sub>ny</sub> (kN)	0,167828	0,167828	0,167828	0,155223	0,150997	0,116535	0,097367	0,131188	0,091222	0,136297	0,167828
	P	365,52	365,52	365,52	365,52	365,52	365,52	365,52	365,52	365,52	365,52	365,52
	P esc.	0,111186	0,112026	0,214593	0,389865	0,36722	0,094479	0,111727	0,000514	0	0	0,008247
		0,031802						0,01988				
	P	0,094852	0,174117	0,288698	0,393953	0,411618	0,23757	0,169135	0,000301	1,11E-16	0,000768	0,058784
	P esc.	0,08153	0,16712	0,288698	0,393953	0,411618	0,2199	0,054707	0,000301	1,11E-16	0,000768	0,016052



UL Stern

	Jan I	Feb II	Mar III	April IV	May V	June VI	July VII	Aug VIII	Sept IX	Oct X	Nov XI	Dec XII
<div>h<sub>e</sub> (m)</div>	1,5	1,74	1,92	2,05	2,17	2,17	1,25	0,97	0,68	0,36	0,74	1,09
<div>Ni (days) Ni esc.</div>	1,57	1,65	1,75	1,81	1,89	1,32	9,43	1,89	1,02	1,28	2,86	6,74
<div>a<sub>i</sub></div>	0,139	0,139	0,139	0,143	0,157	0,155	0,90	0,190	0,218	0,202	0,162	1,45
<div>m<sub>vy</sub> (kN)</div>	370,18	370,18	370,18	370,18	370,18	370,18	370,18	370,18	370,18	370,18	370,18	370,18
<div>P</div>	0,369417	0,534038	0,650469	0,72321	0,782543	0,657233	0,761493	0,08737	0,005224	0	0,027152	0,436229
<div>P esc.</div>							0,127603					0,116124
<div>h<sub>e</sub> (m)</div>	1,41	1,65	1,84	2,07	2,09	1,65	1,3	0,95	0,7	0,36	0,7	1,11
<div>Ni (days)</div>	1,49	1,60	1,72	1,91	1,72	1,44	1,01	1,76	1,22	1,19	2,44	6,76
<div>a<sub>i</sub></div>	0,130	0,130	0,130	0,133	0,131	0,162	0,176	0,177	0,254	0,188	0,151	1,37
<div>m<sub>vy</sub> (kN)</div>	370,18	370,18	370,18	370,18	370,18	370,18	370,18	370,18	370,18	370,18	370,18	370,18
<div>P</div>	0,298309	0,468421	0,604505	0,749631	0,720583	0,433747	0,163393	0,073627	0,007819	0	0,015576	0,464263
<div>P esc.</div>												0,119066
<div>h<sub>e</sub> (m)</div>	1,05	1,31	1,5	1,75	1,77	1,44	1,18	0,92	0,73	0,21	0,5	0,8
<div>Ni (days)</div>	6,68	1,99	2,18	2,43	2,16	1,07	3,41	0,95	0,65	0,48	1,56	3,66
<div>a<sub>i</sub></div>	1,83						0,58					
<div>m<sub>vy</sub> (kN)</div>	0,168	0,168	0,168	0,155	0,151	0,117	0,097	0,114	0,131	0,091	0,136	0,168
<div>P</div>	370,18	370,18	370,18	370,18	370,18	370,18	370,18	370,18	370,18	370,18	370,18	370,18
<div>P esc.</div>	0,382956	0,305466	0,473901	0,680913	0,64939	0,240362	0,33797	0,034605	0,005818	0	0	0,058734
	0,123996						0,0675					
<div>P</div>	0,271708	0,398556	0,536108	0,651916	0,659572	0,468393	0,409337	0,094644	0,006036	1,11E-16	0,011823	0,214074
<div>P esc.</div>	0,228247	0,37486	0,536108	0,651916	0,659572	0,421601	0,158112	0,094644	0,006036	1,11E-16	0,011823	0,070885

ULA Bow

	Jan	Feb	Mar	April	May	June	July	Aug	Sept	Oct	Nov	Dec
	I	II	III	IV	V	VI	VII	VIII	IX	X	XI	XII
Sea Area I	$h_a$ (m)	0,68	0,84	1,06	1,17	1,17	0,74	0	0	0	0,25	0,46
	$N_i$ (days)	0,97	1,33	2,57	4,00	3,00	0,41	0,00	0,00	0,00	0,27	0,69
	$a_i$	0,053	0,053	0,053	0,055	0,045	0,028	0,000	0,000	0,000	0,031	0,053
	$m_{ry}$ (kN)	1641,66	1641,66	1641,66	1641,66	1641,66	1641,66	1641,66	1641,66	1641,66	1641,66	1641,66
	P	0	0	0	0	0	0	0	0	0	0	0
Sea Area II	$h_a$ (m)	0,84	1,06	1,24	1,35	1,47	1,17	0,57	0,25	0,1	0,36	0,57
	$N_i$ (days)	2,54	4,90	1,09	1,00	1,03	6,10	0,16	0,00	0,17	0,91	1,56
	$a_i$	0,101	0,101	0,101	0,094	0,103	0,113	0,034	0,000	0,037	0,094	0,101
	$m_{ry}$ (kN)	1641,66	1641,66	1641,66	1641,66	1641,66	1641,66	1641,66	1641,66	1641,66	1641,66	1641,66
	P	0	0	0	0,000128	0,000399	0	0	0	0	0	0
Sea Area III	$h_a$ (m)	1,19	1,36	1,58	1,71	1,76	1,47	0,84	0,68	0,25	0,57	0,84
	$N_i$ (days)	2,14	2,21	2,29	2,37	2,17	1,58	2,00	1,09	1,21	2,76	5,00
	$a_i$	0,199	0,199	0,199	0,205	0,202	0,194	0,272	0,234	0,217	0,208	2,02
	$m_{ry}$ (kN)	1641,66	1641,66	1641,66	1641,66	1641,66	1641,66	1641,66	1641,66	1641,66	1641,66	1641,66
	P	0	0,000333	0,001509	0,002498	0,002671	0,000612	0	0	0	0	0
Sea Area IV	$h_a$ (m)	1,27	1,5	1,81	1,94	2,05	1,75	1,09	0,69	0,2	0,69	0,97
	$N_i$ (days)	2,25	2,36	2,57	2,62	2,50	2,02	3,03	0,76	1,38	3,44	7,07
	$a_i$	0,209	0,209	0,209	0,215	0,212	0,232	0,213	0,163	0,265	0,218	2,14
	$m_{ry}$ (kN)	1641,66	1641,66	1641,66	1641,66	1641,66	1641,66	1641,66	1641,66	1641,66	1641,66	1641,66
	P	0	0,001074	0,003645	0,005208	0,006399	0,002406	0	0	0	0	0

ULA Bow

	Jan	Feb	Mar	April	May	June	July	Aug	Sept	Oct	Nov	Dec
	I	II	III	IV	V	VI	VII	VIII	IX	X	XI	XII
$h_a$ (m)	1,5	1,74	1,92	2,05	2,17	2,17	1,25	0,97	0,68	0,36	0,74	1,09
$N_i$ (days)	1,57	1,65	1,75	1,81	1,89	1,32	9,43	1,89	1,02	1,28	2,86	6,74
Sea Area $a_i$							0,90					1,45
$m_{ny}$ (kN)	0,139	0,139	0,139	0,143	0,157	0,155	0,162	0,190	0,218	0,202	0,162	0,139
V	1641,66	1641,66	1641,66	1641,66	1641,66	1641,66	1641,66	1641,66	1641,66	1641,66	1641,66	1641,66
P	0,000696	0,001873	0,00325	0,004575	0,006126	0,004303	0	0	0	0	0	0
P esc.							0					0
$h_a$ (m)	1,41	1,65	1,84	2,07	2,09	1,65	1,3	0,95	0,7	0,36	0,7	1,11
$N_i$ (days)	1,49	1,60	1,72	1,91	1,72	1,44	1,01	1,76	1,22	1,19	2,44	6,76
Sea Area $a_i$												1,37
$m_{ny}$ (kN)	0,130	0,130	0,130	0,133	0,131	0,162	0,176	0,177	0,254	0,188	0,151	0,130
V	1641,66	1641,66	1641,66	1641,66	1641,66	1641,66	1641,66	1641,66	1641,66	1641,66	1641,66	1641,66
P	0,000377	0,001341	0,002605	0,005035	0,004732	0,001207	3,69E-05	0	0	0	0	0
P esc.												0
$h_a$ (m)	1,05	1,31	1,5	1,75	1,77	1,44	1,18	0,92	0,73	0,21	0,5	0,8
$N_i$ (days)	6,68	1,99	2,18	2,43	2,16	1,07	3,41	0,95	0,65	0,48	1,56	3,66
Sea Area $a_i$	1,83						0,58					
$m_{ny}$ (kN)	0,168	0,168	0,168	0,155	0,151	0,117	0,097	0,114	0,131	0,091	0,136	0,168
V	1641,66	1641,66	1641,66	1641,66	1641,66	1641,66	1641,66	1641,66	1641,66	1641,66	1641,66	1641,66
P	0	8,84E-05	0,000985	0,002875	0,002714	0,000342	0	0	0	0	0	0
P esc.							0					
P	0,000146	0,000741	0,002019	0,003416	0,003926	0,001579	7,91E-05	0	0	1,11E-16	0	0
P esc.												
	0,000146	0,000741	0,002019	0,003416	0,003926	0,001579	7,91E-05	0	0	1,11E-16	0	0

## ULA Midship

	Jan	Feb	Mar	April	May	June	July	Aug	Sept	Oct	Nov	Dec
	I	II	III	IV	V	VI	VII	VIII	IX	X	XI	XII
Sea												
Area												
I	0,68	0,84	1,06	1,17	1,17	0,74	0,36	0	0	0	0,25	0,46
$N_I$ (days)	0,97	1,33	2,57	4,00	3,00	0,41	0,08	0,00	0,00	0,00	0,27	0,69
$a_I$	0,053198	0,053198	0,053198	0,05467	0,044872	0,027704	0,01286	0	0	0	0,03086	0,053198
$m_{IV}$ (kN)	670,51	670,51	670,51	670,51	670,51	670,51	670,51	670,51	670,51	670,51	670,51	670,51
P	0	0	0	0	0	0	0	0	0	0	0	0
Sea												
Area												
II	0,10133	0,10133	0,10133	0,093719	0,102564	0,112577	0,078383	0,034483	0	0,036718	0,094048	0,10133
$m_{IV}$ (kN)	670,51	670,51	670,51	670,51	670,51	670,51	670,51	670,51	670,51	670,51	670,51	670,51
P	0	0	0,000194	0,000939	0,002458	0	0	0	0	0	0	0
P esc.	0	0				0						
Sea												
Area												
III	1,19	1,36	1,58	1,71	1,76	1,47	1,19	0,84	0,68	0,25	0,57	0,84
$N_I$ (days)	2,14	2,21	2,29	2,37	2,17	1,58	9,00	2,00	1,09	1,21	2,76	5,00
$a_{III}$							1,29					2,02
$m_{IV}$ (kN)	0,199493	0,199493	0,199493	0,205011	0,201923	0,193931	0,231476	0,271552	0,233911	0,216867	0,208303	0,199493
P	670,51	670,51	670,51	670,51	670,51	670,51	670,51	670,51	670,51	670,51	670,51	670,51
P esc.	0	0,002293	0,010208	0,019163	0,021456	0,003761	0	0	0	0	0	0
Sea												
Area												
IV	1,27	1,5	1,81	1,94	2,05	1,75	1,39	1,09	0,69	0,2	0,69	0,97
$N_I$ (days)	2,25	2,36	2,57	2,62	2,50	2,02	1,39	3,03	0,76	1,38	3,44	7,07
$a_{IV}$												2,14
$m_{IV}$ (kN)	0,208993	0,208993	0,208993	0,214774	0,211538	0,23219	0,242498	0,213362	0,163366	0,26506	0,218222	0,208993
P	670,51	670,51	670,51	670,51	670,51	670,51	670,51	670,51	670,51	670,51	670,51	670,51
P esc.	0,000746	0,006692	0,03038	0,047719	0,062584	0,019095	0,001839	0	0	0	0	0

## ULA Midship

	Jan I	Feb II	Mar III	April IV	May V	June VI	July VII	Aug VIII	Sept IX	Oct X	Nov XI	Dec XII
$h_e$ (m)	1,5	1,74	1,92	2,05	2,17	2,17	1,25	0,97	0,68	0,36	0,74	1,09
$N_l$ (days)	1,57	1,65	1,75	1,81	1,89	1,32	9,43	1,89	1,02	1,28	2,86	6,74
Sea Area $a_l$							0,90					1,45
$m_{IV}$ (kN)	0,139329	0,139329	0,139329	0,143183	0,156695	0,154793	0,161666	0,189655	0,217822	0,201951	0,161646	0,139329
$V$	670,51	670,51	670,51	670,51	670,51	670,51	670,51	670,51	670,51	670,51	670,51	670,51
$P$	0,004171	0,014421	0,029158	0,044647	0,063406	0,044928	0,001494	0	0	0	0	0
$P$ esc.						0,000142						0
$h_e$ (m)	1,41	1,65	1,84	2,07	2,09	1,65	1,3	0,95	0,7	0,36	0,7	1,11
$N_l$ (days)	1,49	1,60	1,72	1,91	1,72	1,44	1,01	1,76	1,22	1,19	2,44	6,76
Sea Area $a_l$												1,37
$m_{IV}$ (kN)	0,129829	0,129829	0,129829	0,13342	0,13141	0,162269	0,17575	0,176724	0,253713	0,188181	0,150625	0,129829
$V$	670,51	670,51	670,51	670,51	670,51	670,51	670,51	670,51	670,51	670,51	670,51	670,51
$P$	0,002109	0,009426	0,021948	0,049623	0,047251	0,008487	0,00045	0	0	0	0	0
$P$ esc.												0
$h_e$ (m)	1,05	1,31	1,5	1,75	1,77	1,44	1,18	0,92	0,73	0,21	0,5	0,8
$N_l$ (days)	6,68	1,99	2,18	2,43	2,16	1,07	3,41	0,95	0,65	0,48	1,56	3,66
Sea Area $a_l$	1,83						0,58					
$m_{IV}$ (kN)	0,167828	0,167828	0,167828	0,155223	0,150997	0,116535	0,097367	0,114224	0,131188	0,091222	0,136297	0,167828
$V$	670,51	670,51	670,51	670,51	670,51	670,51	670,51	670,51	670,51	670,51	670,51	670,51
$P$	0	0,001127	0,006044	0,022594	0,021739	0,002005	0	0	0	0	0	0
$P$ esc.	0					0						
$P$	0,001011	0,005278	0,016332	0,030786	0,037251	0,013729	0,000767	0	0	1,11E-16	0	0
$P$ esc.	0,001011	0,005278	0,016332	0,030786	0,037251	0,013729	0,000548	0	0	1,11E-16	0	0

**UCLA Stern**

	Jan	Feb	Mar	April	May	June	July	Aug	Sept	Oct	Nov	Dec
	I	II	III	IV	V	VI	VII	VIII	IX	X	XI	XII
Sea Area I	$h_a$ (m)	0,68	0,84	1,06	1,17	0,74	0,36	0	0	0	0,25	0,46
	$N_l$ (days)	0,97	1,33	2,57	4,00	3,00	0,41	0,08	0,00	0,00	0,27	0,69
	$a_l$	0,053	0,053	0,053	0,055	0,045	0,028	0,013	0,000	0,000	0,031	0,053
	$m_{IV}$ (kN)	938,25	938,25	938,25	938,25	938,25	938,25	938,25	938,25	938,25	938,25	938,25
	P	0	0	0	0	0	0	0	0	0	0	0
Sea Area II	$h_a$ (m)	0,84	1,06	1,24	1,35	1,47	1,17	0,84	0,57	0,1	0,36	0,57
	$N_l$ (days)	2,54	4,90	1,09	1,00	1,03	6,10	1,02	0,16	0,00	0,17	1,56
	$a_l$	0,101	0,101	0,101	0,094	0,103	0,113	0,078	0,034	0,000	0,037	0,101
	$m_{IV}$ (kN)	938,25	938,25	938,25	938,25	938,25	938,25	938,25	938,25	938,25	938,25	938,25
	P	0	0	0	0,000336	0,001291	0	0	0	0	0	0
Sea Area III	$h_a$ (m)	1,19	1,36	1,58	1,71	1,76	1,47	1,19	0,84	0,25	0,57	0,84
	$N_l$ (days)	2,14	2,21	2,29	2,37	2,17	1,58	9,00	2,00	1,21	2,76	5,00
	$a_l$	0,199	0,199	0,199	0,205	0,202	0,194	1,29	0,272	0,234	0,217	2,02
	$m_{IV}$ (kN)	938,25	938,25	938,25	938,25	938,25	938,25	938,25	938,25	938,25	938,25	938,25
	P	0	0,000876	0,006005	0,012104	0,013819	0,001976	0	0	0	0	0
Sea Area IV	$h_a$ (m)	1,27	1,5	1,81	1,94	2,05	1,75	1,39	1,09	0,2	0,69	0,97
	$N_l$ (days)	2,25	2,36	2,57	2,62	2,50	2,02	1,39	3,03	1,38	3,44	7,07
	$a_l$	0,209	0,209	0,209	0,215	0,212	0,232	0,242	0,213	0,163	0,265	2,14
	$m_{IV}$ (kN)	938,25	938,25	938,25	938,25	938,25	938,25	938,25	938,25	938,25	938,25	938,25
	P	0	0,003648	0,0199	0,032474	0,043719	0,012232	0,000797	0	0	0	0

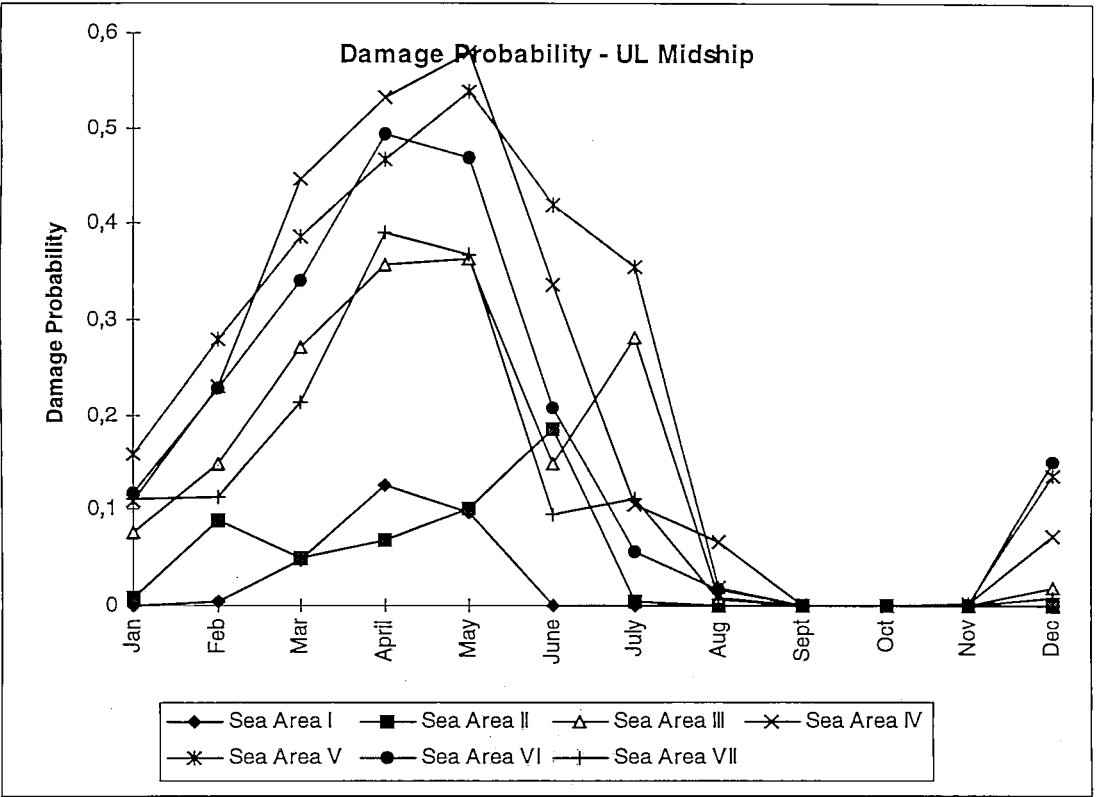
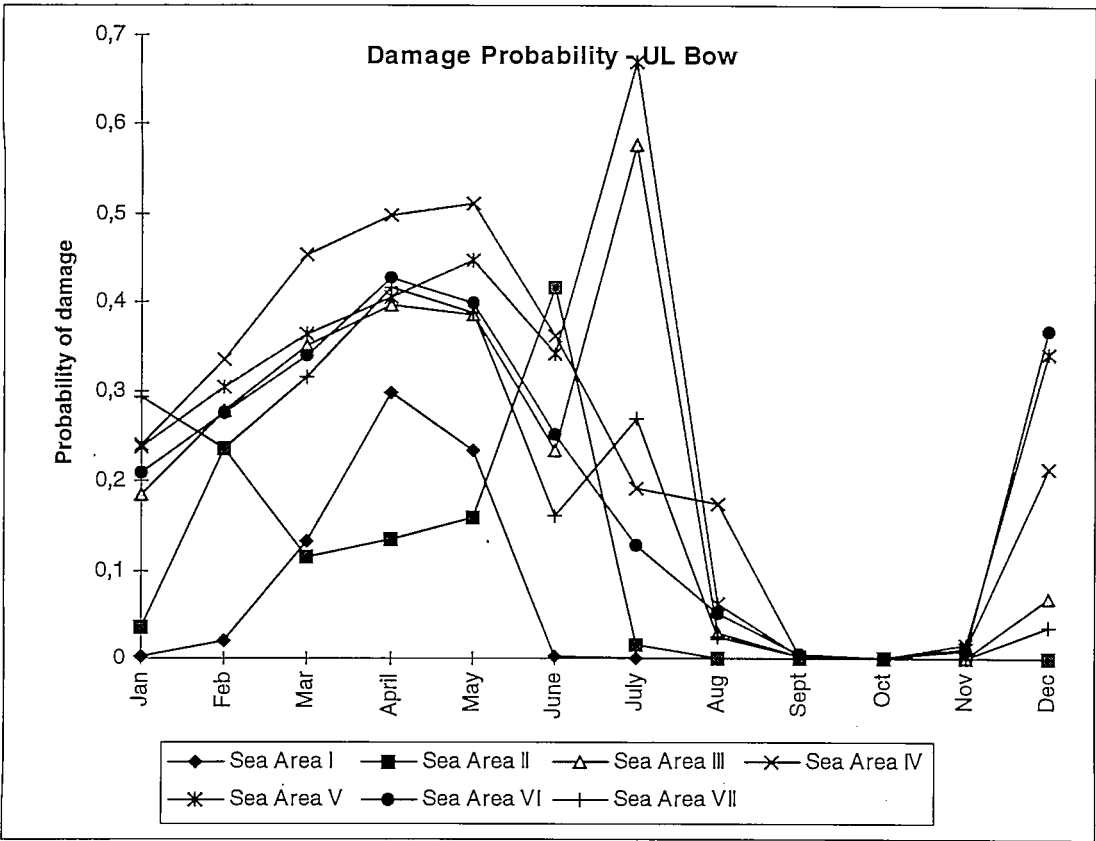


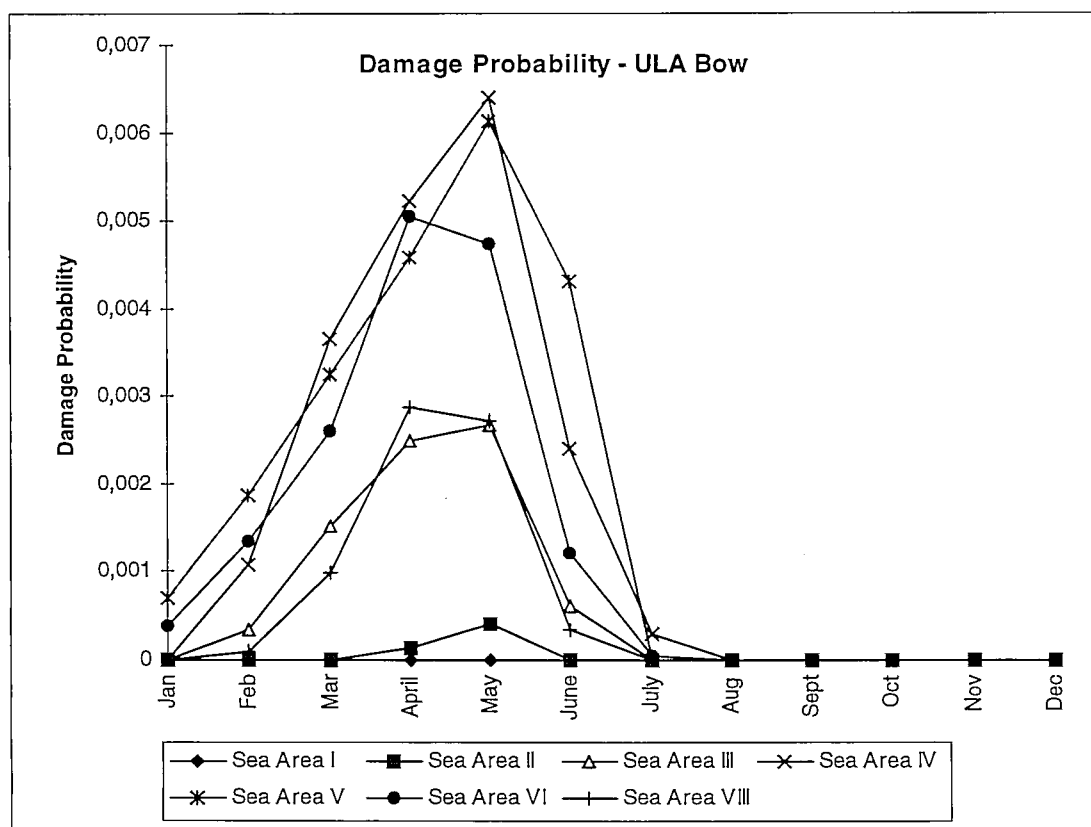
ULA Stern

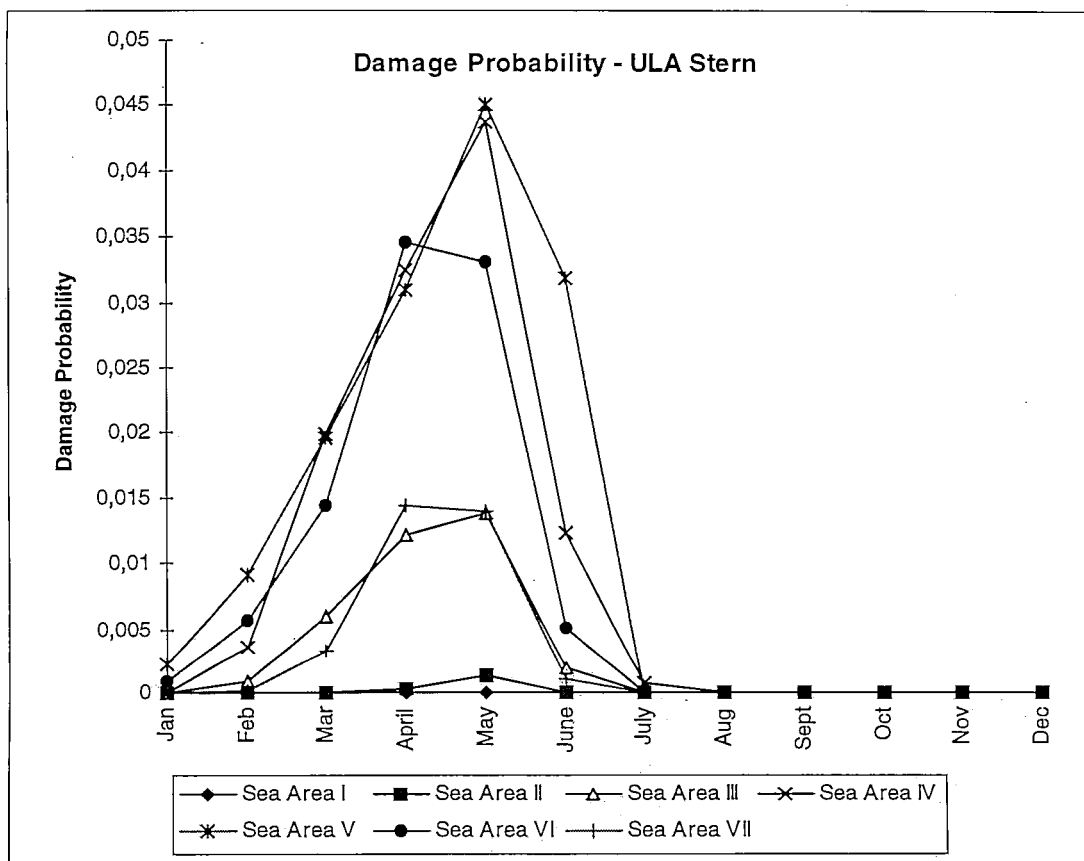
	Jan	Feb	Mar	April	May	June	July	Aug	Sept	Oct	Nov	Dec
	I	II	III	IV	V	VI	VII	VIII	IX	X	XI	XII
$h_e$ (m)	1,5	1,74	1,92	2,05	2,17	2,17	1,25	0,97	0,68	0,36	0,74	1,09
$N_i$ (days)	1,57	1,65	1,75	1,81	1,89	1,32	9,43	1,89	1,02	1,28	2,86	6,74
$N_i$ esc.							0,90					1,45
$a_i$	0,139	0,139	0,139	0,143	0,157	0,155	0,162	0,190	0,218	0,202	0,162	0,139
$m_{xy}$ (kN)	938,25	938,25	938,25	938,25	938,25	938,25	938,25	938,25	938,25	938,25	938,25	938,25
$P$	0,002225	0,009119	0,019568	0,030945	0,045083	0,031854	0	0	0	0	0	0
$P$ esc.							0					0
$h_e$ (m)	1,41	1,65	1,84	2,07	2,09	1,65	1,3	0,95	0,7	0,36	0,7	1,11
$N_i$ (days)	1,49	1,60	1,72	1,91	1,72	1,44	1,01	1,76	1,22	1,19	2,44	6,76
$N_i$ esc.												1,37
$a_i$	0,130	0,130	0,130	0,133	0,131	0,162	0,176	0,177	0,254	0,188	0,151	0,130
$m_{xy}$ (kN)	938,25	938,25	938,25	938,25	938,25	938,25	938,25	938,25	938,25	938,25	938,25	938,25
$P$	0,000932	0,00571	0,014387	0,034561	0,033026	0,00514	3,03E-05	0	0	0	0	0
$P$ esc.												0
$h_e$ (m)	1,05	1,31	1,5	1,75	1,77	1,44	1,18	0,92	0,73	0,21	0,5	0,8
$N_i$ (days)	6,68	1,99	2,18	2,43	2,16	1,07	3,41	0,95	0,65	0,48	1,56	3,66
$N_i$ esc.							0,58					
$a_i$	0,168	0,168	0,168	0,155	0,151	0,117	0,097	0,114	0,131	0,091	0,136	0,168
$m_{xy}$ (kN)	938,25	938,25	938,25	938,25	938,25	938,25	938,25	938,25	938,25	938,25	938,25	938,25
$P$	0	0,000208	0,003269	0,014439	0,013991	0,000984	0	0	0	0	0	0
$P$ esc.							0					
$P$	0,000431	0,002984	0,0105	0,020771	0,025688	0,009103	0,000199	0	0	1,11E-16	0	0
$P$ esc.												
	0,000431	0,002984	0,0105	0,020771	0,025688	0,009103	0,000199	0	0	1,11E-16	0	0

## **APPENDIX 4.**

### **Graphs of damage probability vs month**







## **APPENDIX 5.**

### **Project Review**

## Discussion of INSRP Draft Project - Ice Environment and Ship Hull Loading along the NSR

by  
Claude Daley,  
Memorial University of Newfoundland

Overall the report is well written, clearly presented and makes a significant contribution to our knowledge of the Arctic. I recommend that the report be published after some minor changes as indicated in items 1 and 2 below.

I will make three type of comments on this report; matters of presentation, such as spelling mistakes; matters of clarity, such as areas where the logic is unclear are where further explanation is warranted and; matters of technical debate. The first two items should be fixed prior to publication. The third area, matters of technical debate, are areas where I feel that things may be different than the authors have stated. However, my disagreement or concern should not hinder the publication of the report, as they represent the debate that all technical writings should properly foster.

*(Only the third type of comments included below, the other changes being made.)*

### 3) Comments on Technical Approach

p2

multi-year ice : I find it rather crucial that MY ice is left out of the analysis. If even rare fragments of MY ice are present, they may completely change the situation regarding structural damage. UL class ships would probably be easily damaged by MY ice.

*Reply. The damage probability model is based on observations made in the Baltic and scaled up for the NSR. The multiyear ice can be included into the equivalent thickness similarly to ridges. However, if the multiyear ice is not failing by bending any more the damage probabilities are probably higher than those obtained from the model although the multiyear floes are usually successfully avoided by the ships. A better parameterisation could be made as the Russian data is gradually becoming more available, but a true future strategy to address this question would be to make hull load observations along the NSR..*

p13

ice morphology and "ice state" : I believe that the need for finding an "ice state" is directly related to the issues discussed on this page. However, the idea of having 3 ice codes (geophysical, navigational and observational) goes counter to what I feel an "ice state" model should be. We know that many things (ice cover geophysics, ice loads on ships, etc.), depend on ice morphology and ice physical and mechanical properties. And the morphology, no doubt depends on the ice physical and mechanical properties as well as geophysical processes. The idea of "ice state" is to find a basic way of describing the ice cover that captures the complex morphology, in much the same way

that a sea state captures the complex mix of waves that make it up. It is mentioned that the variation of ice morphology is typically very large, at all scales. Does this not mean that classical geometry is unsuitable? Should we not be using fractal or other measures which elegantly capture these types of complex geometries?

*Reply. As stated on p.13. the threefold description is truly applicable only if connection relations are established. It may be unrealistic to seek a code that would satisfy both navigational and scientific needs. For example, the geometric parameters required by the remote sensing image interpretation contain such that have no relevance to any practical application whatsoever.*

p17

ice thickness : 3 meter ice as a maximum seems to be rather thin, although I understand how you get it. I have difficulty with the idea of separating sheet ice from all other ice. A lot of MY ice is not formed as sheet ice, but as consolidated rubble fields, much thicker than 3 m. The loads in 3 m ice will naturally be very different from loads in 6 m ice.

*Reply. The 3 m default thickness is clearly too small for the Central Arctic or the Canadian Arctic but is realistic for the NSR. This is also supported by observations.*

p20

2.5 Ice Ridges : I am not comfortable with this whole section. I understand the ideas, but I don't think that this approach will be fruitful. It is stated that no generally accepted 2D description of ridge fields exists. Why does it need to be generally accepted? This report is proposing a methodology for treating ship hull loading in the NSR. I don't feel that the proposed methodology must necessarily be founded in the old "generally accepted" approaches. These old methods haven't worked terribly well, and we need new ways. It is clear that ridges represent the single most significant impediment to ships. It is also clear that ridge fields are two-dimensional objects. I believe (see HUT Report M120 - Daley 1992) that ridge fields may be modelled with the aid of fractals and percolation lattices. Clearly more work is needed to place such ideas on a sound footing, but percolation patterns offer two very compelling advantages. One is that they seem to capture the two-dimensional geometry of a ridge field, and secondly they appear to satisfy some physical constraints, that ideas such as "ridge links" do not. Modelling the 2D geometry will result in the various probabilistic distributions (e.g. crossings per km) will be captured naturally. And satisfying the physical constraints is essential if we expect to use our descriptions to calculate ice loads on navigating vessels. A ridge can not form inside an otherwise un-deformed ice floe, ridges/rubble and open water must be contiguous. Of course a ridge segment may be found inside a newly consolidated floe, but that is a further complication. Figure 2.9 seems to indicate that, generally, longer ridges will be wider ridges. I believe that viewing ridges at percolation clusters will confirm this idea, and show causality. I don't want to be too harsh on this point, but I notice that many of the references (other than recent ones by one of the authors) date back to the 1970 s.

*Reply. The 2D description of the ice cover is an unsettled question. The fractal methods are elegant but no systematic applications to the ice cover exist. The data obtained from the ice cover is usually analysed in terms of distributions which makes*



*the parameterisation of distribution based models for different sea areas feasible. The fractal methods and distributions are not incommensurable and have clear theoretical connections.*

p33

Ice Pressure : These references seem rather old (1977). There have been various studies of pressure in ice conducted since then. The values are, I believe generally similar to the values given, but higher values have been reported.

*Reply. As the ice can fail by crushing against the hull the loads can locally be much larger than 100 kN/m which is a typical value for the onset of ridging. The loads also vary much with the hull geometry and the hazardousness of the situation is dependent on the contact area involved.*

p68

first yield : It seems strange to use first yield as the damage limit state. First yield produces no visible effects, and is much more likely than limit states involving some visible damage. Possibly the authors could clarify this point.

*Reply. The absence of yield is a traditional design criterion and can be related to the ultimate strength.*

p73

icebreaker assistance : It is reported that icebreaker assistance reduces the probability of damage considerable. I have some difficulty with this conclusion, although I accept that in certain cases this may be true. Firstly I would like to see more explanation of how loads are calculated for the icebreaker assistance case. I am not clear on how Baltic damage statistics could be modified to be suitable for this case. Surely the collision speeds are still quite high, and the ice thickness is quite large. I might agree that the number of collisions would be less, but how much less would depend on many factors. In established channels in fast ice, there may be few collisions, but in open pack the number of collisions may be quite high. And secondly, in the arctic, icebreaker assistance might lead to collisions with MY ice, further complicating the situation.

*Reply. The model is not intended for situations where the ship cannot navigate unassisted. If a channel is made through a thick multiyear ice the situation may change. The probabilities are based on observations from the Baltic and similar measurements should be made along the NSR to clarify matters like this.*

## The three main cooperating institutions of INSROP



### **Ship & Ocean Foundation (SOF), Tokyo, Japan.**

SOF was established in 1975 as a non-profit organization to advance modernization and rationalization of Japan's shipbuilding and related industries, and to give assistance to non-profit organizations associated with these industries. SOF is provided with operation funds by the Sasakawa Foundation, the world's largest foundation operated with revenue from motorboat racing. An integral part of SOF, the Tsukuba Institute, carries out experimental research into ocean environment protection and ocean development.



### **Central Marine Research & Design Institute (CNIIMF), St. Petersburg, Russia.**

CNIIMF was founded in 1929. The institute's research focus is applied and technological with four main goals: the improvement of merchant fleet efficiency; shipping safety; technical development of the merchant fleet; and design support for future fleet development. CNIIMF was a Russian state institution up to 1993, when it was converted into a stock-holding company.



### **The Fridtjof Nansen Institute (FNI), Lysaker, Norway.**

FNI was founded in 1958 and is based at Polhøgda, the home of Fridtjof Nansen, famous Norwegian polar explorer, scientist, humanist and statesman. The institute specializes in applied social science research, with special focus on international resource and environmental management. In addition to INSROP, the research is organized in six integrated programmes. Typical of FNI research is a multi-disciplinary approach, entailing extensive cooperation with other research institutions both at home and abroad. The INSROP Secretariat is located at FNI.

